

Modelling of aerosol and cloud processes in the summertime high Arctic

Ruth Sarah Price

Submitted in accordance with the requirements for the degree of
Doctor of Philosophy

The University of Leeds
School of Earth and Environment

September 2022

The PGR confirms that the work submitted is her own, except where work which has formed part of jointly authored publications has been included. The contribution of the PGR and the other authors to this work has been explicitly indicated below. The PGR confirms that appropriate credit has been given within the thesis where reference has been made to the work of others.

The contents of Chapter 3 are from a jointly authored publication which is yet to be submitted for publication, titled “Late summer transition from a free tropospheric to boundary layer source of Aitken mode aerosol in the high Arctic” (Price et al. 2022, to be submitted). Co-author Ken Carslaw provided guidance during model output analysis. Co-author Paul Field assisted with model simulations. Co-author Ian Brooks provided scientific guidance. Co-authors Julia Schmale, Andrea Baccharini and Paul Zieger performed aerosol measurements during the Arctic Ocean 2018 campaign. All authors were involved in discussion of results and reviewing of the manuscript. The PGR carried out the necessary simulations, analysis and drafting of the manuscript.

This copy has been supplied on the understanding that it is copyright material and that no quotation from the thesis may be published without proper acknowledgement

Copyright © 2022 The University of Leeds and Ruth Sarah Price
The right of Ruth Sarah Price to be identified as Author of this work has been asserted by her in accordance with the Copyright, Designs and Patents Act 1988.

Acknowledgements

I'd like to thank my supervisors, Ken Carslaw, Ian Brooks and Paul Field, for their support and guidance during my PhD. I'm also grateful to NERC for funding my studentship under the SPHERES Doctoral Training Partnership (NE/L002574/1).

Thank you to my parents, Tim and Kate, for being enthusiastic and generous supporters of all my academic pursuits, leading up to and including this PhD. Thanks also for being enthusiastic and generous supporters of all my non-academic pursuits! Thank you to my grandparents for unconditional and unwavering grandparental pride in the things I do. Thank you to Mary and Sam for many things – career advice, proof-reading of PhD applications, free accommodation during AGU, midnight (UK time..) phone calls, and of course, literally feeding and housing me while I wrote most of this thesis.

To the girls – Bec, Bird, Foynes and Liz – thanks both for the support (weekly zooms in lockdown that kept us all going), and for the distractions (endless tiktoks and general group chat nonsense), both of which were a very important part of this process.

To the boys – George, Joe Lee, Mei, Lewis and Simms – thanks for getting me through 4 years of lectures with awful physics puns. Thanks even more for getting me through 4 years of PhD with awful physics puns, and a variety of excellent European train holidays.

To Alice, my lab partner for life. Research is obviously less fun without you, but having you around still makes it better. I would never have made it through the insanity of Friday lab without you, and I probably wouldn't have done this without you as my inspo.

To Rachel, my PhD twin. It is the honour of my life to be constantly confused for you. I'm so proud of how far we've come over the past 4 years, and excited for what's next. Girls. Get it. Done.

It is a truth universally acknowledged that a first-year PhD student in possession of a 9am meeting, must be in want of caffeine. Hannah, I'm so glad you were the person to provide that caffeine to me, and that the magical power of Elle Woods ignited our friendship. I am proud to be one of your cloud friends.

To the ICAS fourth years and Beechwood View crew, there is no way I'd be handing this in without all of you. Thanks for making PhD life more fun. To the regulars of atmosphere and Filthy Fenton Fridays, I'm so grateful for the community you provided, both during the weird goat cult we accidentally created during lockdown, and when making new connections and seeing old faces once we allowed back in the pub over the last year.

Thank you to everyone from my research group and office 11.121, from the postdocs and other students who made me feel welcome when I arrived, to the new faces who arrived after me. You were a constant source of technical help, science ideas, motivational pep talks, poster templates, and so much more.

Abstract

Warming in the Arctic region is significantly faster than the global average rate, and drives further climate changes. Clouds play a major role in the energy budget of the Arctic and are a key uncertainty in projections of Arctic climate change. The behaviour of aerosol particles and their interactions with clouds is particularly uncertain. Measurements of Arctic clouds have revealed a high sensitivity to perturbations in aerosol concentrations, but climate models show large differences in projections of the Arctic aerosol budget depending on parameterisations used for key processes, such as sea spray aerosol emissions, new particle formation, and wet removal. In this thesis, we use novel measurements of aerosol size distributions from the Arctic Ocean to evaluate Arctic aerosol and cloud processes in regional and global models. We examine primary marine organic carbon, biomass burning, wet removal and new particle formation. Our results show that there is a seasonal transition at the end of summer in the high Arctic from a free-tropospheric source of particles to a boundary layer source of particles. The transition is driven by declining photochemical rates at the end of summer, and coincides with the onset of iodine acid emissions which drive new particle formation in the high Arctic boundary layer during the sea ice freeze period. We show that simulating this transition improves model-observation agreement in the concentration of particles smaller than 100 nm diameter, something that could not be achieved by modifying the primary carbon emissions or wet removal in the model. However, we also reveal biases in the simulation of Arctic clouds in the regional model. Our results show that aerosol processes cannot be considered in isolation, but rather that to model the impact of the changing Arctic aerosol budget on the regional climate system, accurate simulations of cloud behaviour are required.

Contents

List of Figures	xiii
1 Introduction	1
1.1 Arctic clouds in observations and models	1
1.2 Arctic aerosol processes	2
1.2.1 Aerosol-cloud interactions	3
1.2.2 Seasonal cycle	5
1.2.3 Sensitivity to climate change	6
1.3 Model predictions of the future Arctic aerosol budget	9
1.4 Research questions	11
2 The role of scavenging and primary emissions in the Arctic aerosol seasonal cycle in UKESM	13
2.1 Introduction	14
2.2 Methods	15
2.2.1 Model	15
2.2.2 Observations	17
2.3 High Arctic summer size distribution	20
2.4 Emissions	23
2.4.1 Biomass burning	24
2.4.2 Primary marine organic carbon	25
2.4.3 Effect of biomass burning and primary marine organics on summer size distribution	27
2.5 Wet scavenging	30
2.5.1 Cloud phase	30
2.5.2 Model parameters	35
2.5.3 Effect of wet scavenging on summer size distribution	37
2.6 Discussion and conclusion	40
3 Late summer transition from a free-tropospheric to boundary layer source of Aitken mode aerosol in the high Arctic	45

3.1	Introduction	46
3.2	Observations	49
3.3	Model description	49
3.3.1	Ageing of insoluble particles	49
3.3.2	New particle formation schemes	50
3.3.3	Iodic acid	51
3.3.4	Secondary organic vapours	53
3.4	Results	54
3.4.1	Iodic acid concentration	54
3.4.2	Effect of NPF in the boundary layer	55
3.4.3	Effect of free-tropospheric NPF	60
3.4.4	Combining local and non-local NPF	65
3.5	Discussion and conclusion	65
4	Activation of Aitken mode aerosols into cloud droplets during the high Arctic summer in a high-resolution nested model	71
4.1	Introduction	72
4.2	Model description	74
4.2.1	Regional model configuration	74
4.2.2	Cloud scheme	76
4.2.3	Aerosol activation scheme	76
4.3	Observations	78
4.3.1	Cloudnet	78
4.3.2	Surface radiation	78
4.3.3	Vertical wind velocity	79
4.4	Clouds	79
4.5	Vertical wind velocity	83
4.6	Aerosols	87
4.6.1	Aerosol time series and activated fractions	87
4.6.2	Sensitivity of aerosol activation to accumulation mode concentration and updraft velocity	91
4.7	Discussion and conclusions	93
5	Conclusions	95
5.1	Summary of findings	95
5.2	Future work	98
	Bibliography	101
A	Appendix	117
A.1	Particle ageing	117

A.2	Latitude limit for prescribed FT NPF rate	117
A.3	Aerosol precursor vapours and growth rate	118

List of Figures

2.1	Map showing locations of ground stations from which we use measurements of aerosol mass.	19
2.2	Times series and PDFs of aerosol concentration at the surface during AO2018 from observations and model output. Model output is from simulation BASELINE. Observations are shown as 3-hourly mean (black lines) and standard deviation (grey shading). Aerosol concentrations are shown for particles with diameter (a-c) 2.5-15 nm, (d-f) 15-100 nm and (g-i) 100-500 nm. Red dashed lines in (a, d, g) show observed NPF events. PDFs are separated by observed sea ice freeze-up date, 27th August 2018 (day 239).	21
2.3	Aerosol vertical profiles from model output and ASCOS campaign observations from 2008. Model output is from colocated 2018 monthly mean concentrations from simulation BASELINE. Observed concentrations are given as the mean profile from each ASCOS flight (grey lines), overall mean (solid black) and overall median (dashed black). Profiles are for particles with size (a) 3-14 nm, measured during ASCOS using a UCPC and (b) 14-300 nm, measured using a CPC (particles greater than 14 nm) and a CLASP instrument (particles greater than 300 nm).	22
2.4	BC aerosol mass concentration at Alert, Utqiagvik, Tiksi and Ny-Ålesund from measurements and model output. Model output is shown for simulations BASELINE (purple lines) and BIOMASS (green lines) for the years 2017–2018. Monthly means are shown as solid lines, standard deviation in shading.	24
2.5	Map of modelled primary OC particle flux for ocean gridboxes. Output is taken from (left) BIOMASS and (right) PMOC August 2018 mean. The red line marks the monthly mean extent of 90% gridbox sea ice fraction. Area averages for the regions in the white boxes are quoted in the text.	26

2.6	Times series and PDFs of aerosol concentration at the surface during AO2018 from observations and simulation PMOC. Observations are shown as 3-hourly mean (black lines) and standard deviation (grey shading). Aerosol concentrations are shown for particles with diameter (a-c) 2.5-15 nm, (d-f) 15-100 nm and (g-i) 100-500 nm. Red dashed lines in (a, d, g) show observed NPF events. PDFs are separated by observed sea ice freeze-up date, 27th August 2018 (day 239).	28
2.7	Aerosol vertical profiles from model output and ASCOS campaign observations from 2008. Model output is from colocated 2018 monthly mean concentrations from simulations BIOMASS and PMOC. Observed concentrations are given as the mean profile from each ASCOS flight (grey lines), overall mean (solid black) and overall median (dashed black). Profiles are for particles with size (a) 3-14 nm, measured during ASCOS using a UCPC and (b) 14-300 nm, measured using a CPC (particles greater than 14 nm) and a CLASP instrument (particles greater than 300 nm).	29
2.8	BC aerosol mass concentration at Alert, Utqiagvik, Tiksi and Ny-Ålesund from measurements and model output. Model output is shown for simulations BIOMASS (green lines) and ICE_THRESH (pink lines) for the years 2017–2018. Monthly means are shown as solid lines, standard deviation in shading.	31
2.9	Sulphate aerosol mass concentration at Ny-Ålesund and Villum Research Station from measurements and model output. Model output is shown for simulations BIOMASS (green lines) and ICE_THRESH (pink lines) for the years 2017–2018. Monthly means are shown as solid lines, standard deviation in shading.	31
2.10	Maps showing the seasonal mean of f_{ICE} for DJF 2018 at the surface and 2 km altitude from simulation ICE_THRESH. Red contours mark regions where $f_{ICE} > 10\%$	32
2.11	Maps showing the seasonal mean of f_{ICE} for JJA 2018 at the surface and 2 km altitude from simulation ICE_THRESH. Red contours mark regions where $f_{ICE} > 10\%$	33
2.12	Maps showing fraction of each model grid column where (a) clouds are present ($TWC > 0$), (b) clouds are present at $T < -15^\circ\text{C}$, (c), liquid clouds are present ($LWC > 0$) and (d) clouds with $f_{ICE} < 10\%$ are present ($IWC/TWC < 0.1$). Fractions are calculated using 2018 annual mean values of LWC, IWC and temperature from simulation ICE_THRESH. .	34

- 2.13 BC aerosol mass concentration at Alert, Utqiagvik, Tiksi and Ny-Ålesund from measurements and model output. Model output is shown for simulations BIOMASS (green lines), RSCAV_2 (brown lines), RSCAV_0.5 (yellow lines) and IMP_SCAV_OFF (blue lines) for the years 2017–2018. Monthly means are shown as solid lines, standard deviation in shading. 35
- 2.14 Sulphate aerosol mass concentration at Villum Research Station and Ny-Ålesund from measurements and model output. Model output is shown for simulations BIOMASS (green lines), RSCAV_2 (brown lines), RSCAV_0.5 (yellow lines) and IMP_SCAV_OFF (blue lines) for the years 2017–2018. Monthly means are shown as solid lines, standard deviation in shading. 36
- 2.15 Times series and PDFs of aerosol concentration at the surface during AO2018 from observations and model output. Model output is from simulations BIOMASS, ICE_THRESH, RSCAV_2, RSCAV_0.5 and IMP_SCAV_OFF. Observations are shown as 3-hourly mean (black lines) and standard deviation (grey shading). Aerosol concentrations are shown for particles with diameter (a-c) 2.5-15 nm, (d-f) 15-100 nm and (g-i) 100-500 nm. Red dashed lines in (a, d, g) show observed NPF events. PDFs are separated by observed sea ice freeze-up date, 27th August 2018 (day 239). 38
- 2.16 Aerosol vertical profiles from model output and ASCOS campaign observations from 2008. Model output is from colocated 2018 monthly mean concentrations from simulations ICE_THRESH, RSCAV_2, RSCAV_0.5 and IMP_SCAV_OFF. Observed concentrations are given as the mean profile from each ASCOS flight (grey lines), overall mean (solid black) and overall median (dashed black). Profiles are for particles with size (a) 3-14 nm, measured during ASCOS using a UCPC and (b) 14-300 nm, measured using a CPC (particles greater than 14 nm) and a CLASP instrument (particles greater than 300 nm). 39
- 3.1 Times series and PDF of surface iodic acid concentration during AO2018 from observations and model output. Model output is from simulation IA_BL (orange lines). Observations are shown as 3-hourly mean (black lines). Red dashed lines in (a) show periods of observed NPF events. PDF of concentration is for freeze season only, i.e. after 27th August 2018 (day 239). 55

- 3.2 Times series and PDFs of surface aerosol concentration during AO2018 from observations and model simulations with various boundary layer NPF mechanisms. Model output is from simulations CONTROL (pink lines), K06.BL (grey lines), M10.BL (blue lines), IA.BL (thick orange lines) and IA.BL.SecOrg (thin orange lines). Observations are shown as 3-hourly mean (black lines) and standard deviation (grey shading). Aerosol concentrations are shown for particles with diameter (a-c) 2.5-15 nm, (d-f) 15-100 nm and (g-i) 100-500 nm. Red dashed lines in (a, d, g) show observed NPF events. PDFs are separated by observed sea ice freeze-up date, 27th August 2018 (day 239). 56
- 3.3 Nucleation mode aerosol profiles simulated for AO2018 campaign period. Model output is from simulations (a) CONTROL, (b) M10.BL and (c) M10.BL.85N. Model output was colocated with the position of the *Oden*. White lines show BL height. 59
- 3.4 Aerosol vertical profiles from model output and ASCOS campaign observations from 2008. Model output is from colocated 2018 monthly mean values from simulations CONTROL (pink), M10.ALL (thick orange lines), M10.ALL.SecOrg (thin orange lines) and M10.Prsc (dark green). Observed values are given as the mean profile from each ASCOS flight (grey lines), overall mean (solid black) and overall median (dashed black). Profiles are for particles with size (a) 3-14 nm, measured during ASCOS using a UCPC and (b) 14-300 nm, measured using a CPC (particles greater than 14 nm) and a CLASP instrument (particles greater than 300 nm). 61
- 3.5 Aerosol vertical profiles from model output and ATom campaign observations from 2016. Model output is from colocated 2018 monthly mean values from simulations CONTROL (pink), M10.ALL (thick orange lines), M10.ALL.SecOrg (thin orange lines) and M10.Prsc (dark green). ATom observations are taken from leg 1 of the campaign and restricted to measurements that were taken north of 60°N. Observations correspond to mean profiles from different days (grey lines), the overall mean (black solid lines) and overall median (black dashed lines). Profiles are for particles with size (a) 5–10 nm, (b) 10–100 nm and (c) 100–500 nm. Observations were recorded at standard temperature and pressure, model output has been adjusted to account for this. 61

- 3.6 Time series and PDFs of aerosol concentration at the surface during AO2018 from observations and model output. Model output is from simulations M10_ALL (orange lines), M10_Prsc (thick green lines), M10_Prsc_SecOrg (thin green lines) and IA_BL_M10_ALL (red lines) Other than IA_BL_M10_ALL and the observations, lines have been made slightly transparent on this figure so that it is easier to view the results from IA_BL_M10_ALL. Observations are shown as 3-hourly mean (black lines) and standard deviation (grey shading). Aerosol concentrations are shown for particles with diameter (a–c) 2.5–15 nm, (d–f) 15–100 nm and (g–i) 100–500 nm. Red dashed lines in (a, d, g) show observed NPF events. PDFs are separated by observed sea ice freeze-up date, 27th August 2018 (day 239). 63
- 3.7 Schematic of processes controlling the concentration of nucleation mode particles at the surface in the high Arctic. The summer sea ice melt period is on the left and the freeze-up period in late summer/early autumn is on the right. A cartoon of the nucleation mode particle concentration is shown at the bottom. 67
- 4.1 Time series and PDFs of measured and simulated (a, b) surface SW radiation, (b, c) surface LW radiation and (d, e) total surface radiation (sum of SW and LW). All values are defined as positive in the downwards direction. Measured values (black lines) are given once a minute. Model output is for simulations CONTROL (pink lines) and IA_BL_M10_ALL (blue lines). Model output is output once an hour and has been colocated with the ship. Dashed lines on the PDFs mark the median of each distribution. 80
- 4.2 Mean cloud fraction from model output and observations over the period 17th August - 13th September 2018. Observations are shown in black. Model output is from CONTROL (pink) and IA_BL_M10_ALL (blue) and was colocated with the ship before taking the average. Cloud fraction is calculated using a mask based on TWC as described in the text. 82
- 4.3 Average profiles of (a) LWC and (b) IWC from observations (black) and model output. Mean profiles are shown as solid lines, median profiles are shown as dashed lines. Model output is from simulation CONTROL (pink) and IA_BL_M10_ALL (blue). Averages are taken over non-zero values of LWC and IWC (i.e. values where cloud is present). 83

- 4.4 Time series and PDFs of vertical wind velocity measured at cloud base by the cloud lidar during AO2018. Measurements are for 03:00–06:00 and 08:00–11:00 UTC on 13th September 2018 and represent a single layer of low level cloud (black lines) and a low level cloud with another cloud layer aloft (grey lines). 84
- 4.5 PDFs of vertical wind velocity from simulations CONTROL (pink line) and IA_BL_M10_ALL (blue line) and observations (grey and black lines). Model PDFs are shown for in-cloud gridboxes (solid lines) and cloud base gridboxes (dashed lines). Inset shows detail of model PDFs. 85
- 4.6 Time series of $\sigma_{w,sgs}$, the sub-grid scale component of vertical wind velocity in each gridbox along the AO2018 route, diagnosed from output from simulation IA_BL_M10_ALL. 85
- 4.7 Relative frequency distributions of w_{act} for (a) the default values using $\sigma_{w,sgs}$ derived from BL TKE and (b) double the default values. Distributions are shown for in-cloud output from CONTROL (pink bars) and IA_BL_M10_ALL (blue bars). The frequency distributions of vertical wind velocity are also shown for the measurements for the single cloud layer (black bars) and the multi-layer cloud (grey bars). 86
- 4.8 Times series and PDFs of aerosol concentration at the surface during AO2018 from observations and model output. Model output is from simulations CONTROL (solid pink lines) and IA_BL_M10_ALL (solid blue lines). UKESM output is also shown, lines have been made slightly transparent for ease of viewing UKCA-CASIM output. Observations are shown as 3-hourly mean (black lines) and standard deviation (grey shading). Aerosol concentrations are shown for particles with diameter (a-c) 2.5-15 nm, (d-f) 15-100 nm and (g-i) 100-500 nm. Red dashed lines in (a, d, g) show observed NPF events. PDFs are separated by observed sea ice freeze-up date, 27th August 2018 (day 239). 88
- 4.9 Profiles of (a) accumulation mode total concentration, (b) accumulation mode activated concentration and (c) fraction of activated accumulation mode particles from ARG2000-offline output, run using model output from IA_BL_M10_ALL. 89
- 4.10 Profiles of (a) Aitken mode total concentration, (b) Aitken mode activated concentration and (c) fraction of activated Aitken mode particles from ARG2000-offline output, run using model output from IA_BL_M10_ALL. 90

- 4.11 Time series of the total number concentration of activated particles at the surface (blue line) as predicted by ARG2000-offline, using model output from IA_BL_M10_ALL, with the fraction of activated particles coming from the accumulation mode (black line) and Aitken mode (grey line). The predicted number concentration of activated particles excluding those from the Aitken mode is also shown (blue dashed line). 91
- 4.12 Time series of the total number concentration of activated particles at the surface (blue line) as predicted by ARG2000-offline, using model output from IA_BL_M10_ALL with the number concentration of the accumulation mode reduced by a factor of 100 and the width of the updraft PDF increased by a factor of 2. The fraction of activated particles are shown for particles from the accumulation mode (black line) and Aitken mode (grey line). The predicted number concentration of activated particles excluding those from the Aitken mode is also shown (blue dashed line). 93
- A.1 Time series and PDFs of surface aerosol concentration during AO2018 from observations and model output. Model output is from simulations BIOMASS (green lines), CONTROL (pink lines), K06_BL_DEFAULT (thin grey lines), K06_BL (thick grey lines), M10_BL_DEFAULT (thin blue lines) and M10_BL (thick blue lines). Observations are shown as 3-hourly mean (black lines) and standard deviation (grey shading). Aerosol concentrations are shown for particles with diameter (a–c) 2.5–15 nm, (d–f) 15–100 nm and (g–i) 100–500 nm. Red dashed lines in (a, d, g) show observed NPF events. PDFs are separated by observed sea ice freeze-up date, 27th August 2018 (day 239). 118
- A.2 Aerosol vertical profiles from model output and ASCOS campaign observations. Model output is from colocated monthly mean values from simulations M10_Prsc (thick dark green) and M10_Prsc_60N (thin dark green). Observed values are given as the mean profile from each ASCOS flight (grey lines), overall mean (solid black) and overall median (dashed black). Profiles are for particles with size (a) 3–14 nm, measured during ASCOS using a UCPC and (b) 14–300 nm, measured using a CPC (particles greater than 14 nm) and a CLASP instrument (particles greater than 300 nm). 119

A.3	Aerosol vertical profiles from model output and ATom campaign observations. Model output is from colocated monthly mean values from simulations M10_Prsc (thick dark green) and M10_Prsc_60N (thin dark green). ATom observations are taken from leg 1 of the campaign and restricted to measurements that were taken north of 60°N. Observations correspond to mean profiles from different days (grey lines), the overall mean (black solid lines) and overall median (black dashed lines). Profiles are for particles with size (a) 5–10 nm, (b) 10–100 nm and (c) 100–500 nm. Observations were recorded at standard temperature and pressure, model output has been adjusted to account for this.	119
A.4	Zonal means and maps of simulated monthly mean H ₂ SO ₄ concentration from simulation CONTROL. Maps are taken from model level (c–d) at surface and (e–f) with altitude 2 km.	121
A.5	Zonal means and maps of simulated monthly mean secondary organic vapour concentration from simulation CONTROL. Maps are taken from model level (c–d) sat surface and (e–f) with altitude 2 km.	122
A.6	Zonal means and maps of aerosol growth rates from simulation CONTROL. Growth rates are calculated offline using model output of temperature and concentrations of H ₂ SO ₄ and secondary organic vapour. Maps are taken from model level (c–d) at surface and (e–f) with altitude 2 km.	123

Nomenclature

AO2018 Arctic Ocean 2018

ASCOS Arctic Summer Cloud Ocean Study

ATom Atmospheric Tomography Mission

CASIM Cloud AeroSol Interacting Microphysics

CCN Cloud condensation nuclei

CDNC Cloud droplet number concentration

H₂SO₄ Sulphuric acid

HIO₃ Iodic acid

INP Ice nucleating particle

IWC Ice water content

LW Longwave

LWC Liquid water content

MIZ Marginal ice zone

MOCCHA Microbiology-Ocean-Cloud Coupling in the High Arctic

NPF New particle formation

SW Shortwave

TWC Total water content

UKCA UK Cloud and Aerosol

UKESM UK Earth System Model

Chapter 1

Introduction

1.1 Arctic clouds in observations and models

In the present day, clouds have a net cooling effect on the Earth's surface. Their global cooling effect from reflecting incoming solar radiation is only partially offset by their absorption and re-emission of longwave radiation back to the surface. However, in the Arctic, clouds have a net warming effect on the surface for most of the year (Curry et al., 1992; Curry et al., 1993; Wang et al., 2005; Kay et al., 2016). This regional difference results from the high albedo of the Arctic surface (from ice and snow) and the lack of incoming solar radiation during polar night, making the shortwave (SW) cooling from the clouds relatively less important than the longwave (LW) warming. Clouds are common in the Arctic, with average cloud fractions almost always over 50%, higher over the Arctic Ocean and in summer (Intrieri et al., 2002; Wang et al., 2005; Shupe et al., 2011). Mixed-phase clouds are common in the Arctic and can persist for timescales on the order of days, despite the typically unstable relationship in clouds between ice formation and liquid water (Shupe, 2011). Low-level clouds have a greater effect on the surface energy budget than clouds at higher altitudes and are also the most frequently occurring. Frequent cloud occurrence and the net warming effects of the clouds result in a strong coupling between Arctic clouds and sea ice. Thermodynamic model results and observations both suggest that cloudiness can be a controlling factor in the onset of the annual sea ice melt season (Curry et al., 1993; Sedlar et al., 2011).

Because of the key role that clouds play in controlling the Arctic energy budget, there is a high sensitivity to changes in cloud cover or cloud microphysical properties (Garrett and Zhao, 2006). Moreover, model uncertainties in Arctic clouds create uncertainties in predictions of Arctic climate change. Using satellite observations of albedo for the Arctic region, Pistone et al. (2019) found that the global heating resulting from total ice loss from the Arctic Ocean varies by a factor of 6 between completely overcast or completely cloud-free conditions. Although climate models are robust in their

predictions of increased surface temperatures and continued sea ice loss, the speed and magnitude of these changes is the subject of considerable inter-model spread (Pithan and Mauritsen, 2014; Notz and SIMIP Community, 2020; Cai et al., 2021) and does not always agree with the observational record, e.g. for the speed and magnitude of sea ice loss since the beginning of this century (Shu et al., 2020) or for the rate of warming in the Arctic relative to the global mean, known as Arctic amplification (Rosenblum and Eisenman, 2017; Rantanen et al., 2022). Hodson et al. (2013) attribute a large proportion of the uncertainty in projections of Arctic climate change to differences in the ways that different models parameterise the same processes. Clouds constitute a major source of model uncertainty, due to the complexity of processes that govern their behaviour, the wide spread of length and time scales involved, and the large sub-grid scale variability in thermodynamical fields necessitating empirical parameterisations. This difficulty in simulating clouds and the uncertainty that results is widely acknowledged as a challenge for global models, but is particularly acute for the Arctic region (Vihma et al., 2014). Biases were seen in the cloud radiative effects of CMIP5 models for the Arctic region (Boeke and Taylor, 2016). The model biases were linked to errors in the annual cycle of Arctic cloud fraction and in the surface albedo (i.e. the interactions between clouds and sea ice).

In the rest of this chapter we will explain how aerosols can influence clouds in the Arctic, introduce the processes that control the seasonal cycle of aerosol in the Arctic, and how such processes will be affected by climate change. We will review results from previous modelling studies that have examined how the changing Arctic aerosol budget affects the energy budget of the region. We will then lay out the research questions that motivate this thesis.

1.2 Arctic aerosol processes

Aerosol particles in the atmosphere interact with clouds by acting as cloud condensation nuclei (CCN) or ice-nucleating particles (INP) on which liquid drops and ice crystals form. Cloud model behaviour therefore depends on the parameterisations of aerosols in the model, from microphysical and chemical processes on molecular scales to transport of particles over synoptic distances. Aerosols affect the global energy balance directly via aerosol-radiation interactions and indirectly via aerosol-cloud interactions. Two of the most commonly studied aerosol-cloud interactions are the albedo effect and the lifetime effect. The Twomey effect (also referred to as the albedo or first indirect effect) is when an increase in the number of CCN in a cloud of given liquid water content raises the albedo of the cloud, because the higher CCN leads to a higher number of smaller cloud droplets (Twomey, 1977). The lifetime effect (also referred to as the second indirect effect) happens as a consequence of the lower efficiency of rain drop formation from the smaller cloud droplets at high CCN concentrations, leading to a suppression of pre-

precipitation and therefore the possibility of a longer cloud lifetime relative to a low CCN case (Albrecht, 1989). There are many other aerosol-cloud interaction mechanisms, for example related to entrainment, sedimentation, or glaciation. In this section we will discuss the sources and sinks of aerosol in the Arctic, and processes which govern their impacts on Arctic clouds.

1.2.1 Aerosol-cloud interactions

Aerosol and CCN concentrations in the Arctic are often much lower than other regions in the globe which makes Arctic clouds particularly sensitive to aerosol perturbations. Garrett et al. (2002) used in-cloud measurements from the SHEBA campaign and a simple radiative transfer model to demonstrate an increase in downwelling LW radiation from a cloud following an increase in background aerosol concentration, cloud droplet number, and liquid water path. They therefore proposed a mechanism where an increase in aerosols can increase the emissivity of a liquid cloud, creating a warming effect at the surface. This mechanism is opposite to the albedo effect, where more aerosols create smaller cloud drops and therefore cool the surface by increasing reflectivity. Garrett et al. (2002) proposed that the LW emissivity effect is particularly relevant to the Arctic since cloud drop numbers can be very low ($\sim 5 \text{ cm}^{-3}$) and the LW effects of Arctic clouds dominate over the SW effects. Later studies measured the LW warming effect from increased aerosol concentrations using larger datasets of cloud properties from a ground station in Alaska (Garrett and Zhao, 2006; Lubin and Vogelmann, 2006). Mauritsen et al. (2011) also investigated the possibility of a warming effect of Arctic clouds caused by increased aerosol concentrations. Using measurements from the ASCOS campaign in the central Arctic Ocean and a radiative transfer model, they investigate a case study of a “tenuous” cloud regime, where low aerosol concentrations are found to limit cloud liquid water. Adding aerosols to the cloud therefore results in higher emissivity and an associated warming effect. The results from Mauritsen et al. (2011) also identify a threshold (10 cm^{-3}) for the initial CCN concentration below which more aerosols lead to warming due to LW effects and above which the cooling from SW dominates. They analysed measurements from other Arctic campaigns to conclude that the tenuous cloud regime ($\text{CCN} < 10 \text{ cm}^{-3}$) is not limited to the single case study they present. Birch et al. (2012) report that the tenuous regime occurs 10–30% of the time. Several modelling studies have focussed on the tenuous case study from ASCOS (Birch et al., 2012; Loewe et al., 2017; Stevens et al., 2018). The studies concluded that the use of fixed aerosol concentrations inhibits the ability of models to capture the tenuous cloud regime and the dissipation of clouds due to low aerosol concentrations. For example, Birch et al. (2012) found that the modelled cloud did not dissipate as observed using a prescribed CCN concentration of 100 cm^{-3} , but that a concentration of 1 cm^{-3} led to improved model performance. The studies carry an implication that fixed aerosol, CCN, or cloud drop number concentrations in models

are not sufficient to capture the unique behaviour and radiative effects of Arctic clouds.

The frequent occurrence of mixed-phase Arctic clouds makes simulations of cloud radiative effects in the Arctic particularly sensitive to the treatment of ice formation. Concentrations of INPs measured in the Arctic are generally lower than those measured in mid-latitudes (Bigg et al., 1996; Wex et al., 2019). Wex et al. (2019) report that concentrations appear to be higher in the spring and summer and lower in the winter, possibly linked to the exposure of terrestrial sources during the snow melt season. They show that data from Arctic ground stations combined with back trajectory analyses indicate sources close to land are stronger than those from pack ice regions. Marine sources from open water could include polymer gels and other biogenic material from the sea surface microlayer, as well as wind-driven sea spray (Bigg et al., 1996; Wex et al., 2019). Recent measurements from a ship campaign close to the North Pole indicated very variable INP concentrations at the highest latitudes (Porter et al., 2022). Sporadic periods of high ice nucleating activity were linked to biological sources from open water near the coast of Russia. Dust is also a key source of INPs, with a growing focus on high-latitude sources from glacial and river outflows (Tobo et al., 2019; Sanchez-Marroquin et al., 2020; Meinander et al., 2022).

INP concentrations affect cloud phase partitioning. Model studies have shown an increase in ice water content and decrease in liquid water content with increasing INPs, tending towards cloud glaciation at some critical threshold of prescribed INP or ice crystal concentration (Morrison et al., 2011; Ovchinnikov et al., 2014; Loewe et al., 2017; Young et al., 2017; Stevens et al., 2018). However, models rarely agree on the threshold at which cloud glaciation occurs, likely as result of different approaches to the parameterisation of ice formation. Prenni et al. (2007) conducted a multi-model assessment of cloud behaviour using measurements from the M-PACE experiment. The results showed that the model parameterisations simulated INP concentrations that were too high, and/or were not depleted strongly enough by ice formation. The model bias in INP concentration caused underestimations in cloud liquid water path, and associated errors in the cloud radiative effects. In addition to the link between INP concentrations and glaciation, perturbations to INPs or ice crystals can also affect liquid precipitation formation (Young et al., 2017) or sedimentation and growth rates of ice crystals (Ovchinnikov et al., 2014).

Observations have shown that CCN perturbations can also impact cloud phase. Changes to the liquid drop size distribution brought on by changing CCN concentrations can suppress ice mass growth in clouds (Lance et al., 2011; Norgren et al., 2018). However, polluted conditions have also been linked to more efficient freezing in observations of Arctic clouds (Coopman et al., 2018), and increased CCN concentrations have been shown to promote ice formation in a model via an increase in cloud-top radiative cooling (Possner et al., 2017).

1.2.2 Seasonal cycle

In the Arctic, aerosol properties are controlled by a seasonal cycle in emissions, transport and removal, resulting in a distinct seasonal cycle in Arctic aerosol mass and number concentration. In a phenomenon known as Arctic haze, aerosol mass is lowest in summer and autumn, higher in the winter months and peaks in springtime (Shaw, 1995; Ström et al., 2003; Engvall et al., 2008a; Tunved et al., 2013; Schmale et al., 2022). This peak in mass is linked to a stronger anthropogenic influence on Arctic aerosol during winter months, as shown by trajectory analysis (Eneroth et al., 2003; Stohl, 2006) and aerosol composition measurements (Ström et al., 2003; Sharma et al., 2019). Transport from lower latitudes to the Arctic is more efficient in winter because the polar dome extends further south, making it thermodynamically easier for air masses to enter the Arctic region (Shaw, 1995). Additionally, wet removal of aerosols during transport is less efficient in winter because of the cold and relatively dry air (Garrett et al., 2010; Garrett et al., 2011). This combination of efficient transport and inefficient removal is what drives the anthropogenic influence on the Arctic aerosol during winter.

Following the Arctic haze peak in spring, there is a transitional period of decreasing aerosol mass and increasing aerosol number, after which the summer season (June–August) is dominated by a high number of smaller (Aitken mode) particles (Ström et al., 2003; Engvall et al., 2008a; Tunved et al., 2013; Schmale et al., 2022). This has primarily been observed at the surface, but measurements above the surface indicate that the transition occurs aloft as well (Engvall et al., 2008b). The lower concentration of large particles and the onset of photochemistry at polar sunrise promote new particle formation and growth during Arctic spring and summer. In the Arctic marine boundary layer, phytoplankton blooms are a source of sulphuric acid (H_2SO_4 , from dimethylsulphide, DMS) and methanesulfonic acid (MSA), two main drivers of new particle formation events (Chang et al., 2011; Willis et al., 2017; Beck et al., 2020). Marine organic vapours can also contribute to particle formation and subsequent growth (Willis et al., 2016; Beck et al., 2020). Other precursor vapours are ammonia, for example from seabird colonies (Croft et al., 2016a), and iodic acid, from both coastal kelp sources (Allan et al., 2015; Sipilä et al., 2016) and from snow, ice or water sources in the central Arctic Ocean, where it has been observed to be the main driver of new particle formation events (Baccarini et al., 2020).

The distinct Arctic seasonal regimes have been the subject of multiple modelling studies. Browse et al. (2012) and Korhonen et al. (2008b) used the global aerosol transport model GLOMAP to study Arctic aerosol processes at different times of year. Browse et al. (2012) used monthly mean aerosol mass concentration measurements from Arctic ground stations to study the seasonal aerosol cycle, while Korhonen et al. (2008b) focussed on the spring–summer transition and instead used size-resolved mea-

measurements of aerosol number concentration. Another study, Croft et al. (2016b) also used size-resolved measurements to evaluate GEOS-Chem-TOMAS, a different aerosol transport model. These three studies found model-observation biases that required adjustments to model processes to capture the features of the Arctic aerosol cycle. Wet scavenging was examined in all three studies. Global parameterisations of wet scavenging proved to be insufficient for the specific conditions of the Arctic. For example, Korhonen et al. (2008b) found that doubling the fixed activation diameter of aerosols being removed by precipitation led to more accurate springtime aerosol size distributions, but worse distributions in summer. The authors concluded that a fixed diameter for all seasons and locations was probably inadequate. Croft et al. (2016b) found that fixed cloud water contents, that were unrepresentative of Arctic clouds, led to too-weak scavenging in GEOS-Chem-TOMAS. Browse et al. (2012) added a drizzle rate from low-level clouds and a temperature dependence of scavenging efficiency to represent less efficient scavenging from ice and mixed-phase clouds. They found that both adjustments to the model were needed to improve the aerosol seasonal cycle in GLOMAP. Korhonen et al. (2008b) and Croft et al. (2016b), the two studies using size-resolved aerosol measurements, both concluded that increases in the concentration of the accumulation mode size range (roughly 100 nm diameter particles and above) will result in decreases in the concentration of smaller particles. The sink for condensable and nucleating vapours is dominated by the largest particles due to their larger surface area. The accumulation mode concentration is therefore a controlling factor of new particle formation and growth rates. This coupling between the larger and smaller aerosol particles makes modelling the Arctic aerosol size distribution complex, since the aerosol processes governing the seasonal cycle are finely balanced.

1.2.3 Sensitivity to climate change

The seasonal cycle of Arctic aerosol presents challenges, not just for simulating the present-day, but also the future, when aerosol processes will be subject to dramatic change along with other components of the Arctic climate. Sources from lower latitudes will change, and there may be changes to the large-scale dynamics that transport aerosol into the Arctic. Warmer temperatures will affect precipitation both in the Arctic region and along the transport routes that bring moisture and aerosols to the Arctic. Climate models predict both increased total precipitation and an increased fraction of precipitation falling as liquid relative to snow in the Arctic throughout the course of this century (Pan et al., 2020; McCrystall et al., 2021). Łupikasza and Cielecka-Nowak (2020) have reported trends of increasing probability of days with rainfall and decreasing probability of days with snowfall in Svalbard and the surrounding areas. The implications of such trends are complicated by the variations in season, location, and the spatial pattern of warming relative to current patterns in snowfall and freezing thresholds (Bintanja, 2018). Increased precipitation, or increased rainfall at the expense of

snowfall, could lead to a cleaner Arctic by increasing rates of wet removal. However, increases in the proportion of liquid precipitation relative to other phases is more pronounced in summer and autumn, when wet removal rates are already higher than in the winter, so changes could be minimal. The transport of aerosols into the Arctic will also be affected by changes in emissions at source, particularly from East Asia where anthropogenic sources of aerosols are expected to decrease over the next few decades (Samset et al., 2019; Ramachandran et al., 2022). Wildfires are a source of smoke and organic carbon to the Arctic and the frequency and severity of fires may increase with further warming. Biomass burning has already been seen to increase in North America (Turetsky et al., 2011; Veraverbeke et al., 2017; Walker et al., 2019). However, it is difficult to predict how more frequent, longer, or more intense fires translate to aerosol emissions, since assumptions must be made about the relationships between e.g. area burned and aerosol emissions (Carslaw et al., 2010). Finally, the large-scale circulation patterns in the northern hemisphere can change as temperature gradients between the high and mid-latitudes change (Overland and Wang, 2010). Such changes could alter the pathways for aerosol, heat and moisture transport into the Arctic (Heslin-Rees et al., 2020; Pernov et al., 2022), though there is little consensus on how the links between Arctic temperature changes and mid-latitude atmospheric systems manifest themselves (Cohen et al., 2020).

Aerosol sources within the Arctic will change under global warming as well as the transport of aerosol from lower latitudes. The observational record shows a clear link between rising global temperatures and loss of Arctic sea ice (Notz and Stroeve, 2018) and models consistently predict that this trend will continue, likely to the point of an ice-free Arctic Ocean during summer for the first time in the coming decades (Notz and SIMIP Community, 2020). The marginal ice zone (MIZ) will also continue to change, having been measured to increase in width during summer and decrease in width during winter over the period 1979–2011 (Strong and Rigor, 2013). The increased area of open water in summer will perturb gas, heat, moisture and particle fluxes between the atmosphere and the Arctic Ocean. Sea salt particle fluxes are predicted to increase with ice loss (Jones et al., 2007; Struthers et al., 2011) and this could create a surface cooling effect via cloud brightening - such a mechanism has even been studied as a possible global geoengineering technique (Korhonen et al., 2010). However, the overall radiative effect of increased sea salt particle fluxes is difficult to predict because of uncertainties in the present-day baseline sea salt source, both globally and from the Arctic Ocean. Global models typically use parameterisations of sea salt flux as a function of wind speed, sometimes including temperature or salinity dependencies as well (e.g. Monahan et al., 1986; Gong, 2003; Mårtensson et al., 2003; Zinke et al., 2022). Different parameterisations produce large differences in sea salt emissions, and even the same parameterisation can produce different results when used in different models because

of the high sensitivity to wind speeds (Tsigaridis et al., 2013). Interactions with clouds and other aerosol sources also lead to non-linear behaviour. These parameterisations are derived empirically from either idealised laboratory experiments or limited observational datasets without input of measurements from the Arctic region, thus they may not be able to produce accurate predictions of how perturbations to the Arctic Ocean will influence the particle size distributions that are generated from sea salt emissions. In particular, Nilsson et al. (2001a) measured particle fluxes from open leads in the Arctic pack ice that were lower than the fluxes from open water for a given wind speed, because of the smaller fetch associated with the limited areas of open water in the ice regions. Global models simply scale the particle flux with open water fraction, failing to take account of this effect.

Strongly linked to the emissions of sea salt particles are sources of primary marine organic matter. The sea surface microlayer contains organic material that can coat sea salt particles, or otherwise be emitted into the atmosphere by wave or bubble processes. This has been observed to occur in the Arctic (Leck and Bigg, 2010; Orellana et al., 2011; Karl et al., 2013). Like sea salt, this source of organic aerosol to the atmosphere may increase with retreating sea ice but is subject to uncertainty in global models. Parameterisations of the primary marine organic source typically define a fraction of the sea salt mass to be emitted as organic carbon to represent their co-emissions. This means that the uncertainties in the sea salt emissions (discussed above) also affect the organic sea spray component (Albert et al., 2012; Tsigaridis et al., 2013). The organic fraction of the sea spray is also not well constrained. Particularly for the Arctic, the physical mechanisms by which the marine organic material becomes atmospheric particles of CCN-relevant sizes are not well understood. Theories include the break-up of larger biological gel structures into nanogel particles, which can be triggered by exposure to UV radiation or cloud processing (Leck and Keith Bigg, 1999; Lawler et al., 2021). Such complex molecular interactions are not included in models. The sensitivity of emissions to the underlying biological activity is also difficult to model because of the complex relationships between changing ocean circulation, sea ice loss, and nutrient cycles, all of which are unlikely to be captured by models using a simple dependence on chlorophyll concentration (De Leeuw et al., 2011; Albert et al., 2012).

Finally, sea ice loss affects Arctic aerosol sources by increasing the emissions of marine precursor vapours that drive new particle formation and growth (Dall'Osto et al., 2017; Dall'Osto et al., 2018). However, like the primary marine emissions, the effect of increased marine gases from the Arctic Ocean is not straightforward to predict. New particle formation is a parameterised process in climate models since it is not feasible to simulate explicitly the molecular processes that govern the formation rates. The large number of potential species involved, and the seasonal and regional variations in the drivers of Arctic new particle formation, make such parameterisations uncertain, with

formation rates often tuned to limited sets of field or laboratory observations (Kulmala et al., 2006; Metzger et al., 2010; Dunne et al., 2016). There are also knowledge gaps, for example the role of iodic acid as discussed above. The specific formation mechanisms of iodic acid in the Arctic are relatively poorly understood and could be related to snow, ice, or water, obscuring the picture of how new particle formation precursors will respond to sea ice loss (Baccarini et al., 2020).

1.3 Model predictions of the future Arctic aerosol budget

Section 1.2.3 described the ways in which rising temperatures will affect the regional aerosol budget and the impacts and feedbacks resulting from such change. Several modelling studies have made predictions of future aerosol emissions, taking account of climate feedbacks and adjustments. Different model results reveal key uncertainties that stem from different parameterisations of the processes described in section 1.2.

The response of DMS emissions to sea ice loss is uncertain because of a strong dependence on future seawater DMS concentrations. Mahmood et al. (2019) used a global climate model to investigate the aerosol effects of ice loss under 4 different future scenarios of DMS concentration, based on different methods of parameterising DMS concentration in atmospheric models. The increase in Arctic mean DMS emissions between 2000–2050 varied by up to 20% depending on the method of prescribing future DMS seawater concentrations, though an increase in emissions is a robust feature across all parameterisations. The response of the aerosol budget to increased DMS emissions is also uncertain, because it is determined by a balance of condensation and new particle formation. Browse et al. (2014) used a global aerosol transport model to investigate the response of aerosols to Arctic sea ice loss. Emissions of sea salt, DMS, and primary organic carbon under present-day sea ice conditions and ice-free summer conditions were simulated. The effect on particle number concentration was examined for different particle sizes. When sea salt alone is allowed to increase, the concentration of small particles decreases (as inferred from the change in concentration of particles with diameter greater than 3 nm, N_3 , relative to the concentration of particles with diameter greater than 100 nm, N_{100}) because the larger sink of condensable vapours from the sea salt emissions suppressed new particle formation, a key source of small particles. However, when DMS emissions are allowed to increase, either on their own or concurrently with sea salt, the concentration of small particles increases because of stronger new particle formation. The change in concentration of larger particles (N_{100}) and CCN is spatially heterogeneous, however. Over the central Arctic Ocean where sea salt emissions increase, the increased DMS burden leads to more condensational growth of particles. As such, the aerosol size distribution shifts to larger sizes, where more particles are more easily removed by precipitation. The overall effect of this process is a decrease in N_{100} and CCN concentrations. In the continental Arctic, away

from sea salt emissions, the condensation sink is lower so the new particle formation response is stronger than the condensation response. N_{100} and CCN therefore increase in these regions. Perturbations to oxidant concentrations can also play a role in the overall aerosol response to increased DMS emissions. For example, an increase in cloud fraction or liquid water path in the future Arctic could increase the occurrence of in-cloud aqueous oxidation, resulting in a reduction in the amount of oxidants available to convert DMS to SO_2 in the process of forming H_2SO_4 . Browse et al. (2014) ran a sensitivity simulation using coupled chemistry (as opposed to fixed oxidant concentrations) and found no such limit from oxidants on the aerosol response to increased DMS. However, the clouds in their model were fixed so did not respond to the reduction in sea ice.

The net effect of concurrent increases in emissions of sea salt and DMS depend on the relative balance between new particle formation, condensational growth, and wet removal. Modelling studies do not agree on the balance of these processes, because of a large number of differences in parameterisations in different model set-ups. New particle formation parameterisations are diverse across models and the response to increased DMS emissions appears to depend strongly on what kind of parameterisation is used. Browse et al. (2014) used a binary H_2SO_4 - H_2O nucleation scheme (Vehkamäki et al., 2002) as well as an H_2SO_4 nucleation scheme using cluster activation. The temperature dependence in the binary scheme effectively limits new particle formation to the upper free troposphere, where temperatures are colder, whereas the cluster activation scheme leads to new particle formation in the Arctic boundary layer. Gilgen et al. (2018) used a global climate model to simulate Arctic aerosol under the ice conditions of the present day and of 2050. Their model also included a binary H_2SO_4 - H_2O scheme and a cluster activation scheme, but the cluster activation scheme was only applied in the forested boundary layer, due to the high concentrations of organic vapours there which can promote new particle formation. As such, new particle formation in the Arctic boundary layer in their model was likely to be much weaker than in Browse et al. (2014). Thus, their modelled response to increased DMS concentrations was much weaker than that seen in Browse et al. (2014). The influence of condensational growth is also uncertain due to differences in sea spray parameterisation, for both sea salt and primary marine organics, as discussed in section 1.2.3. For example, Struthers et al. (2011), using a global climate model to simulate the aerosol budget over an ice-free Arctic Ocean, used a sea spray parameterisation with a sea surface temperature dependence. Their results showed a sensitivity in the change in sea salt emissions to the sea surface temperature.

There is also uncertainty in the parameterisation of wet scavenging. Aerosol wet removal is typically parameterised as a function of precipitation rate and aerosol size, and the removal rates can be very sensitive to the parameters used, as shown for example

by Korhonen et al. (2008b) and discussed in section 1.2.2. Since total precipitation and the fraction of liquid precipitation are projected to increase in the Arctic, simulations of future aerosol budgets should take this into account. The aerosol transport model used by Browse et al. (2014) uses ECMWF reanalysis products to prescribe meteorology, so the cloud fields and precipitation rates do not change between the present-day and ice-free simulations. Thus, their prediction of the overall response of Arctic aerosol to sea ice loss was missing the coupling between increased precipitation rates and aerosol wet removal.

1.4 Research questions

This thesis aims to assess the simulation of Arctic aerosol and cloud processes in state-of-the-art atmospheric models. To evaluate model output, we make use of novel measurements made during summer 2018 in the central Arctic Ocean. We use measurements of size-resolved aerosol concentrations, vapour concentrations, cloud properties and surface fluxes. Size-resolved measurements of aerosol concentrations from the central Arctic Ocean have previously been sparse. The new dataset we use provides an uninterrupted time series of nearly two months in duration and is therefore a valuable tool to evaluate model behaviour.

We use two distinct modelling set-ups in this thesis. Firstly, we use the UK Earth System Model (UKESM) in atmosphere-only configuration. UKESM is a global model developed for the CMIP6 assessment and uses a two-moment aerosol microphysics scheme, capable of simulating aerosol size and mass, coupled to the model radiation scheme and the precipitation rates calculated by the cloud scheme. The model is therefore well-equipped to simulate the aerosol processes described in section 1.2, the interactions between aerosols of different sizes, and the influence of clouds on aerosol behaviour. Secondly, we use a high-resolution regional model configuration, using the same dynamical core and aerosol microphysics scheme as that in UKESM, and with the addition of two-moment cloud microphysics. The cloud microphysics has recently been coupled to the aerosol scheme in the model, allowing prognostic simulation of the cloud drop number concentration. As such, this high-resolution model does not rely on fixed aerosol, CCN, or cloud drop number concentration, so we can use it to examine the behaviour of Arctic cloud regimes which are very sensitive to aerosol concentrations, as discussed above.

Chapter 2 compares aerosol number and mass concentrations from atmosphere-only UKESM to novel Arctic Ocean measurements and to measurements from continental Arctic ground stations. The ground stations provide a multi-year dataset with which to evaluate the seasonal cycle of Arctic aerosol in the model. Our research questions for chapter 2 are as follows:

- Can the global climate model capture the Arctic aerosol seasonal cycle?
- How is the modelled seasonal cycle affected by the parameterisations of wet scavenging?
- What role do primary marine organic carbon emissions play in the summertime high Arctic aerosol budget?

In chapter 3, we use the same global model to investigate new particle formation in the high Arctic summer. In particular, following observations that iodic acid drives new particle events that have been observed towards the end of high Arctic summer, we implement an empirical scheme for iodic acid concentration in the model and use it to drive new particle formation in the Arctic boundary layer. We explore the following questions:

- What is the effect of iodic acid new particle formation on the modelled aerosol size distribution?
- How important for the aerosol budget and CCN concentrations is such a source compared to other new particle formation mechanisms?

Finally in chapter 4, having implemented sensitivity tests in chapter 3 that reveal ways to reduce the model bias in small particle concentrations, we use the high-resolution model configuration to examine the activation of Aitken mode particles into cloud droplets. We ask the following questions:

- Under what conditions do Aitken particles activate into cloud droplets in the high Arctic?
- Is the model capable of simulating such conditions?
- What are the implications of Aitken activation for modelling the Arctic aerosol budget?

Chapter 5 presents the overall conclusions from these three studies, and suggests pathways for future work.

Chapter 2

The role of scavenging and primary emissions in the Arctic aerosol seasonal cycle in UKESM

Abstract

The Arctic aerosol budget poses a challenge for global aerosol models because of a complex balance of source and sink processes affecting different sizes of aerosol. Previous modelling studies have highlighted wet removal of aerosols by precipitation as a key controlling factor in the aerosol seasonal cycle, while the aerosol budget in a warming Arctic will depend on the net effect of changes in primary marine emissions, condensation, new particle formation, and aerosol removal. Here, we use novel measurements from the high Arctic during summer to assess Arctic aerosol processes in a global climate model. We find that there is an underestimation in the number concentration of particles less than 100 nm in diameter. We examine primary marine organic carbon emissions and aerosol wet removal processes in the model as potential sources of the model bias. We also use aerosol mass concentration measurements from Arctic ground stations to evaluate the model. We find that the primary marine particle flux required to explain the aerosol size distribution in the high Arctic is a factor of 200 greater than the flux that has been observed from open leads in the Arctic pack ice, though our approach does not account for any particle break-up after emissions as has been proposed in the literature. The results also show that changes to the wet scavenging scheme create some improvements in the seasonal cycle of sulphate mass in the Arctic, but they cannot account for the model underestimation of sub-100 nm diameter particles in the high Arctic summer.

2.1 Introduction

As explained in section 1.2 of the previous chapter, the seasonal cycle of aerosol in the Arctic has proved challenging to simulate in global aerosol models (Korhonen et al., 2008b; Browse et al., 2012; Croft et al., 2016b). Wet scavenging is a particularly important process in the Arctic seasonal cycle, to some extent accounting for the difference in aerosol number and mass between the relatively polluted winter months and relatively cleaner summer and autumn. Wet scavenging rates in global models rely on parameterisations of precipitation and removal rates. Often, such parameterisations are designed using data from mid-latitudes and are unsuited to the different conditions of the Arctic. For example, drizzle from low clouds acts a sink of aerosol in the Arctic summer (Browse et al., 2012), but is relatively less important further south, where wet scavenging is dominated by precipitation from large convective or frontal systems.

The uncertainty resulting from parameterisations of aerosol removal rates is compounded by the fine balance of different processes in the Arctic seasonal cycle. In the summer when wet removal is relatively more efficient, the sink of aerosol is balanced by sources such as primary marine emissions, transport of wildfire emissions, and secondary processes triggered by the onset of photochemistry and emissions of marine precursor vapours. All of these sources are also subject to uncertainty, so biases in source terms and removal rates can offset each other or combine.

Recent observations of aerosol size distributions from the central Arctic Ocean provide a new opportunity for model evaluation (Baccarini et al., 2020). Furthermore, new modelling tools allow the coupling of aerosol transport and microphysics to clouds, allowing processes such as autoconversion to respond to simulated aerosol properties and for aerosols to be controlled by activation and removal by clouds and precipitation. The UK Earth System Model (UKESM) uses the GLOMAP aerosol transport model to simulate aerosol microphysics in fully-coupled Earth system simulations. Here, we use UKESM in its atmosphere-only configuration to simulate summertime Arctic aerosol size distributions. Model output is compared to the measurements presented in Baccarini et al. (2020) from the central Arctic Ocean during late summer and early autumn. In evaluating the ability of the model to simulate the Arctic aerosol budget, we use measurements from continental Arctic ground stations to evaluate the effect of model processes on the seasonal cycle, such as scavenging, carbon emissions and primary marine organics.

Section 2.2 introduces UKESM and the observations we use. Section 2.3 compares output from the baseline version of the model to the summertime size distribution measured by Baccarini et al. (2020). Section 2.4 looks at emissions of carbon in the model from biomass burning and primary marine organics. Section 2.5 shows the effect of changes to the scavenging routine on the simulated summer size distribution.

Conclusions are presented in section 2.6.

2.2 Methods

2.2.1 Model

We used the UK Earth System Model version 1 (UKESM1, Mulcahy et al., 2020; Sellar et al., 2019) in its atmosphere-only configuration, which uses output from a fully-coupled run of UKESM1 to prescribe sea surface temperatures (SSTs) and some biogenic emissions, such as DMS from the ocean. The dynamical core of the model is the UK Met Office Unified Model (UM) in global atmosphere configuration version 7.1 (GA7.1, Walters et al., 2019) with a horizontal resolution of 1.875° longitude by 1.25° latitude and 85 vertical levels. The vertical resolution is approximately 50 m at the surface, 150 m at 1 km altitude and on the order of kilometres at the highest model level. We ran the model in its nudged configuration, which means horizontal winds and potential temperature are relaxed to ERA-Interim values on a 6-hourly time scale above approximately 1 km altitude.

The model simulates gas and aerosol chemistry using the UK chemistry and aerosols model (UKCA, Morgenstern et al., 2009; O’Connor et al., 2014). Aerosol microphysics is simulated by the Global Model of Aerosol Processes (GLOMAP-Mode, Mann et al., 2010) using 5 log-normal aerosol modes (4 soluble and 1 insoluble). The model uses 2-moment aerosol microphysics, meaning that the number and mass in each mode are prognostic variables. There are four aerosol species: sulphate, organic carbon, black carbon and sea salt. Processes handled by GLOMAP include primary emissions, coagulation within and between modes, condensational growth and ageing, new particle formation (NPF), dry deposition, wet deposition within and below clouds, and aqueous sulphate production in cloud droplets.

Emissions of SO_2 , black carbon (BC) and organic carbon (OC) are for the year 2014 for all emissions sectors. 2014 was the latest year for which the emissions were available. The emissions datasets used for aerosols and precursor vapours are Hoesly et al. (2018) (SO_2 , anthropogenic OC and BC), Van Marle et al. (2017) (biomass burning OC and BC) and Sindelarova et al. (2014) (monoterpenes). Boreal forest fires are a major source of aerosols to the Arctic region. The number of particles from biomass burning emissions (including forest fires) is calculated by fitting the aerosol mass from Van Marle et al. (2017) to a log-normal mode of mean diameter 150 nm and width 1.59, following Stier et al. (2005). The particles are then added to the insoluble mode. Ageing from condensation of soluble mass onto insoluble particles can move insoluble mass into soluble modes; this is discussed in the following chapter in section 3.3.1. Boreal forest fires experience considerable interannual variability, therefore using emissions from a different year (2014 emissions for a 2018 simulation) could be a source

of bias in our simulations. To test this, we ran a simulation with biomass burning emissions prescribed from a climatology of the years 1995–2004 instead of the year 2014.

Sea salt emissions are calculated using the Gong (2003) parameterisation. The mass flux of primary marine organic carbon is then calculated using the sea spray flux, 10 m wind speed and chlorophyll-a concentration, using the Gantt et al. (2015) parameterisation. Note that because we use an atmosphere-only configuration in this study, the chlorophyll-a concentration is taken from an ancillary file, produced using model output from the fully-coupled model. Marine emissions are scaled by gridbox open water fraction for sea ice regions. The size distribution of primary marine organic particles is assumed to be lognormal, with a mean size of 160 nm and standard deviation of 2. This size does not account for a primary marine source of sub-100 nm particles, which has been suggested to exist in the Arctic following several studies using observations from field campaigns (Leck and Bigg, 2010; Orellana et al., 2011; Karl et al., 2013). It has been proposed that nanogel particles of biological origin can be emitted from the sea surface microlayer, activated into cloud and fog droplets, and broken up during droplet evaporation. The process leaves behind organic particles with sizes on the order of tens of nanometres. We adjusted the primary marine organic carbon parameterisation in UKESM to test whether a primary, marine source of sub-100 nm particles could account for aerosol size distributions measured in the high Arctic. We changed the mean size of the primary marine organic particles from 160 nm to 20 nm in simulation PMOC. A diameter of 20 nm represents a lower limit on the range of possible diameters for these primary organic particles (Karl et al., 2013). We do not perturb the mass flux of the primary marine organic carbon, because this is calculated online by the Gantt et al. (2015) parameterisation. The smaller particle size will therefore lead to an increased particle flux in our sensitivity simulation, so the 20 nm diameter is both a lower limit on the particle size and an upper limit on the particle flux, allowing us to test the sensitivity of the high Arctic aerosol size distribution to a strong source of small primary marine particles. Note that changing the size of the emitted particles is a simplification of the hypothesised process, which includes emissions of larger particles followed by break-up into smaller particles due to atmospheric processing. However, our approach allows us to test this source of particles in the model in the absence of more observation data on emission and break-up rates.

Wet removal of aerosols in UKESM occurs via two processes: in-cloud scavenging (also called nucleation scavenging) and below-cloud scavenging (impaction scavenging). In-cloud scavenging is the removal of aerosol particles by precipitation after they have been activated into cloud droplets. The number of particles removed this way for each mode, ΔN_i , is defined by

$$\Delta N_i = F_{liq} \times N_i \times R_{SCAV} \times \left(1 - \exp\left(-\frac{A}{L} \times dt\right) \right) \quad (2.1)$$

where F_{liq} is the grid-box liquid cloud fraction, N_i is the number of aerosols in mode i , dt is the model timestep, A is the parameterised rate describing how cloud droplets collide and coalesce to form rain drops (autoconversion rate), L is cloud liquid water content and R_{SCAV} is a scavenging coefficient defined for each mode. The value of R_{SCAV} is zero for the nucleation mode and insoluble Aitken mode, and one for the coarse mode. For the soluble Aitken and accumulation modes, $R_{SCAV} = 1 - frac$, where $frac$ is the fraction of particles in the mode larger than a prescribed activation diameter, set to a dry diameter of 206 nm. To test the sensitivity of Arctic aerosol to the strength of in-cloud scavenging, we ran a simulation where the value of R_{SCAV} was halved for all modes and a simulation where R_{SCAV} was doubled for all modes. To test the sensitivity of Arctic aerosol to below-cloud scavenging, we ran a simulation where below-cloud scavenging was turned off.

Liquid clouds are more efficient at removing aerosol than ice clouds, and this is a controlling factor in the Arctic aerosol seasonal cycle. More efficient scavenging of aerosol in late spring and summer acts to reduce the aerosol mass entering the Arctic by transport from lower latitudes. Browse et al. (2012) found that the inclusion of a lower temperature threshold for in-cloud aerosol scavenging in GLOMAP led to better agreement of modelled and measured BC and sulphate mass at Arctic ground stations. We took a different approach to investigate the effect of cloud phase on scavenging, which makes use of the explicit simulation of cloud phase by UKESM. We defined a threshold for the cloud ice fraction, f_{ICE} , above which a cloud is assumed to be mixed phase and therefore less efficient at scavenging aerosol. Hence in-cloud scavenging is switched off where f_{ICE} exceeds the threshold. We calculated f_{ICE} as

$$f_{ICE} = \frac{I}{I + L} \quad (2.2)$$

where I and L are the ice and liquid water contents of the cloud respectively. We used a threshold of 10%.

2.2.2 Observations

Ground stations

Multi-year records of aerosol mass concentration are available from several surface-level ground stations in the continental Arctic. Here we have used mass concentrations of BC from Alert in the Canadian Arctic archipelago (82.5°N, 62.3°W); Utqiagvik in northern Alaska (formerly Barrow, 71.3°N 156.6°W); Tiksi in Russia (71.6°N, 128.9°E) and Ny-Ålesund in Svalbard (78.9°N, 11.9°E). We have used mass concentrations of

Table 2.1: List of simulations.

Simulation	Description
BASELINE	The default set-up of UKESM in its atmosphere-only configuration.
BIOMASS	Emissions of black and organic carbon from biomass burning are taken from a 1995–2004 climatology instead of emissions values for the year 2014.
PMOC	As BIOMASS and the mean emission size of primary marine organic carbon particles is reduced from 160 nm to 20 nm.
ICE_THRESH	As BIOMASS and in-cloud scavenging is switched off in gridboxes with an ice water content of more than 10% of the total water content.
RSCAV_0.5	As BIOMASS and the in-cloud scavenging efficiency is reduced by a factor of 2.
RSCAV_2	As BIOMASS and the in-cloud scavenging efficiency is increased by a factor of 2.
IMP_SCAV_OFF	As BIOMASS and below-cloud aerosol scavenging is switched off.

sulphate from Ny-Ålesund and Villum Research Station in north-eastern Greenland (81.6°N, 16.4°W). The locations of these stations are displayed in figure 2.1.

BC absorption coefficients for each station were downloaded from the World Meteorological Organisation (WMO) Global Atmosphere Watch (GAW) World Data Centre for Aerosols (WDCA) and converted to mass concentrations using a specific attenuation coefficient of $19 \text{ m}^2 \text{ g}^{-1}$ as given in Sharma et al. (2002). Concentrations were averaged to give monthly means. For most sites, the observational data covers 2017 and 2018; data from 2018 was not available from Alert so data from 2009–2017 was used instead.

Sulphate mass concentrations were downloaded directly from the WDCA database. More data was available for sulphate than for BC, so longer time series of sulphate mass were used than for BC. Monthly means were taken from 2009–2018 for Ny Ålesund and 2013–2017 for Villum.

Arctic Ocean 2018

The Arctic Ocean 2018 (AO2018) expedition took place in August and September 2018 aboard the Swedish icebreaker *Oden*. The ship travelled from Svalbard to the North pole and then drifted with an ice floe for four weeks before travelling back to Svalbard. Further details and meteorological conditions of the campaign are presented

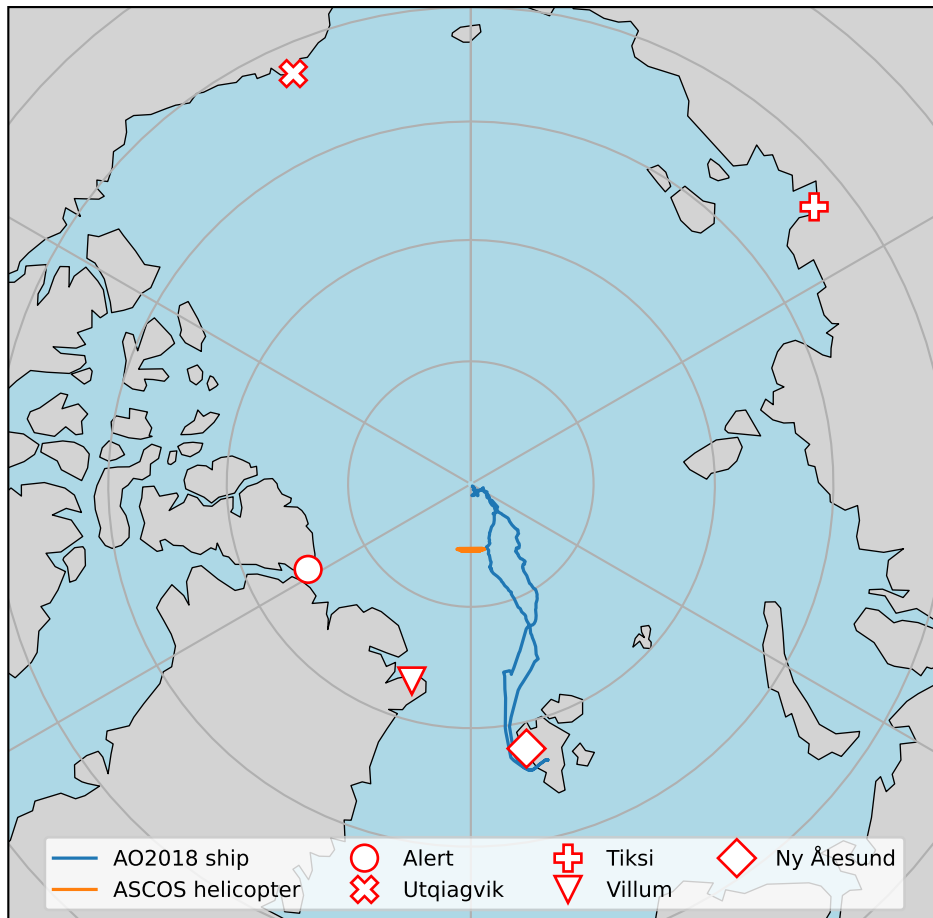


Figure 2.1: Map showing locations of ground stations from which we use measurements of aerosol mass.

in Vüllers et al. (2020). Here, we compare model output to aerosol and gas-phase measurements, which were measured during AO2018 as part of the Microbiology-Ocean-Cloud Coupling in the High Arctic (MOCCHA) campaign.

We use two aerosol datasets from the AO2018 campaign, involving three different instruments (Baccarini et al., 2020). A differential mobility particle sizer (DMPS) measured particles in the size range 10–959 nm (Karlsson and Zieger, 2020). We integrate this size distribution over the ranges 15–100 nm and 100–500 nm, sizes representative of the Aitken and accumulation modes. Total particle concentration for diameters greater than 2.5 nm was measured by an ultrafine condensation particle counter (UCPC). The UCPC and integrated DMPS data were used to calculate the concentration of all particles in the size range 2.5–15 nm (Baccarini and Schmale, 2020). This 2.5–15 nm time series was also supplemented by a Particle Size Magnifier during periods when the UCPC was not in operation. All data has been selected for “clean” periods, i.e. when pollution from the ship’s exhaust was not influencing the measurements.

Arctic Summer Cloud Ocean Study

The Arctic Summer Cloud Ocean Study (ASCOS) campaign also took place on the icebreaker *Oden*, at roughly the same time of year as AO2018 but a decade earlier (2008). The ASCOS drift period was from 12th August until 2nd September 2008 and took place close to 87°N. A full description of the campaign is given in Tjernström et al. (2014).

A helicopter was used during ASCOS to make measurements above the surface. Two condensation particle counters (CPCs) and one optical particle counter (OPC) were used on the helicopter to measure aerosol concentrations. The CPCs and OPC detected particles larger than 3 nm, 14 nm, and 300 nm respectively, giving an overall aerosol size distribution in the ranges 3–14, 14–300 and >300 nm. The aerosol measurements are presented in Kupiszewski et al. (2013).

During the ASCOS drift period, *Oden* was situated next to an open lead in the sea ice. Turbulent aerosol number fluxes were measured from the open lead using an eddy covariance system (a sonic anemometer, a gas analyzer and a condensation particle counter, CPC). A full description of the measurements and calculations of the aerosol flux is given in Held et al. (2011).

2.3 High Arctic summer size distribution

Figure 2.2 shows observations of aerosol concentrations in three particle size ranges measured at the surface during the AO2018 campaign. The nucleation mode (2.5–15 nm) behaves differently in the sea ice melt period (before 27th August 2018, day 239) and the sea ice freeze period (after day 239). In the melt period, the concentration is usually between 1–100 cm⁻³, occasionally reaching concentrations greater than 100 cm⁻³. After the freeze period, the concentration is typically higher, rarely dipping below 10 cm⁻³ and with peaks of order 1000 cm⁻³ that last on the order of a few hours. These peaks are associated with NPF events which were observed to be driven by iodic acid. The times of the events are marked in red. The Aitken mode (15–100 nm) concentration varies from about 1–1000 cm⁻³ with a mean of 60 cm⁻³. The accumulation mode (100–500 nm) concentration is generally lower than the smaller modes. The concentration is rarely greater than 50 cm⁻³, mostly at the beginning of the campaign period when the ship was in transit, and is occasionally less than 1 cm⁻³. Such periods of very low accumulation mode concentration are typical of the pristine Arctic summer environment (Mauritsen et al., 2011).

Simulation BASELINE underestimates the aerosol concentration in both the nucleation and Aitken modes (figure 2.2(a) and (d)). The simulated nucleation mode concentration has a maximum of 0.01 cm⁻³, such that observations are underestimated

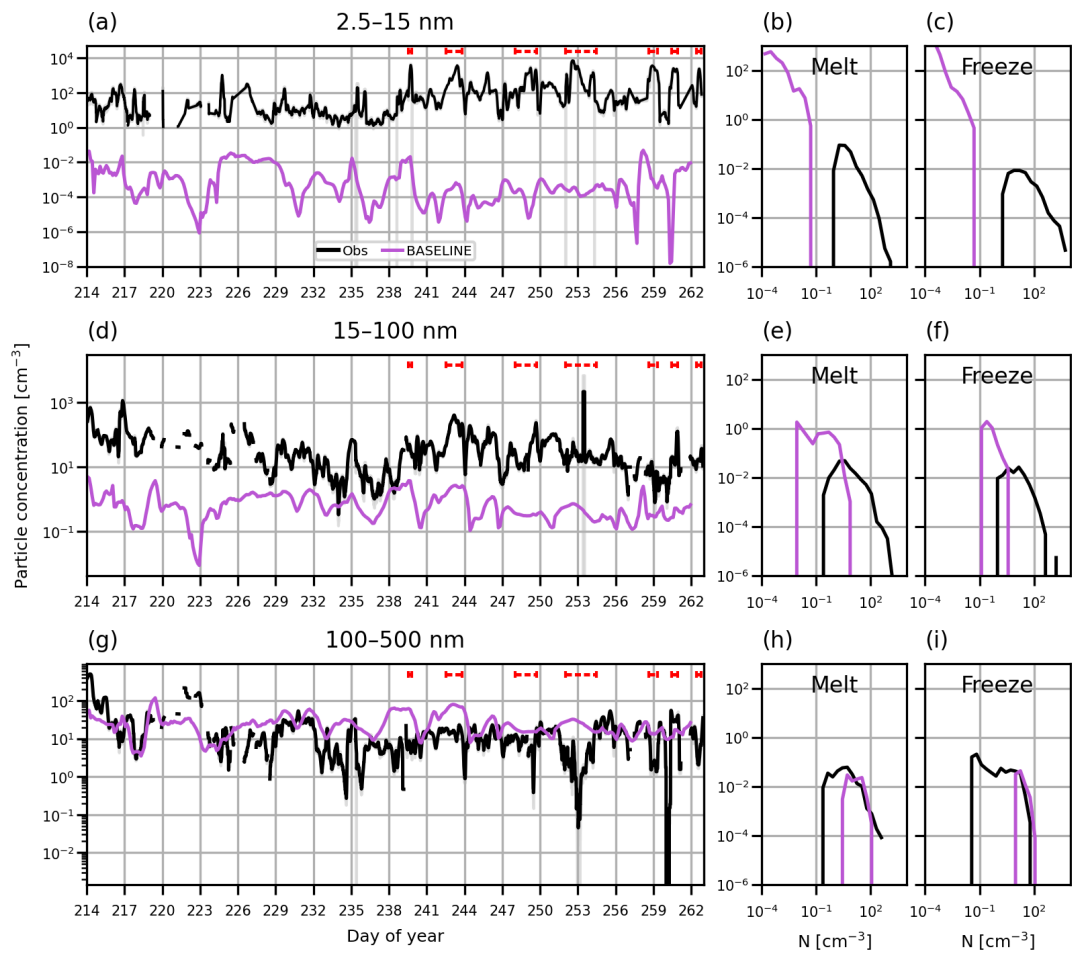


Figure 2.2: Times series and PDFs of aerosol concentration at the surface during AO2018 from observations and model output. Model output is from simulation BASELINE. Observations are shown as 3-hourly mean (black lines) and standard deviation (grey shading). Aerosol concentrations are shown for particles with diameter (a-c) 2.5-15 nm, (d-f) 15-100 nm and (g-i) 100-500 nm. Red dashed lines in (a, d, g) show observed NPF events. PDFs are separated by observed sea ice freeze-up date, 27th August 2018 (day 239).

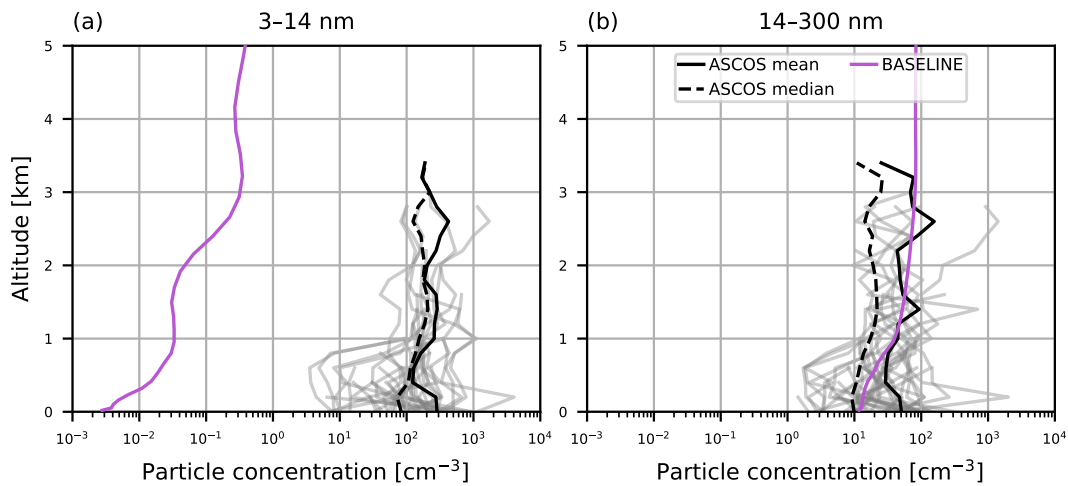


Figure 2.3: Aerosol vertical profiles from model output and ASCOS campaign observations from 2008. Model output is from colocated 2018 monthly mean concentrations from simulation BASELINE. Observed concentrations are given as the mean profile from each ASCOS flight (grey lines), overall mean (solid black) and overall median (dashed black). Profiles are for particles with size (a) 3–14 nm, measured during ASCOS using a UCPC and (b) 14–300 nm, measured using a CPC (particles greater than 14 nm) and a CLASP instrument (particles greater than 300 nm).

by at least 2 orders of magnitude in both periods and the PDFs of particle concentration do not overlap with the measured PDFs (figure 2.2(b) and (c)). The Aitken mode concentration in the model is most often between about $0.1\text{--}10\text{ cm}^{-3}$, with one day where the concentration reaches about 0.01 cm^{-3} (day 223). The lowest measured Aitken concentrations are sometimes captured by the model, for example between days 234–239, but the model does not simulate the highest concentrations that were measured. As such, the model is usually underestimating the Aitken concentration by 1 or 2 orders of magnitude.

In the accumulation mode, the simulated concentration is between about $5\text{--}100\text{ cm}^{-3}$ and performs better than the smaller modes (figure 2.2(g)). The observed concentration is often produced by the model, however there are also periods of overestimation, such as days 238–240. The troughs of 1 cm^{-3} and below observed in the accumulation mode concentration are never produced by the model.

Figure 2.3 shows aerosol concentrations measured by helicopter during the ASCOS campaign. The nucleation mode (here measured as 3–14 nm diameter particles) varies across nearly 3 orders of magnitude at the surface and in the lowest 1 km of the atmosphere, and by about 1 order of magnitude in the free troposphere. Both the median and mean profile from all the flights are on the order of 100 cm^{-3} . The accumulation mode (14–300 nm particles) has an equally large range but smaller concentrations, with the mean and median profiles both on the order of 10 cm^{-3} . The lowest concentrations

at the surface for the accumulation mode are approximately 20 cm^{-3} , 1–2 orders of magnitude higher than the lowest concentrations recorded during AO2018. This could be due to the different size ranges used for the particle concentrations. Since these profiles were measured during ASCOS with CPC instruments, it is not possible to resolve the particle concentration further between 14–300 nm.

Figure 2.3 also shows colocated August 2018 monthly mean output from BASELINE. As for the aerosol concentrations at the surface during AO2018, the model underestimates the concentration of the smallest particles (here measured between 3–14 nm) and performs better for the accumulation mode (measured as 14–300 nm during ASCOS). The height profile for 3–14 nm diameter particles shows that the model underestimates the nucleation mode concentration aloft as well as at the surface. The concentration at 3 km is underestimated by about 3 orders of magnitude while at the surface the underestimation is 5 orders of magnitude. In the accumulation mode, the simulated concentration at the surface is approximately equal to the ASCOS median value (about a factor of 5 lower than the mean value), and the mean profile is captured well above 1 km.

In the following sections, we will investigate whether primary marine organic carbon is a missing source of Aitken particles in UKESM. We will also investigate whether the overestimations in the accumulation mode can be corrected by changes to biomass emissions or wet removal, and whether such changes could improve the simulated nucleation and Aitken mode concentrations by promoting more NPF, as was seen in Korhonen et al. (2008b) and Croft et al. (2016b).

2.4 Emissions

In section 2.3, we showed that UKESM underestimates the concentration of aerosol in the nucleation and Aitken modes in the high Arctic during summer, and does not simulate the lowest accumulation mode concentrations. In this section, we investigate primary aerosol emissions in the model and their effect on the high Arctic summer size distribution. Primary aerosol sources affect the high Arctic summer aerosol budget via local, marine emissions and long-range transport of emissions from further south. Since primary particles have a relatively large surface area in the model, they act as a sink for condensable vapours. As such, the behaviour of primary particles affects NPF and growth, affecting the smaller size modes as well as the modes into which the particles are directly emitted. Here we will assess two emissions sectors of particular relevance for the Arctic: primary marine organic carbon and biomass burning. Since biomass burning emissions in the continental Arctic occur further south from the AO2018 campaign region, we use observations of aerosol mass from Arctic ground stations between 71–82°N to assess the changes we make to the biomass burning emissions. For primary

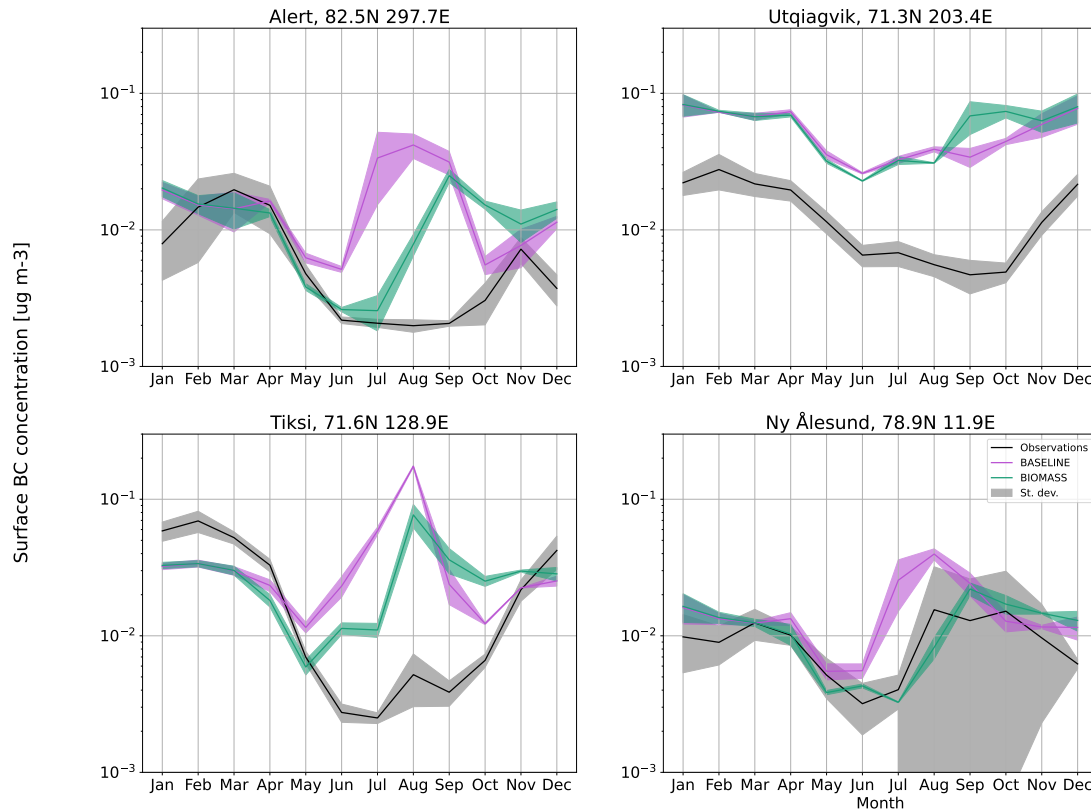


Figure 2.4: BC aerosol mass concentration at Alert, Utqiagvik, Tiksi and Ny-Ålesund from measurements and model output. Model output is shown for simulations BASELINE (purple lines) and BIOMASS (green lines) for the years 2017–2018. Monthly means are shown as solid lines, standard deviation in shading.

marine organic carbon, we use particle flux measurements and particle concentrations from the AO2018 and ASCOS campaigns.

2.4.1 Biomass burning

Figure 2.4 shows BC mass concentrations measured at Alert, Utqiagvik, Tiksi and Ny-Ålesund. The Arctic haze cycle is evident in the observations, with all sites except Ny-Ålesund showing a maximum in BC mass in the winter or early spring. At Ny-Ålesund, BC mass peaks from August–October with a secondary peak in March. All sites also display a minimum in BC mass that is 5–10 times lower than the annual maximum. The timing of the annual minimum is not consistent across these sites. At Ny-Ålesund, the BC concentration is lowest in June before increasing again in August. Tiksi also has lower concentrations in June, with its minimum occurring in July before a slight increase in concentrations again in August. Concentrations at Alert are consistently low from June–September, while at Utqiagvik the annual minimum in BC mass does not occur until September.

Monthly mean BC mass concentrations from simulation BASELINE are shown in

figure 2.4 for the years 2017–2018. Output is shown for gridboxes containing the locations of Alert, Utqiaġvik, Tiksi and Ny-Ålesund. Simulation BASELINE mostly fails to capture the seasonal cycle at these sites. At Alert, BASELINE simulates a peak in the winter months but instead of a summer minimum there is a maximum in concentration in July and August which is approximately 3 times greater than the winter peak. Similarly, BASELINE simulates an August maximum in concentrations at Tiksi that is roughly 2.5 times greater than the observed winter maximum concentration, and more than an order of magnitude greater than the observed concentration for August. The concentrations from December–March are underestimated by the model by approximately a factor of 2. At Ny Ålesund, the model is correct to within a factor of 2 during the build up of Arctic haze (Nov–April) but has a maximum concentration at the end of summer that occurs a month too soon and exceeds the measured concentration in August. At Utqiaġvik, the BC concentrations are consistently too high in the model. BC mass concentration is 2–3 times too high during Arctic haze (December–April) and 5–10 too high when the measurements are lowest (June–October). The model has a minimum in June, rather than the observed minimum in September.

We tested the sensitivity of the BC seasonal cycle to fire emissions by changing the emissions for biomass burning from 2014 monthly means to a climatology for 1995–2004. The output from BIOMASS is shown on figure 2.4. The climatology improves the model performance at Alert, Tiksi and Ny-Ålesund, though biases remain. At Alert, the modelled concentrations for July and August reduce by up to an order of magnitude, shifting the maximum from August to September. Summer mass concentrations also reduce at Tiksi, though the peak concentration in August is still an order of magnitude too high and concentrations remain too high in June, July, September and October. At Ny-Ålesund, the anomalous peak in July and August is removed by using different emissions, leaving a peak in September that is within the standard deviation of the observations. Utqiaġvik behaves differently from the other locations, with concentrations increasing even more in September and October, further overestimating the minimum in the observations.

Overall, the model performs slightly better when a 10 year climatology is used for the biomass emissions (simulation BIOMASS) than when a single year is used (BASELINE). As such, for the rest of this chapter, model perturbations will be relative to simulation BIOMASS rather than to the default settings in BASELINE and will be compared to BIOMASS.

2.4.2 Primary marine organic carbon

Figure 2.5 shows the August 2018 mean modelled particle flux for OC from simulations BIOMASS and PMOC. The red lines mark the region with 90% gridbox sea ice fractions, as calculated from the monthly mean ice fraction output. Area averages for

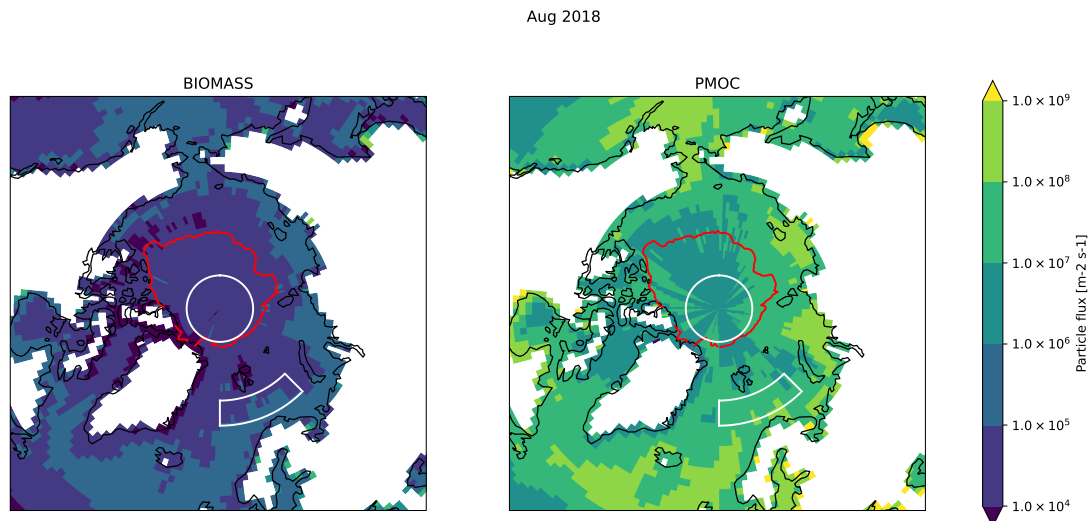


Figure 2.5: Map of modelled primary OC particle flux for ocean gridboxes. Output is taken from (left) BIOMASS and (right) PMOC August 2018 mean. The red line marks the monthly mean extent of 90% gridbox sea ice fraction. Area averages for the regions in the white boxes are quoted in the text.

the central Arctic Ocean (white circle in figure 2.5) and an area of open water between 72–76°N (see white box in figure 2.5) are given in table 2.2 for both simulations. When the mean size of marine organic particles is reduced (PMOC relative to BIOMASS), particle flux values increase by approximately a factor of 500. In simulation PMOC we reduced the mean emission size from 160 to 20 nm, a factor of 8 difference, while leaving the mass flux unchanged. This leads to a factor of $8^3 = 512$ increase in the particle flux. We emphasise that we have changed the size of the emitted particles in simulation PMOC, whereas it is hypothesised that such a source includes emissions of larger particles followed by atmospheric processing which causes particle break-up. As such there are likely to be differences between the observed particle fluxes and the fluxes simulated in PMOC.

Simulation PMOC produces primary marine organic particle fluxes that are greater than particle fluxes previously reported from the Arctic. Using measurements taken during the ASCOS campaign, Held et al. (2011) reported fluxes from an open lead of up to $5 \times 10^4 \text{ m}^{-2} \text{ s}^{-1}$ during a period of net emission from the lead. The mean value from BIOMASS is within the range of their measurements, while the mean value from PMOC is nearly a factor of 200 greater than their maximum reported value. During another icebreaker field campaign, the Arctic Ocean Expedition 1996 (AOE96), particle fluxes were measured both over the open sea and over open leads in the sea ice (Nilsson et al., 2001a). Fluxes reported for the open sea varied from around 5×10^5 to $1 \times 10^7 \text{ m}^{-2} \text{ s}^{-1}$ (depending on wind speed) while fluxes over the open lead were about an order of magnitude lower. The mean flux values from PMOC are 1–2 orders of magnitude greater than the open lead fluxes and about a factor of 4 greater than

Table 2.2: Particle fluxes from open leads and open ocean from model output and field measurements. All values are given in $\text{m}^{-2} \text{s}^{-1}$.

	BIOMASS	PMOC	ASCOS	AOE96
Open ocean	8.09×10^4	4.16×10^7	N/A	$5 \times 10^5 - 1 \times 10^7$
Open leads	1.79×10^4	9.14×10^6	$-5 \times 10^4 - 5 \times 10^4$	$1 \times 10^4 - 5 \times 10^5$

the maximum open water flux. The flux values from BIOMASS are within the range of the measurements for open lead fluxes but about a factor of 6 lower than the minimum reported flux from open water. Hence, simulation PMOC overestimates the particle flux from both open ocean and sea ice open leads, while the default primary marine organic emissions in BIOMASS underestimate the open ocean flux.

The measurements from AOE96 show that the particle flux from open leads is about an order of magnitude less than the flux from open ocean. There are a range of factors that could explain this difference, for example different biological activity in the pack ice region compared to the open ocean, or the smaller fetch over an open lead resulting in calmer waters compared to open ocean. Although the model does produce higher particle fluxes over the open ocean in both simulations, the difference is about a factor of 4 rather than a factor of 10 as seen in the measurements.

2.4.3 Effect of biomass burning and primary marine organics on summer size distribution

So far in this section we have analysed the effects of changing the biomass burning emissions and the primary marine organic emissions. We will now examine how these changes affect the summertime size distribution in the high Arctic.

Figure 2.6 shows aerosol concentrations from measurements and model output during AO2018. Like BASELINE, simulation BIOMASS underestimates the measured nucleation mode concentration by at least 2 orders of magnitude in the melt period, and more than 3 orders of magnitude in the freeze periods. However, there are periods when the nucleation mode concentration in BIOMASS is higher than that of BASELINE, for example on days 230–232, when the concentration from BIOMASS is 3 orders of magnitude greater than BASELINE, somewhat reducing the model bias. PMOC produces nucleation mode concentrations between 1–100 cm^{-3} , an increase of between 2–7 orders of magnitude compared to BIOMASS. In the sea ice melt period (up to day 239), the nucleation mode in PMOC is usually on the same order of magnitude as the observations, but in the freeze period the model does not capture the highest concentrations (caused by NPF events), leading to underestimations of 1–2 orders of magnitude.

In the Aitken mode, the PDFs of particle concentration from BIOMASS and BASE-

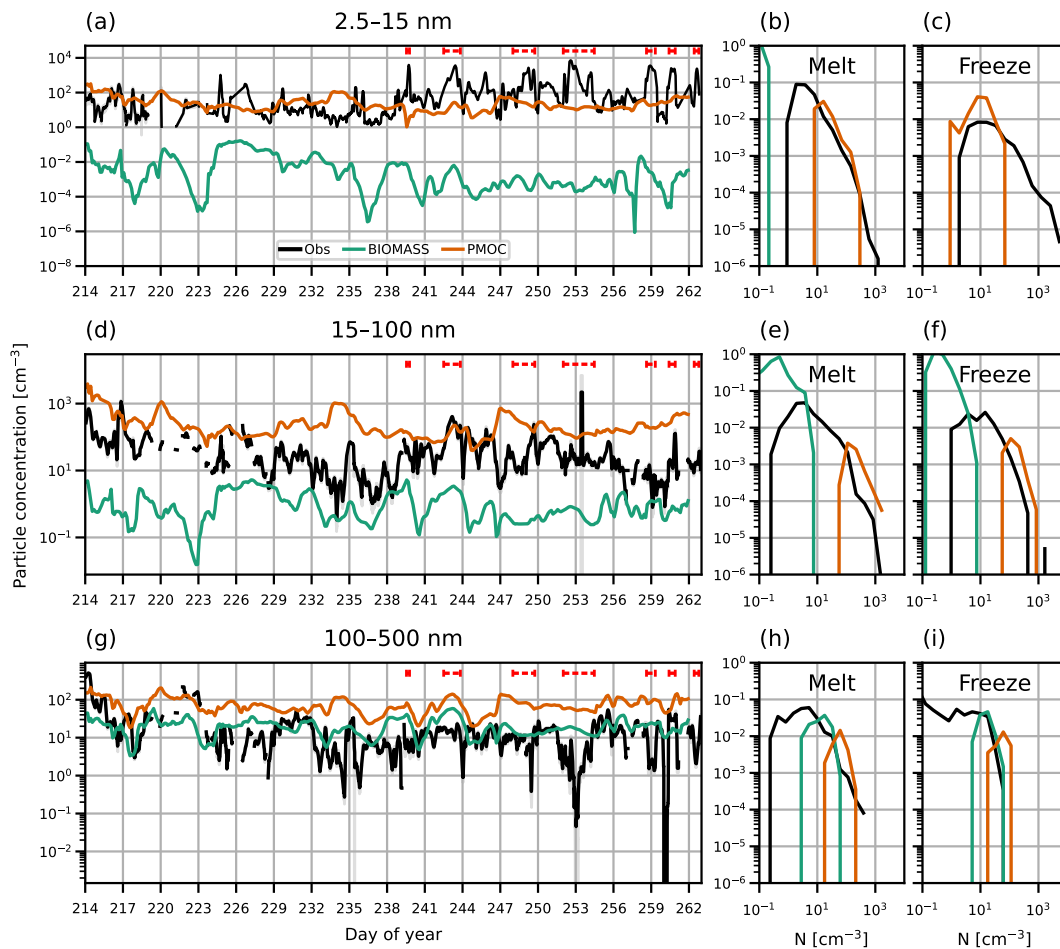


Figure 2.6: Times series and PDFs of aerosol concentration at the surface during AO2018 from observations and simulation PMOC. Observations are shown as 3-hourly mean (black lines) and standard deviation (grey shading). Aerosol concentrations are shown for particles with diameter (a-c) 2.5-15 nm, (d-f) 15-100 nm and (g-i) 100-500 nm. Red dashed lines in (a, d, g) show observed NPF events. PDFs are separated by observed sea ice freeze-up date, 27th August 2018 (day 239).

LINE are largely similar. Again, there are periods when the concentrations from BIOMASS are larger than those simulated by BASELINE (e.g. days 224-229). Like in the nucleation mode, the alterations to the primary marine organic carbon in the model cause a dramatic increase in particles (PMOC relative to BIOMASS). The concentration in PMOC varies from just below 100 particles cm^{-3} to more than 1000 cm^{-3} . The observations rarely reach as high as 1000 cm^{-3} and are occasionally as low as 1 cm^{-3} , so the PMOC simulation does not capture the lowest end of the observed distribution of concentrations in either period and overestimates the observed concentrations by up to 2 orders of magnitude.

The different biomass emissions (BIOMASS) cause only minor changes to the modelled accumulation mode, while the accumulation mode concentration is overestimated

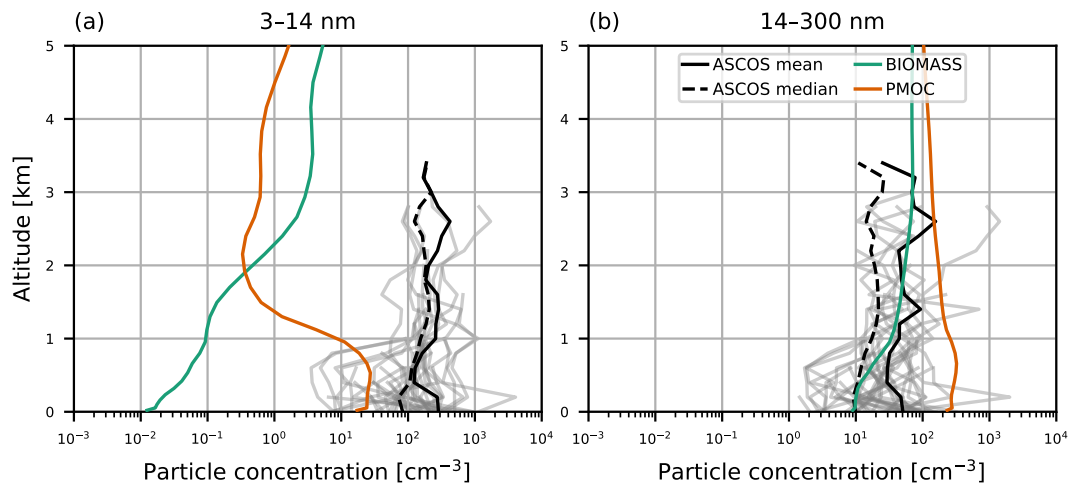


Figure 2.7: Aerosol vertical profiles from model output and ASCOS campaign observations from 2008. Model output is from colocated 2018 monthly mean concentrations from simulations BIOMASS and PMOC. Observed concentrations are given as the mean profile from each ASCOS flight (grey lines), overall mean (solid black) and overall median (dashed black). Profiles are for particles with size (a) 3-14 nm, measured during ASCOS using a UCPC and (b) 14-300 nm, measured using a CPC (particles greater than 14 nm) and a CLASP instrument (particles greater than 300 nm).

by PMOC. While simulation BIOMASS captures the higher end of the PDF of accumulation mode concentration, concentrations in simulation PMOC are typically between $10\text{--}100\text{ cm}^{-3}$, often overestimating the measurements by 1–2 orders of magnitude. Like BASELINE, the lowest measured concentrations are not captured at all in BIOMASS or PMOC. For example on day 253, the overestimation of the measurements by the model is 2 orders of magnitude in the BIOMASS output and 3 orders of magnitude in PMOC.

Aerosol profiles from the ASCOS campaign are shown in figure 2.7 with model output from BIOMASS and PMOC. Model output is from 2018 August monthly mean data that has been colocated with the ASCOS helicopter. The model underestimates the nucleation mode. In BIOMASS, the mean nucleation mode concentration is underestimated by 2 orders of magnitude at 3 km and 4 orders of magnitude at the surface. In PMOC, the nucleation mode concentrations at the surface are within the range of concentrations measured during certain individual flights, but underestimate the median value by about a factor of 4 and the mean value by an order of magnitude. While the observations show little variation in nucleation mode concentration with height, concentrations in BIOMASS increase with height, and concentrations in PMOC decrease with height, such that the measurements are underestimated by PMOC above 1 km by about 2 orders of magnitude. In the accumulation mode, BIOMASS performs better than in the nucleation mode, capturing the mean profile above 1 km and simulating the median concentration at the surface. PMOC overestimates the measured

accumulation mode concentration, particularly at the surface where the concentration from the model is about a factor of 2 higher than the mean profile.

2.5 Wet scavenging

In the previous section we examined primary aerosol emissions as a source of model bias in the high Arctic summer aerosol size distribution. We found that perturbations to the primary marine organic carbon aerosol source in UKESM could not reconcile the simulated aerosol size distribution with measurements from ASCOS or AO2018. Similarly, although changes to the biomass emissions led to model improvements, they were not enough on their own to explain the model bias in the high Arctic size distribution. Here, we will investigate precipitation as a sink of aerosol in order to establish whether too-strong removal of small particles, or too-weak removal of larger particles, can account for the model bias. As we did for biomass burning emissions, we will use measurements of BC and sulphate mass from Arctic ground stations to investigate the effect of changes to wet removal in UKESM on the simulated Arctic aerosol seasonal cycle.

2.5.1 Cloud phase

BC and sulphate aerosol mass from observations and from simulations BIOMASS and ICE_THRESH are shown in figures 2.8 and 2.9 for different Arctic ground stations. Aerosol mass is higher in ICE_THRESH than BIOMASS, which is as expected since the cloud ice threshold acts to suppress aerosol removal in mixed-phase clouds. At Alert, Tiksi and Ny-Ålesund, BC mass concentrations increase by up to about a factor of 5 in all months except for July, August and September. This seasonal behaviour is consistent with a lower fraction of ice clouds in the summer. BC concentrations at Utqiagvik do not see the same increase as the other locations.

Like BC, sulphate mass concentrations show a seasonal cycle at Villum and Ny-Ålesund with a peak in April and a minimum in July or August. At Villum, the springtime peak in sulphate mass is 12 times higher than the summer minimum and at Ny-Ålesund it is 5 times higher. In simulation BIOMASS, the model overestimates sulphate mass at both sites and for all months of the year. At Villum, the model performs worse in the summer than in the winter. The modelled sulphate mass is within about a factor of 2 of the observations in the months October–April, whereas in May–September the bias is larger, reaching about a factor of 5 in July. In contrast to Villum, BIOMASS performs the best during spring. The model overestimates sulphate mass by about a factor of 2 in the months February–May and about a factor of 4 from July–December. January has the highest overestimation of about 5 times the observations.

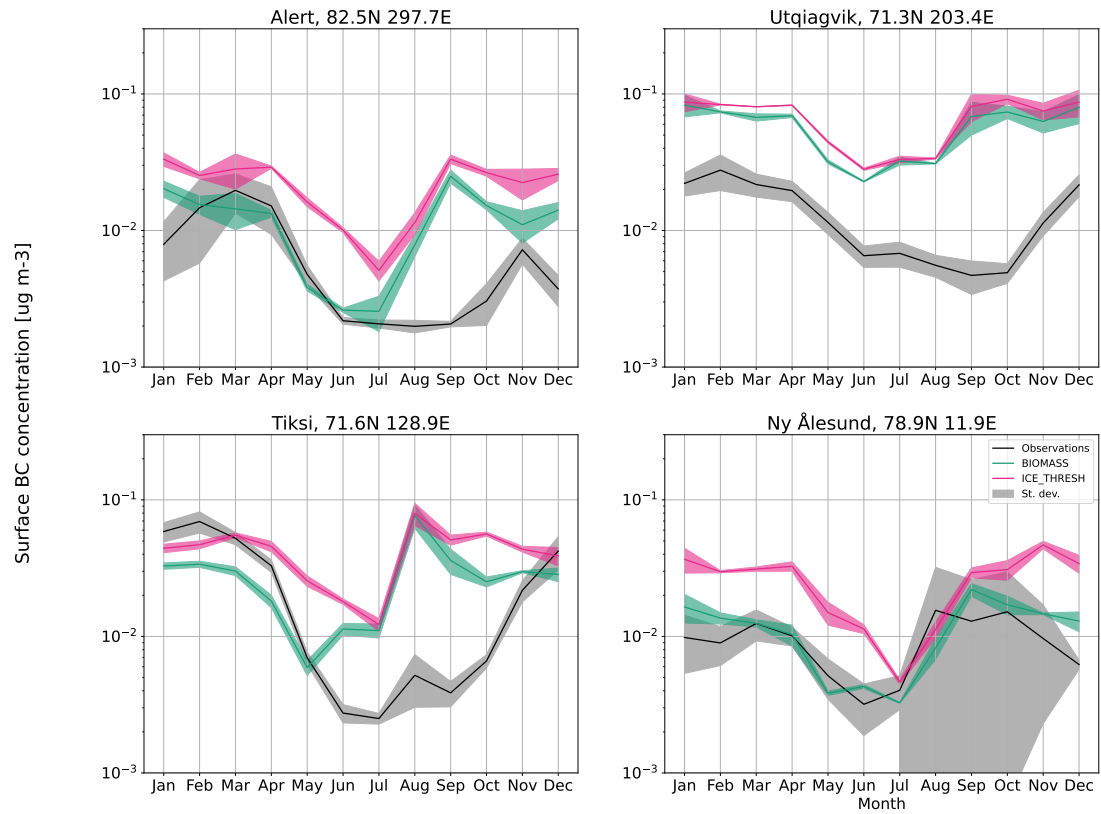


Figure 2.8: BC aerosol mass concentration at Alert, Utqiagvik, Tiksi and Ny-Ålesund from measurements and model output. Model output is shown for simulations BIOMASS (green lines) and ICE_THRESH (pink lines) for the years 2017–2018. Monthly means are shown as solid lines, standard deviation in shading.

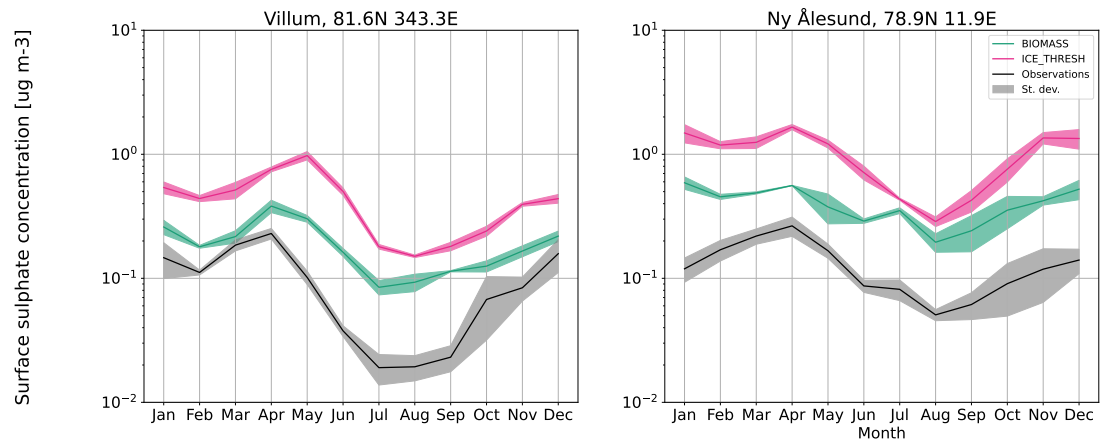


Figure 2.9: Sulphate aerosol mass concentration at Ny-Ålesund and Villum Research Station from measurements and model output. Model output is shown for simulations BIOMASS (green lines) and ICE_THRESH (pink lines) for the years 2017–2018. Monthly means are shown as solid lines, standard deviation in shading.

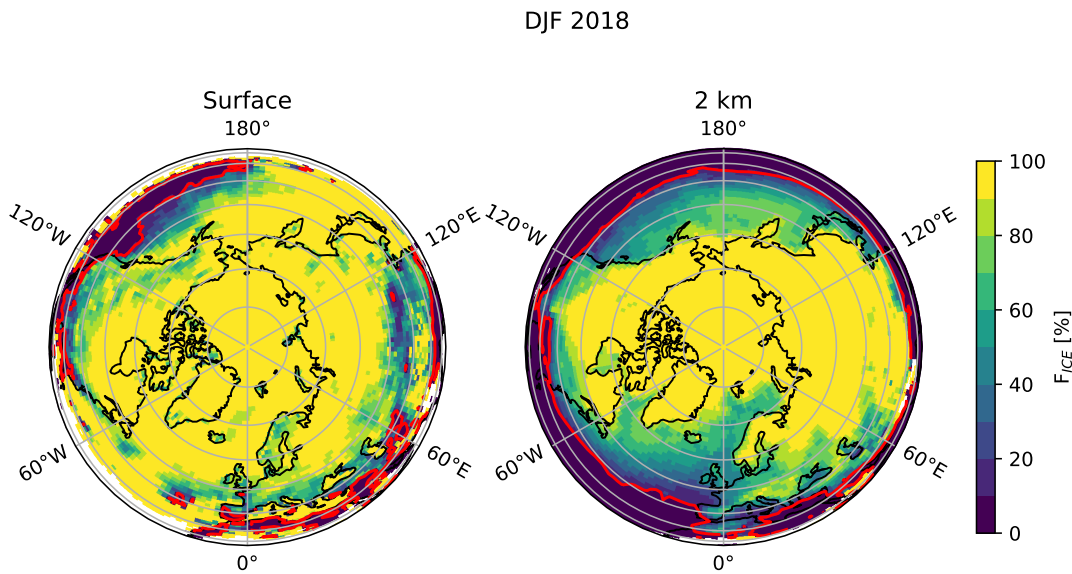


Figure 2.10: Maps showing the seasonal mean of f_{ICE} for DJF 2018 at the surface and 2 km altitude from simulation ICE_THRESH. Red contours mark regions where $f_{ICE} > 10\%$.

In simulation ICE_THRESH, sulphate mass concentrations increase in all months and at both sites relative to BIOMASS, causing even higher overestimations of the observed values. At Ny-Ålesund, sulphate concentration from ICE_THRESH is about 2 times higher than that of BIOMASS except for July–September, where the increase is by about a factor of 1.5 relative to BIOMASS. Similarly at Villum, concentrations from ICE_THRESH are 2–2.5 times higher than BIOMASS in October–April, 3 times higher in May and June, but only 1.5 times higher in August and September. Thus, although the absolute sulphate concentrations are worse in ICE_THRESH than they are in BIOMASS, the smaller increases in summer create a better representation of the seasonal cycle, with the difference between the minimum and maximum concentrations going from a factor of 4.5 to a factor of 6.5 at Villum (observed difference factor of 12) and going from a factor of 3 to 6 at Ny-Ålesund (observed difference factor of 5).

The increase in BC and sulphate aerosol mass in simulation ICE_THRESH leads to worse model performance in terms of the absolute values of the concentrations, but better performance in terms of the relative concentrations in the Arctic annual cycle of sulphate. This suggests that while the ICE_THRESH configuration leads to too weak scavenging overall, it captures the variation in scavenging strength at different times of year better than the default model configuration. Figures 2.10 and 2.11 show maps of f_{ICE} from ICE_THRESH for winter and summer 2018. Model output is shown for the surface and for 2 km and $f_{ICE} = 10\%$ is marked as red contours. In winter, there are no areas north of 50°N where f_{ICE} is less than 10%, meaning all in-cloud scavenging is suppressed for the region $50\text{--}90^\circ\text{N}$. In summer, there is a clear reduction of the area where scavenging is suppressed, both at the surface and at 2 km. At the surface, the

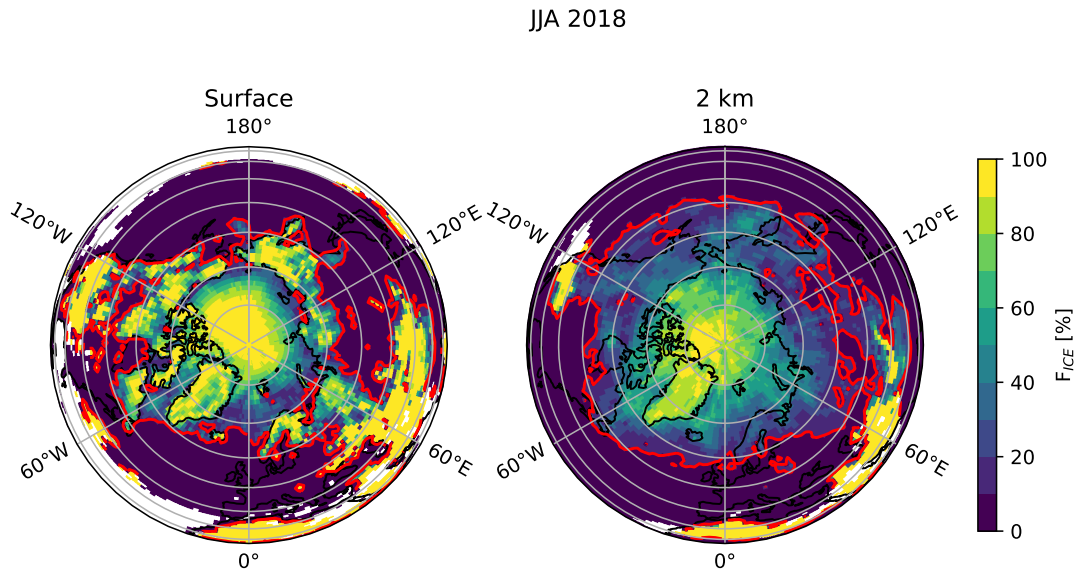


Figure 2.11: Maps showing the seasonal mean of f_{ICE} for JJA 2018 at the surface and 2 km altitude from simulation ICE_THRESH. Red contours mark regions where $f_{ICE} > 10\%$.

extent of the $f_{ICE} > 10\%$ region is inhomogeneous with longitude, extending to the mid-latitudes and further south on the western side of North America and some parts of the Eurasian continent, but not covering large parts of Russia, the North Atlantic and parts of Canada. At 2 km, the southern extent of the $f_{ICE} = 10\%$ region is $10\text{--}30^\circ$ north of the extent of the region during winter, again with the exception of the western side of North America and parts of central Asia. It is clear from the difference in area covered by the f_{ICE} contour that scavenging in the mid-latitudes is suppressed much more in winter than in summer by the ICE_THRESH mechanism.

Figure 2.12 shows the fraction of gridboxes in each model column meeting various thresholds. The thresholds are $TWC > 0$ (i.e. any cloud is present, default GLOMAP scavenging criterion), $TWC > 0$ and temperature is above -15°C (i.e. Browse et al. (2012) GLOMAP scavenging criterion), $LWC > 0$ (i.e. liquid cloud is present, default UKESM scavenging criterion) and clouds containing less than 10% ice (the threshold we apply to f_{ICE} here). We have reduced the 3-dimensional water content thresholds to column fractions for ease of visualisation. The fractions are calculated for 2018 annual mean output from simulation ICE_THRESH. The number of gridboxes meeting these criteria is a proxy for the number of gridboxes where scavenging is occurring under the different model configurations (GLOMAP default and Browse et al. (2012) set-ups and UKESM default and ICE_THRESH set-ups). Note that we have applied the GLOMAP criteria to UKESM output only, so the number of gridboxes meeting the criteria in GLOMAP would be different from what is shown in figure 2.12 because of the use of prescribed cloud fields in GLOMAP. However, by applying the criteria to UKESM output, it gives us an impression of the relative distribution of how widespread

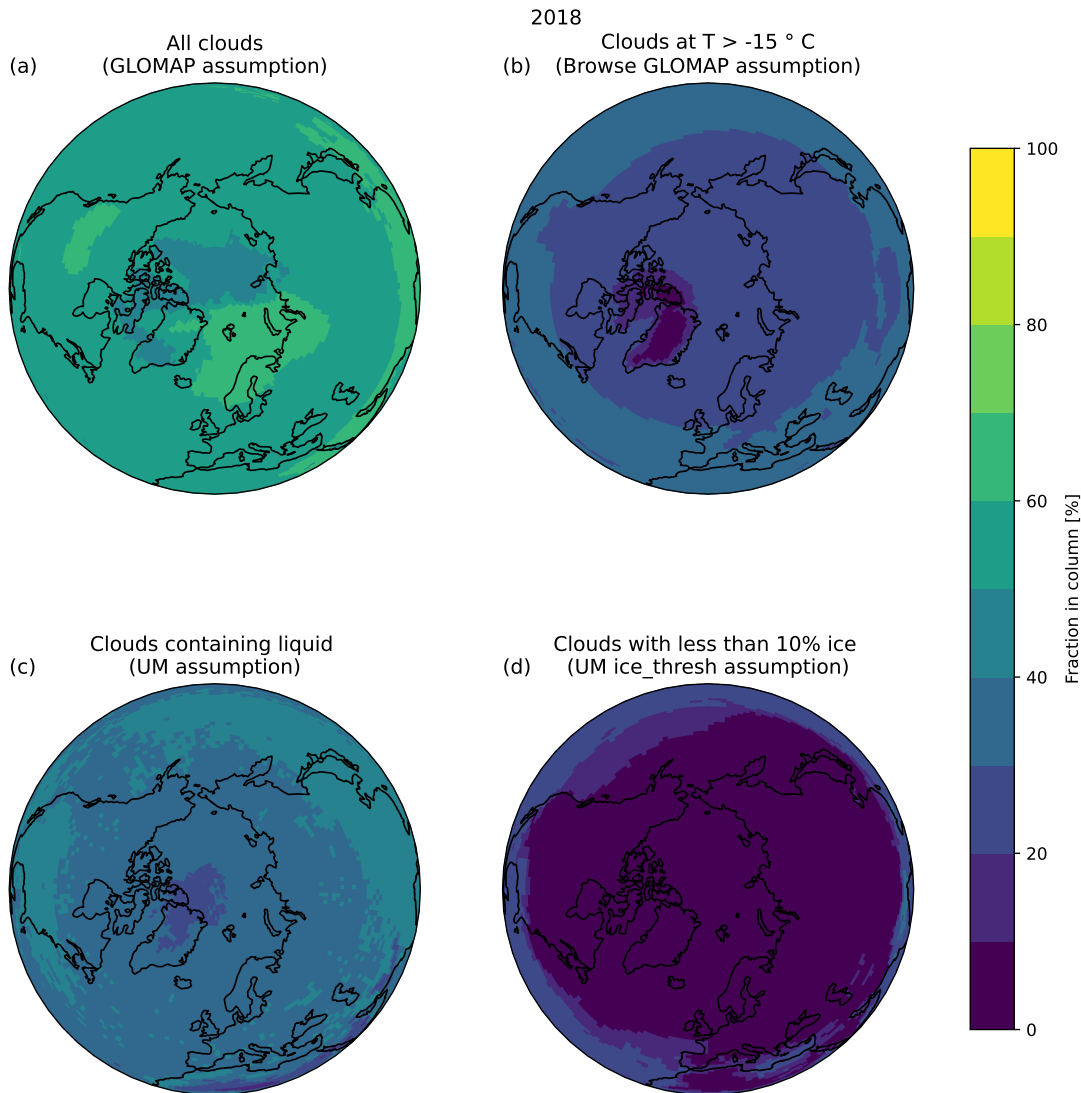


Figure 2.12: Maps showing fraction of each model grid column where (a) clouds are present ($TWC > 0$), (b) clouds are present at $T < -15^\circ\text{C}$, (c), liquid clouds are present ($LWC > 0$) and (d) clouds with $f_{ICE} < 10\%$ are present ($IWC/TWC < 0.1$). Fractions are calculated using 2018 annual mean values of LWC, IWC and temperature from simulation ICE_THRESH.

scavenging is in each model. The highest fractions are seen in figure 2.12(a) where all clouds are selected, implying that the default GLOMAP assumption for scavenging would lead to the most spatially widespread scavenging out of all of these criteria. This is in line with the results from Browse et al. (2012) which showed the the default configuration of GLOMAP was overestimating the removal of aerosol by wet scavenging. The temperature dependence that was added by the authors of that study leads to lower fractions (figure 2.12(b)), indicating that it is successful in reducing the amount of scavenging that takes place. The fractions in the default UKESM configuration are closer to the Browse et al. (2012) configuration of GLOMAP than its default, which suggests that the use of cloud phase in the default UKESM scavenging mechanism is

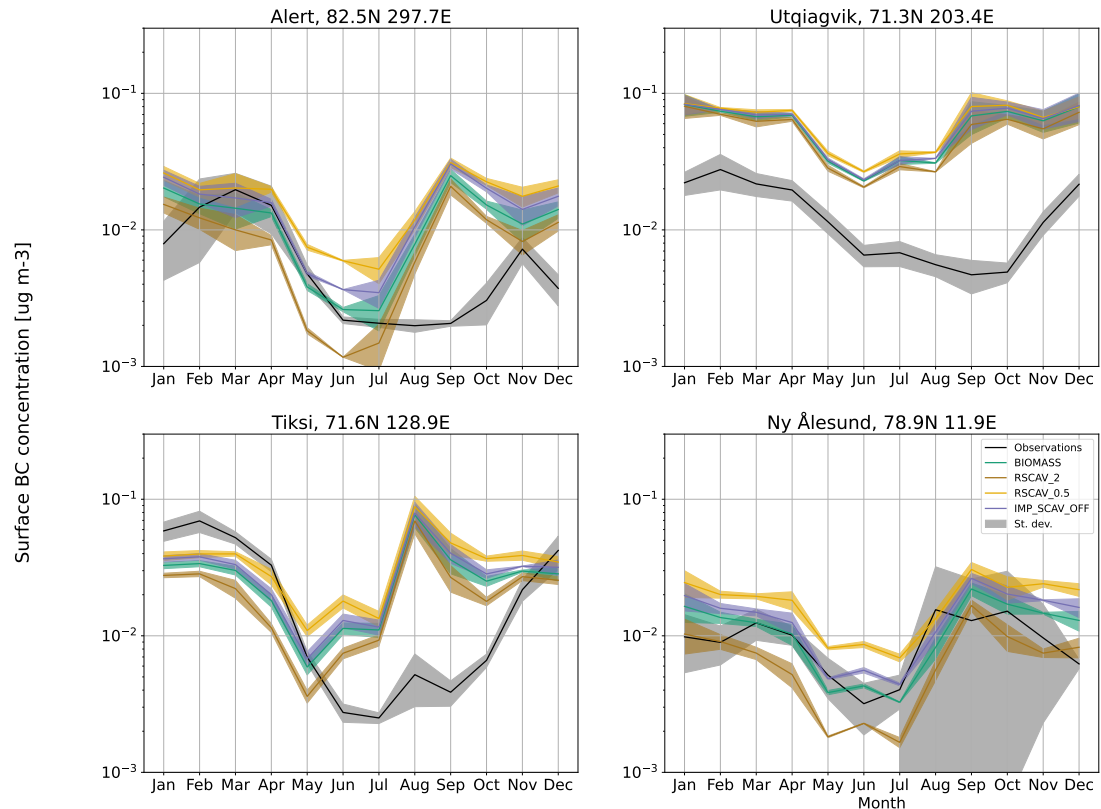


Figure 2.13: BC aerosol mass concentration at Alert, Utqiagvik, Tiksi and Ny-Ålesund from measurements and model output. Model output is shown for simulations BIOMASS (green lines), RSCAV_2 (brown lines), RSCAV_0.5 (yellow lines) and IMP_SCAV_OFF (blue lines) for the years 2017–2018. Monthly means are shown as solid lines, standard deviation in shading.

performing better than GLOMAP was. Moreover, the ICE_THRESH fractions are the lowest of all, suggesting that the ICE_THRESH criteria may be too stringent, therefore not producing enough scavenging in UKESM. This is reflected in the aerosol mass concentrations from ICE_THRESH (figures 2.8 and 2.9), which overestimated measurements from Arctic ground stations. Although the use of ice fraction provides better representation of the seasonal variation in scavenging, the strength of the scavenging overall remains too low.

2.5.2 Model parameters

As well as controlling which gridboxes are subject to wet removal of aerosols, we can control the removal rate in gridboxes where scavenging is taking place. Here we examine the effects of changing the model parameter R_{SCAV} , as described in section 2.2.1. We also examine the effect of switching off impaction scavenging in the model.

Figure 2.13 shows BC aerosol mass concentrations at Arctic ground stations from observations and simulations BIOMASS, RSCAV_0.5 and RSCAV_2. As expected, RSCAV_0.5 increases aerosol mass compared to BIOMASS because of the decreased

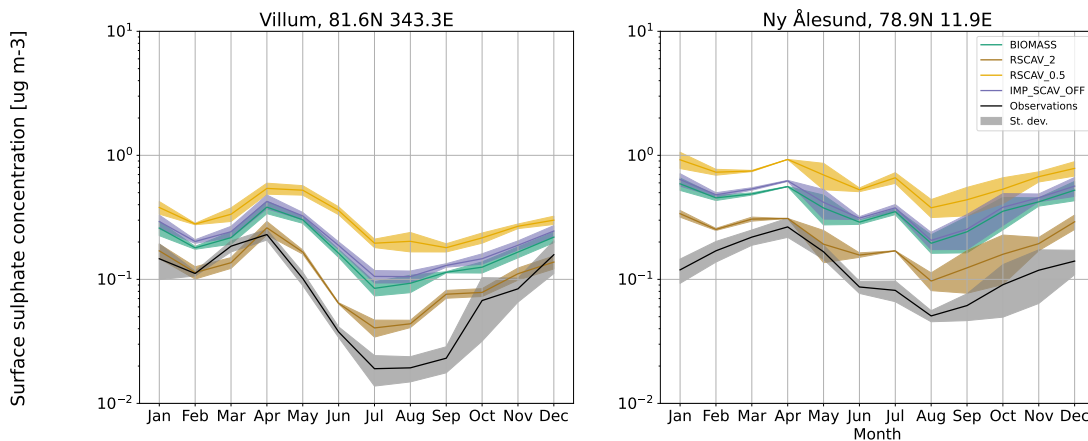


Figure 2.14: Sulphate aerosol mass concentration at Villum Research Station and Ny-Ålesund from measurements and model output. Model output is shown for simulations BIOMASS (green lines), RSCAV_2 (brown lines), RSCAV_0.5 (yellow lines) and IMP_SCAV_OFF (blue lines) for the years 2017–2018. Monthly means are shown as solid lines, standard deviation in shading.

strength of wet scavenging, while RSCAV_2 decreases aerosol mass. The R_{SCAV} perturbations have different effects on model-observation agreement for BC mass at different times of year depending on the model bias in the baseline run, except at Utqiagvik where the R_{SCAV} changes make only a minimal difference to the BC mass concentrations. At Alert, where the concentrations from BIOMASS are within a factor of 2 of the observations in the first half of the year, RSCAV_2 underpredicts BC mass in these months, while doing little to improve the model overprediction of BC mass in late summer. RSCAV_0.5 performs worse than BIOMASS in all months. At Tiksi, where there is also a model bias in late summer of more than an order of magnitude, RSCAV_2 improves the model performance in the months of June–July and September–November (either side of the model’s summer peak) but increases the model underestimation of BC mass in the months of January–May. RSCAV_0.5 has the opposing effect. Ny-Ålesund is the only station where the BC concentrations from BIOMASS are within a factor of 2 of the observations for the entire year, hence neither R_{SCAV} simulation performs better than BIOMASS, which already reproduces the BC seasonal cycle. RSCAV_0.5 overpredicts BC mass while RSCAV_2 overpredicts BC mass, except for December–January when the BC mass from RSCAV_2 is about 1.5 times lower than that of BIOMASS, improving agreement with the observations.

Sulphate mass concentrations at Villum and Ny-Ålesund are shown in figure 2.14. Unlike for BC aerosol mass, sulphate mass was consistently overpredicted by the model in simulation BIOMASS at both stations and in all months. RSCAV_0.5 therefore performs worse than BIOMASS, increasing the overprediction from a factor of 4–5 to a factor of 10 in the summer months at Villum. The sulphate concentrations from RSCAV_2 are approximately a factor of 2 lower than those from BIOMASS at both sites, improving model-observation agreement. At Villum, RSCAV_2 performs best in

the winter months, with overestimations of about a factor of about 2 remaining in the summer months. At Ny-Ålesund, RSCAV_2 performs best in April and is within a factor of 2 of the observations for the rest of the year.

Output from IMP_SCAV_OFF is also shown in figures 2.13 and 2.14. At all sites, the difference in BC mass between IMP_SCAV_OFF and BIOMASS is less than 50%. The sulphate concentrations from IMP_SCAV_OFF are within about 25% of those from BIOMASS at both Villum and Ny-Ålesund.

2.5.3 Effect of wet scavenging on summer size distribution

In this section we have shown that an ice fraction threshold for wet scavenging of aerosol (simulation ICE_THRESH) leads to some improvements to the Arctic aerosol seasonal cycle, but overall it results in overestimations in sulphate mass. Halving nucleation scavenging efficiency (RSCAV_0.5) similarly creates overestimations of aerosol mass. Doubling the efficiency (RSCAV_2) improves the model agreement with measured sulphate concentrations but causes underestimations of BC at some Arctic sites for certain months of the year. Turning off impaction scavenging (IMP_SCAV_OFF) has little effect compared to the other perturbations, producing sulphate and BC mass within 50% of the simulation with impaction scavenging switched on. Here, we will investigate the effects of these model perturbations on the aerosol size distribution in high Arctic summer, where the model is underestimating the nucleation and Aitken mode concentrations.

Figure 2.15 shows time series of aerosol concentration in the nucleation, Aitken and accumulation modes during AO2018 from measurements and model output. Simulations with weaker wet removal (RSCAV_0.5, IMP_SCAV_OFF, ICE_THRESH) generally have larger accumulation and Aitken mode concentrations than BIOMASS and smaller nucleation mode concentrations, and vice versa for RSCAV_2. The smaller concentrations in the nucleation mode when scavenging is weaker is likely a result of the larger accumulation mode concentrations in those simulations, since the sink of condensable vapours is larger so NPF is suppressed.

Although there are differences in the aerosol concentrations when the scavenging is perturbed, these changes in concentrations during AO2018 are not as large as the changes seen in aerosol mass in the continental Arctic. In the accumulation mode, a stronger scavenging efficiency (RSCAV_2) produces concentrations that are within about a factor of 2 of the unperturbed scavenging rate, with the exception of day 223 when the concentration is about an order of magnitude lower than BIOMASS. Likewise, the weaker scavenging efficiency (RSCAV_0.5) produces accumulation mode concentrations that are up to about a factor of 2 higher than BIOMASS. The concentration from simulation IMP_SCAV_OFF is usually within 50% of that from BIOMASS, indicat-

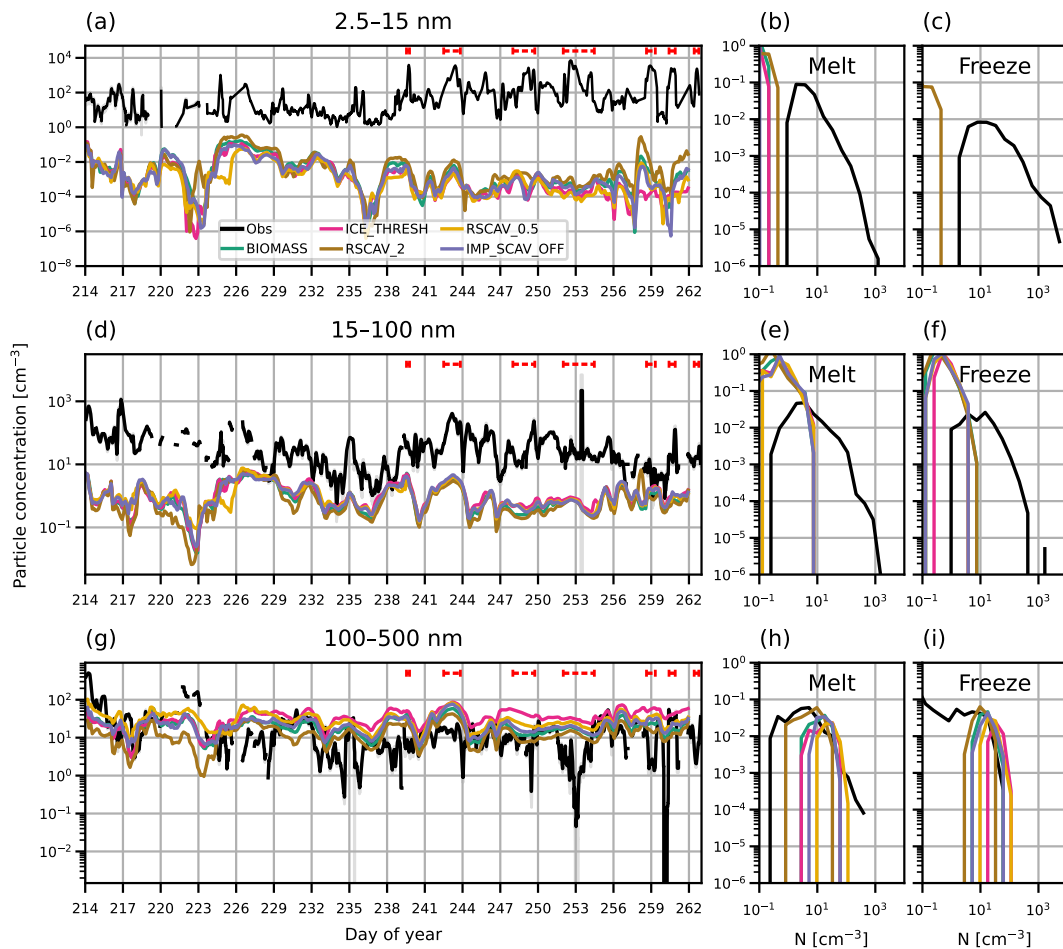


Figure 2.15: Times series and PDFs of aerosol concentration at the surface during AO2018 from observations and model output. Model output is from simulations BIOMASS, ICE.THRESH, RSCAV_2, RSCAV_0.5 and IMP_SCAV_OFF. Observations are shown as 3-hourly mean (black lines) and standard deviation (grey shading). Aerosol concentrations are shown for particles with diameter (a-c) 2.5-15 nm, (d-f) 15-100 nm and (g-i) 100-500 nm. Red dashed lines in (a, d, g) show observed NPF events. PDFs are separated by observed sea ice freeze-up date, 27th August 2018 (day 239).

ing the limited role of below-cloud scavenging in the high Arctic, where precipitation rates are lower than those at lower latitudes. The cloud ice threshold for scavenging (ICE.THRESH) makes little difference to the accumulation mode in the first 10 days of the campaign, but for the rest of the period gives concentrations about a factor of 2 higher than BIOMASS.

In the Aitken mode, the concentrations produced by these perturbations to the scavenging scheme are usually within a factor of 2 of the unperturbed simulation (BIOMASS), though like in the accumulation mode day 223 is an exception. The Aitken concentration in RSCAV_2 is lower than that of BIOMASS on days 221–223 by a factor of 5–10, while the Aitken concentration in RSCAV_0.5 is higher than

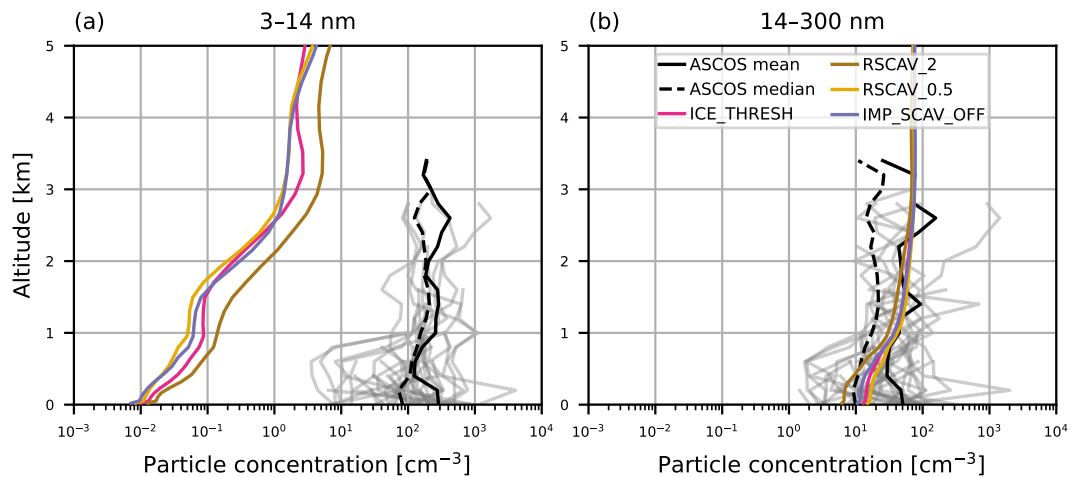


Figure 2.16: Aerosol vertical profiles from model output and ASCOS campaign observations from 2008. Model output is from colocated 2018 monthly mean concentrations from simulations ICE_THRESH, RSCAV_2, RSCAV_0.5 and IMP_SCAV_OFF. Observed concentrations are given as the mean profile from each ASCOS flight (grey lines), overall mean (solid black) and overall median (dashed black). Profiles are for particles with size (a) 3–14 nm, measured during ASCOS using a UCPC and (b) 14–300 nm, measured using a CPC (particles greater than 14 nm) and a CLASP instrument (particles greater than 300 nm).

BIOMASS by about a factor of 5. Since these days are from the transit period of the campaign, they correspond to concentrations from lower latitudes than the drift period, which took place close to the North Pole. The stronger effect of RSCAV_2 and RSCAV_0.5 on these days could therefore suggest that the scavenging efficiency has more of an effect at lower latitudes than it does in the high Arctic.

In the nucleation mode, the concentrations from RSCAV_2, RSCAV_0.5, ICE_THRESH and IMP_SCAV_OFF are all within a factor of 2–5 of BIOMASS, again with the exception of day 223 and also the last few days of the campaign (from approximately day 257 onwards). The nucleation concentration in RSCAV_2 is 2 orders of magnitude greater than BIOMASS on day 223 and reaches up to an order of magnitude greater at the end of the campaign. The opposite is true for ICE_THRESH and RSCAV_0.5. ICE_THRESH produces nucleation concentrations up to 2 orders of magnitude smaller than BIOMASS on days 223 and 257 onwards, while RSCAV_0.5 has concentrations 2 orders of magnitude lower than BIOMASS on day 225 and 260. As for the other modes, turning off impaction scavenging in IMP_SCAV_OFF has less of an effect on the nucleation concentration.

Aerosol profiles from ASCOS measurements and August 2018 model output is shown in figure 2.16. Similarly to the AO2018 aerosol concentrations, the simulations with weaker scavenging (RSCAV_0.5, ICE_THRESH, IMP_SCAV_OFF) have higher concentrations of 14–300 nm particles than BIOMASS and lower concentrations of 3–14 nm particles, and vice versa for stronger scavenging (RSCAV_2). Nucleation mode concen-

trations from simulation RSCAV_2 are about 50% higher than BIOMASS throughout the profile while simulations IMP_SCAV_OFF and RSCAV_0.5 are both about 50% lower. The profile from ICE_THRESH follows that of BIOMASS in the lowest 1 km and is slightly lower aloft, though still exceeding the concentrations from IMP_SCAV_OFF and RSCAV_2. In the accumulation mode, the difference caused by the different scavenging rates is greatest at the surface, with concentrations converging to the BIOMASS profile as altitude increases. The difference between halved and doubled scavenging efficiency (RSCAV_2 relative to RSCAV_0.5) is approximately a factor of 2–3 in the accumulation mode concentration at the surface.

2.6 Discussion and conclusion

The model underestimates the concentration of sub-100-nm diameter particles in the high Arctic summer. The nucleation mode particle concentration at the surface is at least an order of magnitude too low compared to AO2018 observations, sometimes underestimating observed concentrations by as much as 5 orders of magnitude. The surface Aitken mode concentration is also underestimated by up to 3 orders of magnitude. The model performs better at simulating the surface accumulation mode concentration. The accumulation mode concentration in the model is generally within the range of the observations, but does not capture the lowest concentrations (less than 1 cm^{-3}) seen in the time series of AO2018 observations.

We have used pan-Arctic observations of aerosol mass to investigate the possible role of aerosol emissions or aerosol removal in creating the model bias in the summer size distribution. We have tested the sensitivity to carbonaceous particle emissions from biomass burning and marine organics as well as the scavenging rates in the model. The results of these investigations are summarised in the rest of this section.

The model simulates large peaks in black carbon mass at 3 Arctic sites during July and August that are not present or are smaller in magnitude in the observations. Such summer peaks in black carbon mass are likely related to boreal forest fires. Adjusting the biomass emissions in the model so that they are from climatologies rather than a single year improves the seasonal cycle, though biases remain.

Adjusting the mean emission size of primary marine organic carbon particles in the model from 160 nm to 20 nm (considered a lower limit on the range of possible sizes) is effective at creating a source of sub-100 nm particles in the Arctic region. The concentration of the nucleation and Aitken modes at the surface in the central Arctic increases by up to 6 orders of magnitude compared to the default primary marine organic emissions. However, despite these increased particle concentrations, the primary marine organic source does not capture the behaviour of sub-100 nm particles in observations from the Arctic Ocean and is not consistent with observed particle fluxes from

the surface. Firstly, the particle flux in the perturbed simulation is about 500 times greater than the default scheme, since we reduce the mean particle size by a factor of 8 without changing the mass flux. In the central Arctic Ocean, the resulting particle flux is at least a factor of 20 greater than observed fluxes from open leads in the pack ice. These differences between simulated and measured particle fluxes are unsurprising given that we perturb the size of emitted particles, whereas Leck and Bigg (2010) and others have proposed a particle break-up process that alters the size (and number concentration) of the particles after they have been emitted. The 20-nm diameter particle source also overestimates the Aitken mode concentration measured at the surface during AO2018. Secondly, during the sea ice freeze period of the AO2018 campaign, when iodine acid was observed to drive new particle formation events, the perturbed primary marine simulation underestimates the peaks in the nucleation mode concentration by roughly 3 orders of magnitude, suggesting that a secondary source needs to be considered in this regime and a primary source alone would not be sufficient to simulate the observed aerosol concentrations. Finally, the aerosol vertical profiles from the ASCOS campaign in 2008 show that despite higher concentrations in the boundary layer, the marine organic source decreases nucleation mode particle concentrations aloft and underestimates the observations in the free troposphere. This could be because the extra particles in the boundary layer promote condensational growth at lower latitudes, increasing the depletion of vapours and therefore leading to less transport of vapours or secondary particles through the free troposphere to the Arctic, creating a reduction of small particles in the free troposphere.

Simulated sulphate and black carbon mass is sensitive to in-cloud scavenging rates with below-cloud scavenging having only a minimal effect on mass concentrations. Increasing the efficiency of in-cloud scavenging reduces model overestimations of sulphate at Villum and Ny-Ålesund, though it causes underestimations of black carbon at some sites for some months of the year. Conversely, decreasing the scavenging efficiency causes overestimations in the modelled sulphate concentrations.

The use of cloud phase in the default UKESM wet scavenging scheme appears to perform better than the previous version of the same scheme in GLOMAP which had no such cloud phase dependence and had to be adjusted by Browse et al. (2012) to include a temperature dependence in the scavenging rate, with the aim of suppressing scavenging from ice or mixed-phase clouds. When we use the cloud ice fraction to suppress scavenging in the model, the resulting scavenging is too weak and leads to overestimation of aerosol mass at Arctic ground stations. However, because of differences in the ice fraction at different times of year, there are improvements to the simulation of the seasonal cycle when using the ice fraction threshold to suppress scavenging. Scavenging is suppressed more in winter than in summer, increasing the simulated sulphate mass at Villum and Ny-Ålesund in winter and spring relative to the summer months.

Despite the effect that scavenging evidently has on aerosol mass in the continental Arctic, the effect on the high Arctic summer size distribution is minimal. Changes to the accumulation mode concentration are visible at the surface, but still no simulation is routinely able to capture the lowest accumulation mode concentrations of 1 cm^{-3} and below. This is therefore likely a feature of using output from a global, coarse resolution model to compare to point measurements. The large scale of the model gridboxes in the model cannot resolve the variation in meteorological conditions that lead to such fluctuations in the accumulation mode concentration via aerosol removal. The model results also show that while there is some evidence of the nucleation and Aitken mode concentrations responding to changes in the accumulation mode, the magnitude of the underestimations of these small particles are not consistent with a bias in aerosol removal alone. The strong model underestimations of the nucleation and Aitken mode concentrations are relatively unaffected by changes to the model scavenging rates. Along with the results from the primary marine organic simulation, this suggests there is a missing source of aerosols, likely related to secondary sources.

Although we have not been able to explain the source of the model bias in sub-100 nm particle concentrations in the high Arctic summer, these simulations point to areas of the model that warrant further attention. Firstly, the use of a threshold for cloud ice water fraction in the scavenging code improves the seasonal cycle while producing absolute values of sulphate mass concentration that are too high compared to observations. A stronger in-cloud scavenging efficiency improves the sulphate concentrations in the model compared to observations. It is therefore possible that the use of the ice water fraction combined with a higher efficiency in the scavenging rate could produce more accurate monthly mean sulphate mass concentrations than either perturbation on their own. Secondly, the marine carbon particle flux rates from the model suggest that the relationship between open water emissions and emissions from open leads in sea ice is not captured. During AOE96, particle fluxes from open water were 20-50 times higher than fluxes from an open lead. In the model, the open water emissions are only greater than the pack ice region by a factor of 4. It is unsurprising that the model does not capture the difference in emissions between the different environments, since the sea spray parameterisations in the model are global and do not differentiate between emissions from open water and emissions from sea ice regions. The marine organic carbon flux in a gridbox is simply scaled linearly by the open water fraction for that gridbox, with no effect of the smaller fetch in the ice region. The difference in emissions between these two environments is important for the Arctic aerosol budget since it implies a sensitivity of marine aerosol emissions to changes in the ice. The pack ice region is retreating, while the extent of the marginal ice zone is expanding in the summer months. If the primary marine emissions are dependent on the ice fraction in non-linear ways, there could be feedback effects from the reduction of sea ice which the model is currently not

capturing. These potential sources of model biases should be areas of further study in the future. Since these processes have not improved the simulation of the nucleation and Aitken modes in the high Arctic summer, further investigation is beyond the scope of this thesis. Because this chapter has ruled out primary sources or aerosol removal as sources of the model-observation bias in the concentration of small particles in the Arctic, the next chapter will focus on secondary sources. In particular, we examine the effect of new particle formation driven by iodine.

Chapter 3

Late summer transition from a free-tropospheric to boundary layer source of Aitken mode aerosol in the high Arctic

Abstract

In the Arctic, the aerosol budget plays a particular role in determining the behaviour of clouds, which are important for the surface energy balance and thus for the region's climate. A key question is the extent to which cloud condensation nuclei in the high Arctic summertime boundary layer are controlled by local emission and formation processes as opposed to transport from outside. Each of these sources is likely to respond differently to future changes in ice cover. Here we use a global model and observations from ship and aircraft field campaigns to understand the source of high Arctic aerosol in late summer. We find that particles formed remotely, i.e. at lower latitudes, outside the Arctic, are the dominant source of boundary layer Aitken mode particles during the sea ice melt period up to the end of August. Particles from such remote sources, entrained into the boundary layer from the free troposphere, account for nucleation and Aitken mode particle concentrations that are otherwise underestimated by the model. This source from outside the high Arctic declines as photochemical rates decrease towards the end of summer, and is largely replaced by local new particle formation driven by iodine acid emitted from the surface and associated with freeze-up. Such a local source is consistent with strong fluctuations in nucleation mode concentrations that occur in September. Our results suggest a high Arctic aerosol regime shift in late summer, and only after this shift do cloud condensation nuclei become sensitive to local aerosol

processes.

3.1 Introduction

Modelling studies have demonstrated the importance of new particle formation for the budget of Arctic aerosol. Merikanto et al. (2009) and Gordon et al. (2017) used the global aerosol model GLOMAP to show the importance of new particle formation on a global scale. Both studies indicate that a high fraction (greater than 80%) of particles and CCN in the Arctic are derived from new particle formation. While the model configuration in Merikanto et al. (2009) only included parameterisations based on H_2SO_4 , the model used by Gordon et al. (2017) included parameterisations for neutral and ion-induced binary (H_2SO_4 -water) and ternary (H_2SO_4 -ammonia-water) new particle formation, new particle formation from organic molecules and H_2SO_4 , and pure organic new particle formation driven by highly oxygenated molecules (HOMs). The authors found that a significant fraction (greater than 40%) of Arctic CCN originate from secondary organic aerosol, including HOMs. Karl et al. (2012) used an aerosol dynamics model to study new particle formation events that were observed during the summers of 1996, 2001 and 2008. H_2SO_4 and organic vapours were used in the model to drive new particle formation events. Simulations of new particle formation driven by H_2SO_4 followed by growth from condensation of organic vapours were able to reproduce the particle size distributions observed during new particle formation events. The inclusion of organic vapours as a driver of new particle formation led to an overprediction in the concentration of particles, though the authors note significant uncertainty in the sources and concentrations of organic vapours in the high Arctic. Croft et al. (2019) used a chemical transport and aerosol microphysics model to show that condensation of secondary organic vapour played a key role in particle formation events in the Canadian Arctic during the summer. The vapours were assumed to have a marine, biogenic source. Browse et al. (2014), using GLOMAP to investigate the response of Arctic aerosol to sea ice loss, found that boundary layer new particle formation driven by H_2SO_4 was required to explain measured CCN concentrations in the high Arctic during summer.

Boundary layer new particle formation as a source of Arctic aerosol implies a potentially high sensitivity of the local aerosol budget to the changing climate. Any future increase in the extent of open water and the marginal ice zone in summer will affect the emission of aerosol and precursor gases to the atmosphere. Dall'Osto et al. (2017) and Dall'Osto et al. (2018) have found a positive correlation between frequency of new particle formation events and the extent of open water near Svalbard and Greenland, respectively. Such an increase in occurrence of new particle formation with sea ice loss could be expected to increase CCN concentrations in the Arctic under future warmer conditions, though this is far from certain since changing sea ice extent is not the only

controlling factor. Gilgen et al. (2018) found that reduction of sea ice by the year 2050 leads to increased emissions of DMS in a global aerosol-climate model. The increased DMS emissions, along with increased sea spray aerosol and meteorological changes, cause higher cloud drop number concentrations over the Arctic Ocean. This is in line with results from another global model study, Struthers et al. (2011), which used an atmospheric climate model to investigate the response of sea spray aerosol to sea ice loss. They found a strong increase in sea salt emissions and thus higher cloud drop concentrations, but the effect on clouds and energy budget was uncertain due to poor model representations of aerosol-cloud interactions. In contrast to these studies, the results from Browse et al. (2014) suggest that interactions between aerosol particles of different sizes could lead to a suppression of new particle formation in an ice-free Arctic summer. Their results showed an increase in the sink of condensable vapours due to stronger emission of sea spray aerosol from the open water, resulting in a decrease in the concentration of smaller particles from new particle formation. In addition, the growth of sea spray particles from condensation of vapours shifted the size distribution to larger sizes, leading to enhanced scavenging by precipitation and a decrease in drop concentrations.

The conflicting results from Browse et al. (2014), Gilgen et al. (2018) and Struthers et al. (2011) highlight the difficulty in modelling the Arctic aerosol budget and how it might change in future. Uncertainties in model parameterisations stem from the knowledge gaps in processes controlling the aerosol budget, and cause differences in climate projections from different model set-ups. For example, the sea spray parameterisations used in the Gilgen et al. (2018) and Struthers et al. (2011) studies include empirical representations of the effect of temperature on the sea spray aerosol size distribution, while the parameterisation used in the Browse et al. (2014) study does not. This could be a cause of the discrepancy in their predictions of sea spray aerosol response to sea ice loss, though this has not been studied. The studies also differ in their treatment of primary marine organic emissions, with only the Browse et al. (2012) study including such a source. Some field studies from the Arctic have indicated the importance of primary marine organics in the region (Leck and Bigg, 2010; Karl et al., 2013), as well as raising questions about possible recycling mechanisms of particles after they are emitted (i.e. through ageing or the particle break-up theory, Lawler et al., 2021). The open questions surrounding primary marine emissions complicate modelling of Arctic new particle formation due to the the sink of condensable vapours from larger particles. Models with size-resolved aerosol microphysics and chemistry are better equipped to study these questions than bulk, single-moment models considering total mass only.

Aitken mode particles can act as CCN in the Arctic, which increases the influence of new particle formation over the Arctic aerosol budget. Karlsson et al. (2022) used measurements of cloud residual particles (i.e. particles obtained by drying cloud droplets

or ice crystals) from the high Arctic to show that Aitken mode particles were acting as CCN during a period of frequent boundary layer new particle formation. Observations of aerosol size distributions in and out of cloud in sub-Arctic Finland showed that on average 30% of Aitken particles (defined as 25-95 nm) were activated to form droplets (Komppula et al., 2005). In Svalbard, measurements of cloud residuals (Karlsson et al., 2021) and cloud drop number concentrations (Koike et al., 2019) have been used to show the activation of particles smaller than 50 nm diameter during periods of high supersaturation, such as when updraft speeds are high or when accumulation mode concentrations are low. Results from parcel models and large-eddy simulation (LES) models are in agreement with the observations that Aitken particles can act as CCN (Bulatovic et al., 2020; Pöhlker et al., 2021). Activation of Aitken particles means that particles formed by new particle formation and subsequent growth may only need to grow up 20-50 nm diameter to act as CCN in Arctic clouds, making it more plausible that such particles could survive long enough in the atmosphere to be important for cloud formation.

Recent observations from the high Arctic provide a new opportunity to explore the questions surrounding the source of summertime aerosol. The Arctic Ocean 2018 (AO2018) expedition took place in August and September 2018 between Svalbard and the North Pole (Vüllers et al., 2020). The observed properties and behaviour of the aerosol challenge our current understanding of aerosol sources and sinks. Firstly, mass spectrometry measurements clearly show that iodic acid is the main driver of new particle formation events, which occur primarily during sea ice freeze-up (Baccarini et al., 2020). This process was not included in previous large-scale modelling studies. Secondly, the long time series of particle concentrations and size distributions provide an opportunity to understand how sources and sinks are related to the melting/freezing cycle and changes in photochemistry. In particular, the observations show a distinct transition in aerosol behaviour in late summer, when the iodic acid new particle formation events begin to take place. Here we aim to interpret this change in behaviour in terms of changes in the dominant aerosol sources.

In this study we used measurements from AO2018 to evaluate the Arctic aerosol budget in the global climate model UKESM1. We compared the accuracy of simulations with new particle formation in the boundary layer to that of simulations with new particle formation in the free troposphere. We also introduced an iodic acid new particle formation scheme to the model to investigate iodic acid as an Arctic aerosol source compared to other components of the Arctic aerosol budget. The observational datasets are introduced in Sect. 3.2. The model is described in Sect. 3.3, including the different new particle formation schemes and our approach to the inclusion of iodic acid. Results are presented in Sect. 3.4 and discussed in Sect. 3.5.

3.2 Observations

In addition to measurements from the Arctic Ocean 2018 (AO2018) and Arctic Summer Cloud Ocean Study (ASCOS) campaigns introduced in chapter 2, we will use measurements from the Atmospheric Tomography Mission (ATom). ATom was a multi-year flight campaign that used the NASA DC-8 aircraft to study the effects of air pollution on the chemistry of the atmosphere. There were four legs of ATom, each carried out in a different season in different years. Here, we use measurements taken during the first leg, which took place in summer 2016. Measurements were taken over a wide range of latitudes and altitudes. We only use measurements taken north of 60°N .

Aerosol size distributions were measured during ATom using a nucleation-mode aerosol size spectrometer (NMASS), an ultra-high-sensitivity aerosol size spectrometer (UHSAS) and a laser aerosol spectrometer (LAS). The full set of ATom aerosol measurements are presented in Brock et al. (2019). Aerosol size distributions are available for particles between approximately 3 nm and 3.5 μm diameters.

Note that the AO2018, ASCOS and ATom campaigns use instruments with different ways of sizing particles. The DMPS measures the electrical mobility diameter of particles. The CPCs and NMASS measure particles based on the critical diameter for droplet nucleation at the instrument’s operating supersaturation. The OPC, UHSAS and LAS all rely on optical methods to measure particles, meaning they measure the optical equivalent diameter of particles. No attempt has been made to convert from optical equivalent diameter to mobility diameter. Such a conversion would require information about the refractive indices of the particles measured by the optical instruments, which is not available.

3.3 Model description

For this chapter, we use UKESM in the set-up introduced in chapter 2. We showed that changing the source of biomass burning emissions from 2014 data to 1995–2004 data produced more accurate black carbon mass concentrations at Arctic ground stations, so we continue using the 1995–2004 emissions here. This section describes further model perturbations that we make in this chapter.

3.3.1 Ageing of insoluble particles

The default assumptions in UKESM about particle ageing have a very substantial effect on Arctic aerosol, particularly where NPF is a major source of Aitken mode particles. Particle ageing in a model is the transfer of insoluble particles into the soluble particle modes after condensation of water-soluble material. In UKESM, sources of insoluble carbonaceous particles are biofuel and biomass burning emissions (mean diameter 150

nm), fossil fuel burning emissions (mean diameter 60 nm) and primary marine organic carbon emissions (mean diameter 160 nm). By default, the aged mass from the insoluble mode is moved into the soluble Aitken mode (Mulcahy et al., 2020). However, the mean diameter of the insoluble mode does not usually correspond to the size limits of the soluble Aitken mode, and this can lead to undesirable behaviour in the model. Thus, when mass from the insoluble mode is moved into the soluble Aitken mode, it will typically increase the mean diameter of the soluble mode beyond its upper limit (100 nm). When small particles enter the Aitken mode following growth of nucleation mode particles, they are artificially strongly depleted because “mode merging” (Mann et al., 2010) requires that their mass is averaged with the larger particles already existing in the Aitken mode. This combination of assumptions (the size of aged particles and mode merging) is adequate for reproducing size distributions in the mid-latitudes, where anthropogenic and fire emissions are a more dominant source. However, our early simulations showed that this method has a very substantial effect in the Arctic where NPF is occurring in air that has aged during long-range transport from low latitudes to the Arctic (see appendix A.1). In particular, we found that the particle size distribution was insensitive to the NPF rate. We therefore altered the model such that aged carbonaceous particles are moved directly into the soluble accumulation mode (100 – 500 nm), as is appropriate for their diameter. All simulations in this chapter use the altered ageing scheme, we therefore refer to a CONTROL simulation in our comparisons. CONTROL is otherwise the same as simulation BIOMASS from chapter 2.

3.3.2 New particle formation schemes

UKESM includes binary homogeneous nucleation of water and sulphuric acid (H_2SO_4) using the parameterisation of Vehkamäki et al. (2002). In this study, we included two additional NPF formation schemes in the model. We simulated nucleation of H_2SO_4 in the boundary layer (BL) by cluster activation as described by Kulmala et al. (2006) (hereafter K06). We simulated organically mediated H_2SO_4 nucleation using the parameterisation of Metzger et al. (2010) (hereafter M10). Simulations are labelled by their NPF scheme and the region of the atmosphere the scheme is applied to (e.g. BL for a scheme switched on in the boundary layer only or FT for a scheme switched on in the free troposphere only).

The formation rates of 1.5 nm clusters, J_* , used by M10 and K06 are given in $\text{cm}^{-3} \text{s}^{-1}$ by

$$J_{*,K06} = k_{K06}C_{SA} \quad (3.1)$$

$$J_{*,M10} = k_{M10}C_{SA}C_{secorg} \quad (3.2)$$

where k_{K06} is 10^{-6} s^{-1} , k_{M10} is $10^{-13} \text{ cm}^3 \text{ s}^{-1}$, and C_x are the concentrations of the precursor vapours in cm^{-3} . The 3 nm particle formation rate is calculated from the 1.5 nm cluster formation rates using the method from Kerminen and Kulmala (2002), which accounts for growth of clusters and loss to existing particles.

It should be noted that these two BL NPF schemes use empirical parameterisations that have not been developed with or tested against data from the Arctic. Moreover, the parameterisations only consider the influence of H_2SO_4 and secondary organic vapours. MSA and ammonia are not included in UKESM and thus are not modelled as NPF precursors in this study. These omissions are potential sources of bias given the importance of MSA and ammonia in the Arctic (Willis et al., 2018; Beck et al., 2020).

As we show below, entrainment of nucleation mode aerosol from the FT is an important process. To investigate the role of FT entrainment as a source of surface particles in the high Arctic, we ran an additional sensitivity test with an imposed NPF rate in the low FT (simulation M10_Prsc). A rate of $10^{-2} \text{ particles cm}^{-3} \text{ s}^{-1}$ was used for altitudes above the top of the BL and below 7.5 km, and for latitudes north of 80°N . Since this rate is higher than what the M10 scheme typically produces, it allows us to investigate the sensitivity of the surface concentrations to a strong free troposphere source.

3.3.3 Iodic acid

An empirical model for the steady-state concentration of iodic acid has been produced from observations taken in the high Arctic (Baccarini et al., 2020). The concentration in cm^{-3} , C_{IA} , is given by

$$C_{IA} = \frac{E}{v_{dep} + h \cdot CS} \quad (3.3)$$

where E is the emission rate of iodine atoms in $\text{cm}^{-2} \text{ s}^{-1}$, v_{dep} is the dry deposition velocity of iodic acid in cm s^{-1} , h is the surface mixed layer height in cm and CS is the condensation sink due to existing aerosols, given in s^{-1} . It was observed during AO2018 that fog and cloud droplets acted as a strong sink of the iodic acid, however we do not account for that here since the parameterisation of clouds in the coarse resolution model gridboxes is unlikely to be representative of conditions at the ship.

We used Eq. (3.3) to diagnose the steady-state concentration of iodic acid in model gridboxes at each timestep. The iodic acid was then used as a precursor to drive NPF. The dry deposition velocity of iodic acid was calculated by the model assuming a diffusion constant equal to that of H_2SO_4 . The condensation sink due to existing aerosols was calculated during model runs using the aerosol size distribution produced by the model. We use the modelled dry aerosol diameter in the condensation sink calculation, meaning that the effects of water uptake by aerosol are not included. For the surface mixed layer height, we take the BL height calculated by the UM. Finally, we use a value of $5.21 \times 10^6 \text{ cm}^{-2} \text{ s}^{-1}$ for E , which is approximately equal to the median of the distribution of E measured by Baccarini et al. (2020).

The concentration of iodic acid was observed to increase towards the end of summer, during the sea ice freeze-up (Baccarini et al., 2020). It is thought that the freezing of sea water can trigger the emission of iodine from the surface. To incorporate this behaviour into UKESM, we calculate the concentration of iodic acid in gridboxes where sea ice fraction is non-zero and where the surface temperature is less than $-5 \text{ }^\circ\text{C}$. Although the observed freeze-up date is defined as the day when the 14-day running mean of surface temperature reaches $-2 \text{ }^\circ\text{C}$ (the temperature at which sea water freezes), we found that $-5 \text{ }^\circ\text{C}$ acted as a better threshold for ice freeze-up in the model. This is because there is a cold bias in the model such that when the observed 14-day running mean temperature reaches $-2 \text{ }^\circ\text{C}$, the modelled surface temperature is closer to $-5 \text{ }^\circ\text{C}$. The calculated concentration of iodic acid is then equally distributed from the surface to the BL top. This is equivalent to assuming that the lifetime of iodic acid is long enough for the gas to be mixed throughout the BL.

A direct mechanism linking the freeze-up to iodine emissions has not yet been identified. However, our results would remain valid even if the two processes were not directly related. In fact, the surface temperature threshold used in the model is a good tracer for the summer to autumn transition, which has been associated with higher iodine concentration in the Arctic (Sharma et al., 2019; Baccarini et al., 2020)

The iodic acid particle formation rate at 3 nm is calculated using the Kerminen and Kulmala (2002) method as for the H_2SO_4 activation and organically mediated schemes, using a kinetic rate of iodic acid cluster formation. This is in line with recent results from cloud chamber experiments (He et al., 2021). The cluster formation rate in $\text{cm}^{-3} \text{ s}^{-1}$ is given by

$$J_{*,IA} = k_{IA} C_{IA}^2 \quad (3.4)$$

where $k_{IA} = 10^{-13} \text{ cm}^3 \text{ s}^{-1}$. The mass created from HIO_3 -driven new particle formation is added to the sulphate model component.

3.3.4 Secondary organic vapours

Assumptions about the production of secondary organic aerosol (SOA) material have a large effect on modelled Arctic aerosol. SOA is created in the model by the oxidation of monoterpenes by ozone, the hydroxyl radical and the nitrate radical (Spracklen et al., 2006). These reactions produce SOA on the timescale of hours. This is a simplification of the process, since in reality there are many chemical species and reaction pathways involved in the production of SOA, which operate on a range of timescales and produce a range of volatilities. In particular, some SOA precursor species have a longer lifetime than monoterpene and can therefore be transported further in the atmosphere before forming SOA and condensing on existing aerosol. In the model, most monoterpene is oxidized close to the source region (e.g. boreal forests) and quickly condenses onto existing particles, therefore the concentration of SOA precursor gases is very low in the central Arctic; as a consequence, NPF involving organic vapours is extremely weak. To investigate the effect of these assumptions on Arctic NPF, we ran sensitivity simulations where the oxidation rate of monoterpene was reduced by a factor of 100. The labels of these simulations use the suffix `_SecOrg`.

A description of all model simulations presented in this chapter is given in table 3.1. When comparing model output to observations of surface aerosol concentration, we use the overlap index defined in Pastore and Calcagnì (2019) to quantify the similarity between the distribution in aerosol concentration from observations and different model simulations. For two probability density functions $A(x)$ and $B(x)$, the overlap index $\eta(A, B)$ is defined as

$$\eta(A, B) = \int \min[A(x), B(x)] dx \quad (3.5)$$

which can be thought of as integrating the area where the distributions overlap. If the two distributions overlap completely, the entire area under the distribution will be integrated so the index will be 1, whereas if they do not overlap at all, no area will be integrated and the index will be 0. Overlap indices closer to 1 therefore indicate simulations with good model-observation agreement in terms of the magnitude and variability of the two time series even if individual peaks and troughs do not match temporally. In our case, we apply the overlap index to discrete distributions of binned aerosol concentration, so the integral is calculated as the probability density function in each bin multiplied by the bin width, summed over all bins.

Table 3.1: Description of simulations.

Simulation	Description
CONTROL	Model set-up based on BIOMASS simulation from 2, with additional changes to the aerosol ageing scheme. Binary H ₂ SO ₄ -water vapour NPF parameterised as per Vehkamäki et al. (2002).
K06_BL	Additional BL H ₂ SO ₄ NPF parameterised by Kulmala et al. (2006)
M10_ALL	Organically-mediated NPF in all model levels, using Metzger et al. (2010)
M10_BL	Organically-mediated NPF in the BL, using Metzger et al. (2010)
M10_Prsc	As M10_ALL, but with a prescribed NPF rate of $10^{-2} \text{ cm}^{-3} \text{ s}^{-1}$ between the BL top and 7.5 km and north of 80°N
IA_BL	Additional BL NPF driven by IA
IA_BL_M10_ALL	As M10_All but with additional BL NPF driven by IA
M10_BL_75N, M10_BL_80N, M10_BL_85N	Additional NPF in the BL using Metzger et al. (2010) for grid-boxes north of 75°N, 80 °N or 85 °N respectively
M10_Prsc_60N	As M10_Prsc, but the rate is prescribed for gridboxes north of 60°N
XXX_SecOrg	Additional change to oxidation of monoterpenes as described in section 3.3.4

3.4 Results

3.4.1 Iodic acid concentration

Figure 3.1 shows a time series and PDF of surface HIO₃ concentration from observations and model output. To collocate the model output with the ship, we take the model gridbox nearest the ship’s position. In the observations, the surface HIO₃ concentration is lower in the melt period (before day 239) than in the freeze period (after day 239). The surface concentration in the freeze period has a baseline of approximately 10^6 cm^{-3} and peak values 5–6 times higher lasting on the order of hours, whereas in the melt period the concentration reaches 10^6 cm^{-3} only for brief periods, such as on day 228. The periods of peak surface concentration in the freeze period correspond to observed NPF events.

In the model, HIO₃ is only emitted when the surface temperature is -5 °C or less. The modelled temperature reaches this threshold on approximately day 236 at the ship’s position, such that the model starts to emit HIO₃ at a similar time to the observed freeze-up onset (day 239), when HIO₃ concentrations were observed to increase at the ship. After HIO₃ starts to be emitted in the model, the empirical scheme we use for HIO₃ production consistently calculates surface HIO₃ concentration to be the same order of magnitude as the observations. The PDF in Fig. 3.1(b) is for the freeze season only, i.e. day 239 onward. The observed distribution of surface HIO₃

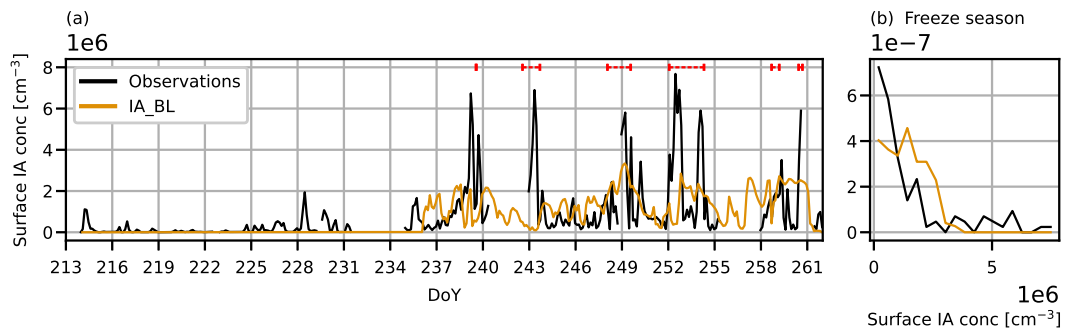


Figure 3.1: Times series and PDF of surface iodic acid concentration during AO2018 from observations and model output. Model output is from simulation IA_BL (orange lines). Observations are shown as 3-hourly mean (black lines). Red dashed lines in (a) show periods of observed NPF events. PDF of concentration is for freeze season only, i.e. after 27th August 2018 (day 239).

concentration is broadly captured, though the model does not reproduce the highest or lowest observed concentrations. This is likely to be because the model does not resolve the spatially heterogeneous sea ice state (which controls the emissions of iodic acid) nor the variability in clouds and fog, which control iodic acid scavenging as well as influencing the condensation sink due to existing aerosols.

3.4.2 Effect of NPF in the boundary layer

Time series of particle concentrations

Figure 3.2 shows time series and PDFs of surface aerosol concentration in three particle size ranges from the AO2018 observations and for simulations CONTROL, K06_BL, M10_BL, IA_BL and IA_BL_SecOrg. Observations are from the ship (approximately 15 m above the surface) and model output is for the first model level, between approximately 0 and 37 m.

A time series of the measured nucleation mode (2.5–15 nm diameter) particle concentration during AO2018 is shown in Fig. 3.2 (a). Periods where iodic acid NPF events were observed are marked with red dashed lines. There is a marked difference in the behaviour of the nucleation mode concentration before and after the onset of sea ice freeze-up (27th August 2018, day 239). In the melt period (up to day 239), the nucleation particle concentration rarely exceeds 100 cm^{-3} and is usually between $1\text{--}10 \text{ cm}^{-3}$. The NPF events, which occurred after the freeze-up began in the vicinity of the ship on day 239, are associated with peaks in the nucleation mode particle concentration lasting a few hours, causing fluctuations in particle concentration between approximately 10 and 10^4 cm^{-3} , consistent with a strong local source.

The modelled nucleation mode particle concentration is underestimated in simulations CONTROL, IA_BL and IA_BL_SecOrg in the melt period, while the inclusion of

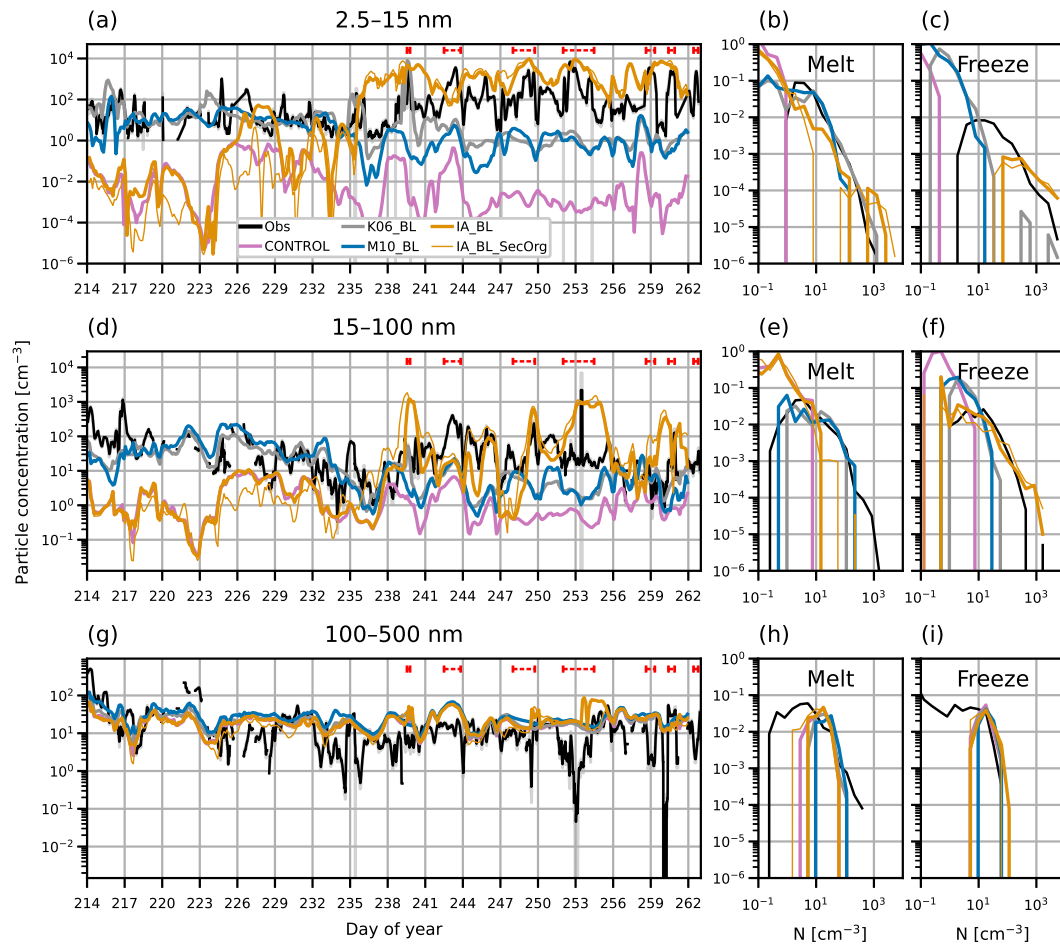


Figure 3.2: Times series and PDFs of surface aerosol concentration during AO2018 from observations and model simulations with various boundary layer NPF mechanisms. Model output is from simulations CONTROL (pink lines), K06_BL (grey lines), M10_BL (blue lines), IA_BL (thick orange lines) and IA_BL_SecOrg (thin orange lines). Observations are shown as 3-hourly mean (black lines) and standard deviation (grey shading). Aerosol concentrations are shown for particles with diameter (a-c) 2.5-15 nm, (d-f) 15-100 nm and (g-i) 100-500 nm. Red dashed lines in (a, d, g) show observed NPF events. PDFs are separated by observed sea ice freeze-up date, 27th August 2018 (day 239).

HIO₃ NPF means that IA_BL and IA_BL_SecOrg perform better in the freeze period than during the melt. The nucleation mode concentration in CONTROL varies from roughly 10^{-6} to 10^{-1} cm^{-3} and is usually at least an order of magnitude lower than observed throughout the whole period. In contrast, simulations with HIO₃ (IA_BL and IA_BL_SecOrg) produce nucleation mode concentrations of roughly the correct order of magnitude during the freeze period (day 239 onwards), with a distinct change in concentration and behaviour around day 235. However, the lack of HIO₃ emissions during the melt period means that the model continues to underestimate the concentration by several orders of magnitude. The model underprediction of nucleation mode particle concentration in the melt period is an indication that HIO₃ NPF is not the only part of

Table 3.2: Overlap indices calculated for the PDFs of nucleation, Aitken and accumulation aerosol concentrations from observations and each simulation, measured at the surface. PDFs are separated into the melt and freeze periods before overlap indices are calculated. Bold text indicates the greatest overlap index in each mode for the melt and freeze periods.

Simulation	Nucleation		Aitken		Accumulation	
	Melt	Freeze	Melt	Freeze	Melt	Freeze
CONTROL	0.01	0.00	0.31	0.12	0.57	0.64
K06_BL	0.75	0.12	0.72	0.31	0.53	0.63
M10_ALL	0.72	0.06	0.71	0.40	0.52	0.55
M10_BL	0.73	0.05	0.73	0.34	0.50	0.55
M10_Prsc	0.35	0.52	0.75	0.37	0.51	0.55
M10_Prsc_SecOrg	0.20	0.61	0.64	0.66	0.57	0.55
IA_BL	0.25	0.47	0.35	0.70	0.58	0.58
IA_BL_SecOrg	0.13	0.40	0.30	0.59	0.65	0.69
IA_BL_M10_ALL	0.63	0.51	0.69	0.77	0.55	0.56

the regional aerosol budget that needs consideration to produce an accurate simulation. Simulations K06_BL and M10_BL both use BL NPF schemes and have higher nucleation mode concentrations than CONTROL as a result. In the melt period, K06_BL and M10_BL both consistently simulate nucleation mode concentrations of the same order of magnitude as the observations. Interestingly, the two simulations have very similar nucleation mode concentrations despite the differences in the NPF schemes. K06_BL occasionally simulates higher nucleation mode concentrations than M10_BL, most notably on days 239–243. In the freeze period, K06_BL and M10_BL still underestimate the nucleation mode concentration despite simulating higher concentrations than CONTROL.

Overlap indices for the PDFs of observed surface aerosol concentration and modelled concentration from all simulations are given in Table 3.2. The underestimation of nucleation mode concentration by simulation CONTROL is highlighted by the fact that its overlap indices are close to 0 in both the melt and the freeze periods. The K06_BL and M10_BL PDFs of nucleation mode concentration for the melt period match the observations well, producing overlap indices of 0.73 for M10_BL and 0.75 for K06_BL, which is the highest value achieved for the nucleation mode in the melt period. In the freeze period, the overlap indices are also low (0.05 for M10_BL and 0.12 for K06_BL).

Observed Aitken mode concentrations (diameter 15–100 nm) lie between about 1 and 1000 cm^{-3} , with a mean of 60 cm^{-3} over the whole period. In contrast, concentrations in the CONTROL simulation are around 1 cm^{-3} , frequently fall below 0.1 cm^{-3} , and never exceed 10 cm^{-3} . The simulations with HIO_3 again show a sharp increase in particle concentration around day 235 when HIO_3 starts being emitted during the freeze period. Model Aitken mode concentrations then vary between being comparable to the observations and being 1–2 orders of magnitude too low. The Aitken

mode concentration in simulation IA.BL.SecOrg behaves similarly to that of IA.BL, although there are some periods where the concentration in IA.BL.SecOrg exceeds those in the IA.BL simulation by a factor of more than 10 and is in better agreement with observed concentrations (notably days 244–247). This is likely because of the extra condensable vapour in IA.BL.SecOrg, which promotes more particle growth from the nucleation mode. As in the nucleation mode, the Aitken mode concentrations from K06.BL and M10.BL are higher than CONTROL, on the same order of magnitude as the observations in the melt period but underestimating observations in the freeze period.

The observed accumulation mode concentrations (diameter 100–500 nm) are typically around 10–100 cm⁻³, with brief periods of less than a day where they fall to 1 cm⁻³ or lower, which is characteristic of the central Arctic (Bigg et al., 1996; Bigg and Leck, 2001; Mauritsen et al., 2011; Leck and Svensson, 2015). All simulations capture the observations well, except for the periods of extremely low concentration. The good agreement shows that NPF is not an important source of accumulation mode aerosol. As shown in e.g. Stevens et al. (2018) and Loewe et al. (2017), the periods of very low concentration are associated with efficient scavenging in drizzle on smaller spatial scales than represented in a global model. Nevertheless, the generally good model-observation agreement means that the aerosol surface area, and hence condensation sink for nucleating vapours, is reasonable in the model, and therefore not a cause of the biases in nucleation and Aitken mode particle concentrations.

Aerosol vertical profiles

In Sect. 3.4.2, we showed that the use of BL NPF schemes (instead of only the default upper tropospheric scheme) increased nucleation and Aitken particle concentrations at the surface during the melt period of AO2018. In this section, we examine the effect of these schemes on particle concentrations aloft.

Figure 3.3 shows simulated nucleation mode aerosol vertical profiles for the AO2018 campaign period. As discussed in Sect. 3.4.2, the nucleation mode concentrations at the surface in CONTROL are typically less than 0.1 cm⁻³ and never above 1 cm⁻³. We showed that this is an underestimation of the measurements taken at the ship. Figure 3.3 shows that despite the low concentrations at the surface, the model produces nucleation mode concentrations of up to 1000 cm⁻³ in the low FT, for example on day 244 above approximately 4 km. These higher concentrations aloft suggest that NPF is being simulated in the FT, but that those particles do not reach the surface.

The vertical profile for simulation M10.BL shows that the nucleation mode concentration is higher than CONTROL above the BL as well as at the surface, even though this simulation is using the same NPF mechanism as CONTROL in the FT.

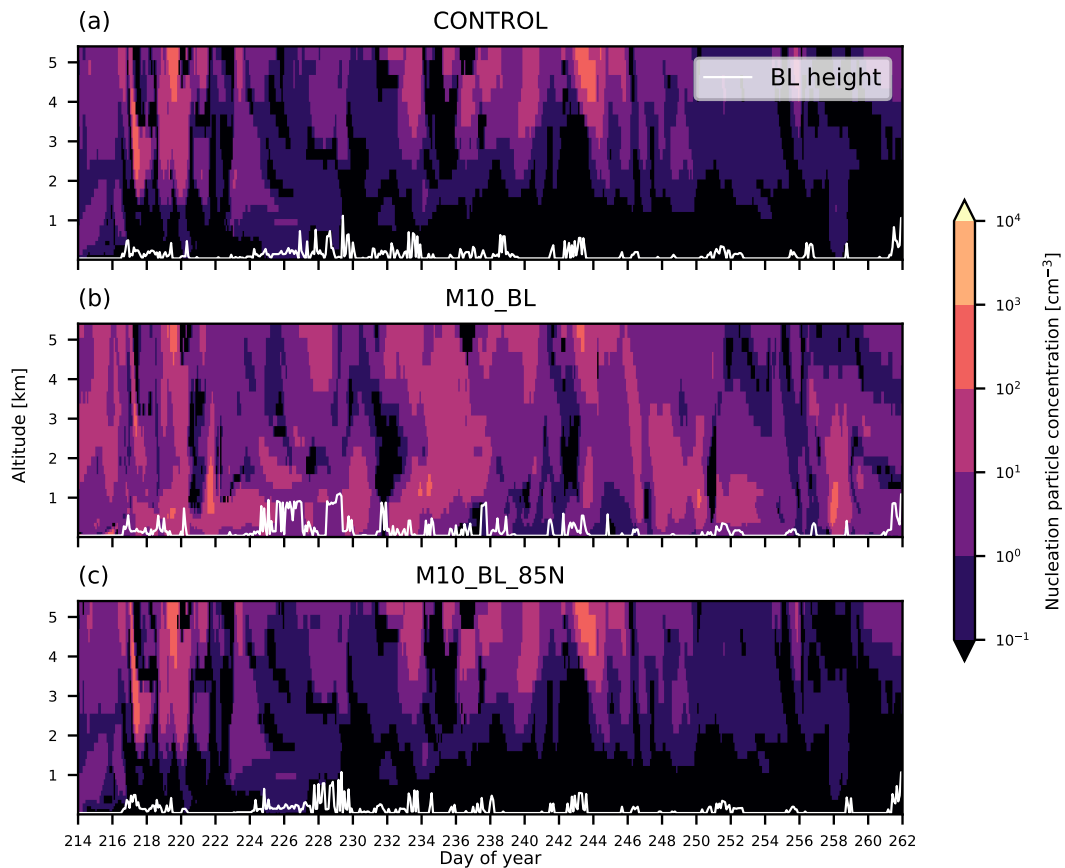


Figure 3.3: Nucleation mode aerosol profiles simulated for AO2018 campaign period. Model output is from simulations (a) CONTROL, (b) M10_BL and (c) M10_BL_85N. Model output was colocated with the position of the *Oden*. White lines show BL height.

We previously showed that M10_BL had nucleation mode concentrations at the surface that were 1–3 orders of magnitude higher than that of CONTROL. In the FT, the increase is up to an order of magnitude. The white lines in Fig. 3.3 show the modelled BL height, which is used by the NPF schemes to separate the BL from the FT. The increased nucleation mode concentrations in M10_BL above this BL height suggest that particles are being created in the BL at lower latitudes and then transported north in the FT. To examine this effect further, we ran a simulation where the M10 scheme was used in the BL only for latitudes north of 85° . The nucleation mode vertical profile for this simulation, M10_BL_85N, is also shown in Fig. 3.3 and shows lower concentrations than M10_BL in both the BL and the FT. In fact, the nucleation mode concentration in M10_BL_85N is mostly the same as that of CONTROL. The output from M10_BL_85N therefore shows that the higher FT and BL concentrations in M10_BL are from latitudes south of 85° . The concentration of organic vapours north of 85°N is much lower than at lower latitudes (see the steep latitudinal gradient in Fig. A.5), which potentially accounts for the low particle concentrations in M10_BL_85N.

Note that the smaller spatial extent of the NPF scheme could lead to less depletion of precursors than when the scheme is used globally, thereby increasing the NPF rate in M10_BL_85N relative to M10_BL. However, this non-linear behaviour would have the opposite effect to what we describe here so we can disregard it.

3.4.3 Effect of free-tropospheric NPF

In Sect. 3.4.2 we showed that the model default NPF scheme is insufficient to produce an accurate simulation of the aerosol concentrations measured at the surface during AO2018. The inclusion of iodine acid NPF improves the concentration in the nucleation and Aitken modes in the freeze period. Nevertheless, substantial model underestimations in particle concentration remain during the melt period, indicating some other missing source. Simulations with BL NPF driven by H_2SO_4 or a combination of H_2SO_4 and secondary organic vapours produce more accurate surface concentrations in the melt period of AO2018 compared to observations. However, as we showed in Sect. 3.4.2, these simulations do not produce more NPF in the BL in the high Arctic. Rather, small particles produced at lower latitudes are transported north, increasing nucleation and Aitken concentrations aloft as well as at the surface. This behaviour in the model suggests that the FT could be a source of particles to the surface, either from particles created by NPF aloft, or in the BL at lower latitudes before being transported into the high Arctic FT. Such a source has been considered before, for example by Korhonen et al. (2008a), who showed that entrainment of secondary particles from the FT is an important source of CCN over the Southern Ocean in GLOMAP, and Igel et al. (2017) who used a high-resolution LES model to show that particles can be transported from the free troposphere to the surface under conditions typical of the high Arctic. Also of relevance to entrainment processes in Arctic clouds, Solomon et al. (2011) used an LES model to show that a humidity inversion and entrainment of water vapour at cloud top helps to maintain the cloud by supplying moisture.

In this section we explore the role of the FT as a source of particles at the surface in both periods. We ran a simulation with M10 switched on at all model levels. We also ran a simulation with a fixed NPF rate for model levels between the top of the BL and 7.5 km.

Aerosol vertical profiles

Figure 3.4 compares simulated aerosol vertical profiles against observations from ASCOS (see Sect. 2.2.2). Model particle concentrations in these size ranges were calculated using August 2018 monthly mean data, colocated with the ASCOS flights which took place in August 2008. Concentrations of 3–14 nm diameter particles were consistently in the range 10^2 – 10^3 cm^{-3} in the FT, with lower values recorded below 1 km. The CONTROL simulation fails to capture these concentrations, underestimating the

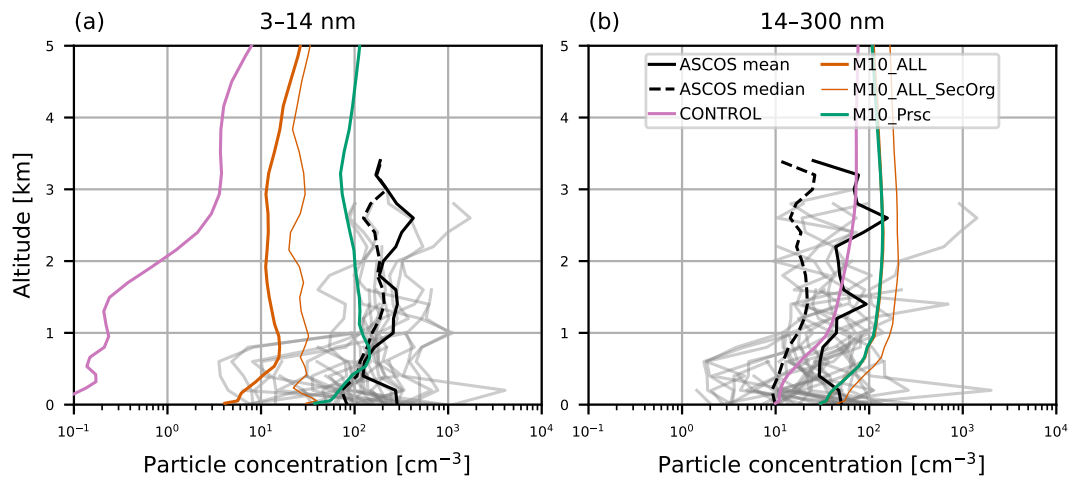


Figure 3.4: Aerosol vertical profiles from model output and ASCOS campaign observations from 2008. Model output is from colocated 2018 monthly mean values from simulations CONTROL (pink), M10_ALL (thick orange lines), M10_ALL_SecOrg (thin orange lines) and M10_Prsc (dark green). Observed values are given as the mean profile from each ASCOS flight (grey lines), overall mean (solid black) and overall median (dashed black). Profiles are for particles with size (a) 3–14 nm, measured during ASCOS using a UCPC and (b) 14–300 nm, measured using a CPC (particles greater than 14 nm) and a CLASP instrument (particles greater than 300 nm).

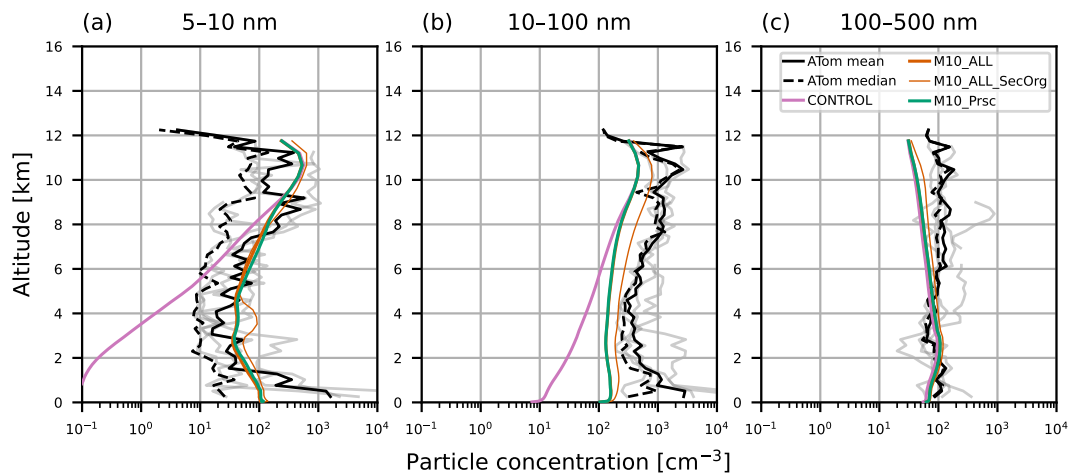


Figure 3.5: Aerosol vertical profiles from model output and ATom campaign observations from 2016. Model output is from colocated 2018 monthly mean values from simulations CONTROL (pink), M10_ALL (thick orange lines), M10_ALL_SecOrg (thin orange lines) and M10_Prsc (dark green). ATom observations are taken from leg 1 of the campaign and restricted to measurements that were taken north of 60°N. Observations correspond to mean profiles from different days (grey lines), the overall mean (black solid lines) and overall median (black dashed lines). Profiles are for particles with size (a) 5–10 nm, (b) 10–100 nm and (c) 100–500 nm. Observations were recorded at standard temperature and pressure, model output has been adjusted to account for this.

ASCOS mean concentration throughout the profile by 2 orders of magnitude in the FT and 3 orders of magnitude at the surface. Inclusion of organic NPF (M10_ALL) substantially increases particle concentrations, but they remain at least 1 order of magnitude lower than observed. Even when we allow much higher concentrations of organic vapours to be transported into the Arctic (M10_ALL_SecOrg), 3–14 nm diameter particle concentration is still underestimated by up to 1 order of magnitude throughout the profile. The model captures the 14–300 nm concentration better than the smaller particles. This is consistent with the results from the AO2018 comparisons, where the accumulation mode was captured much better than the nucleation or Aitken modes. All simulations shown here have 14–300 nm diameter particle concentrations of the same order as those measured in the ASCOS flights.

Aerosol vertical profiles measured in 2016 during the ATom campaign are shown in Fig. 3.5 with model output for the year 2018. Consistent with the ASCOS and AO2018 datasets, the CONTROL simulation predicts 5–10 nm diameter particle concentrations up to 3 orders of magnitude lower than the ATom measurements in the lowest 5 km of the atmosphere, with the largest model-observations discrepancies at the surface. In contrast to ASCOS, the M10_ALL simulations captures the nucleation mode profile better, producing concentrations that are within the range of the ATom measurements. The Aitken mode is underestimated by all simulations, though simulation M10_ALL is closer to the observations than CONTROL in the lowest part of the FT. All simulations capture the accumulation mode well at the surface but underestimate particle number aloft by roughly 50%.

M10_ALL underpredicts the profile of nucleation mode aerosol measured during the ASCOS campaign, even after perturbing the model monoterpenes to increase the availability of precursors in the Arctic (M10_ALL_SecOrg). We therefore artificially tested what NPF rate would be required to explain these observed profiles. We tested various prescribed nucleation rates applied above the boundary layer. A rate of $10^{-2} \text{ cm}^{-3} \text{ s}^{-1}$ produced a nucleation mode profile in best agreement with ASCOS and ATom (M10_Prsc). In the ASCOS region (the central Arctic), M10_Prsc is the only simulation to produce 3–14 nm particle concentrations close to the observed profiles (Fig. 3.4). In the ATom region over continental North America, M10_ALL and M10_Prsc both behave the same. We prescribed the nucleation rate in the model for latitudes north of 80°N , which means it has little effect over the ATom area. We also tested the prescribed rate in gridboxes north of 60°N and still found good agreement with the ATom and ASCOS profiles (Figs. A.2 and A.3).

The model output shown in Figs. 3.4 and 3.5 is for the year 2018, while the observational data is from 2008 (ASCOS) and 2016 (ATom). However, the large underestimations of the nucleation mode by simulation CONTROL (up to 3 orders of magnitude at the surface) for both campaigns is unlikely to be because of interannual variability

alone. The CONTROL simulation also underestimates the particle concentrations from the AO2018 campaign, which was in the same year as our model output.

Time series of particle concentrations

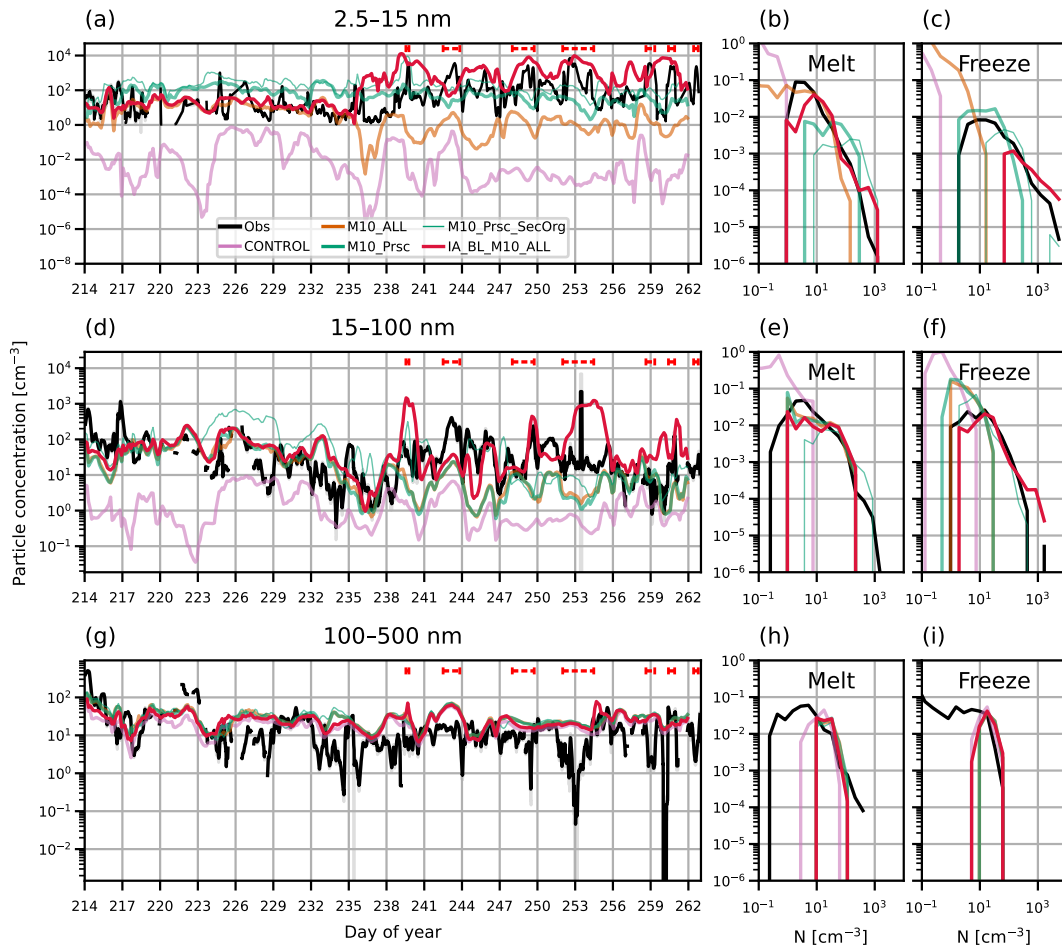


Figure 3.6: Time series and PDFs of aerosol concentration at the surface during AO2018 from observations and model output. Model output is from simulations M10_ALL (orange lines), M10_Prsc (thick green lines), M10_Prsc.SecOrg (thin green lines) and IA_BL_M10_ALL (red lines) Other than IA_BL_M10_ALL and the observations, lines have been made slightly transparent on this figure so that it is easier to view the results from IA_BL_M10_ALL. Observations are shown as 3-hourly mean (black lines) and standard deviation (grey shading). Aerosol concentrations are shown for particles with diameter (a-c) 2.5–15 nm, (d-f) 15–100 nm and (g-i) 100–500 nm. Red dashed lines in (a, d, g) show observed NPF events. PDFs are separated by observed sea ice freeze-up date, 27th August 2018 (day 239).

Time series and PDFs of particle number concentration at the surface from AO2018 observations and simulations M10_ALL and M10_Prsc are shown in Fig. 3.6 for nucleation, Aitken and accumulation mode particles.

In the nucleation mode, simulations M10_ALL and M10_Prsc both increase the simulated particle concentration by 2–3 orders of magnitude in the melt period relative

to CONTROL (Fig. 3.1). Like M10_BL, M10_ALL captures the observed nucleation mode concentration well in the melt period. The higher FT NPF rate in M10_Prsc produces a nucleation mode concentration that is 1–2 orders of magnitude higher than M10_ALL. This higher concentration in M10_Prsc further demonstrates the way the FT is acting as a source of particles to the surface in the model, although the fixed NPF rate in M10_Prsc overestimates the nucleation mode concentration in the melt period. The nucleation mode concentration declines from the melt to the freeze period in M10_ALL. The particle concentration decreases from above 1 cm^{-3} in the melt period to approximately 1 cm^{-3} , occasionally reaching 0.1 cm^{-3} . M10_Prsc produces concentrations close to 100 cm^{-3} in the both periods. As such, M10_Prsc captures the lower end of the observed distribution of nucleation concentration in the freeze periods, but does not capture the highest concentrations seen during the NPF events.

In the Aitken mode, particle concentrations are also higher in M10_ALL and M10_Prsc than in CONTROL. Despite differences between M10_ALL and M10_Prsc in the nucleation mode, they produce the same concentration of Aitken particles. Melt-period Aitken particle concentrations in M10_ALL and M10_Prsc are 1–3 orders of magnitude higher than in CONTROL, taking them to within 1 order of magnitude of the observed particle concentration for most of the melt period. As in the nucleation mode, Aitken concentrations decrease in M10_ALL and M10_Prsc in the freeze period such that the observations are underestimated by 1–2 orders of magnitude in the freeze period. The declining Aitken concentrations in both of these simulations suggests a decrease in the particle growth rates towards late summer, possibly driven by declining photochemical production of precursor vapours (see appendix A.3). The Aitken mode concentration decreases even in M10_Prsc, which has a fixed NPF rate above the BL, highlighting that particle growth by condensation is an important process as well as the particle formation rate itself.

The accumulation mode is well captured by both M10_ALL and M10_Prsc. As for IA_BL, the changes to the model NPF scheme in the M10 simulations have little effect on the accumulation mode concentration relative to CONTROL.

Local formation processes in M10_Prsc are dominated by the fixed nucleation rate above the BL. However, local particle formation is also affected by the availability of condensable vapours (if new particles grow faster, they are more likely to survive in the atmosphere for longer rather than being lost to coagulation with other particles). Therefore, since growth is important, we tested the sensitivity of NPF in the M10_Prsc simulation to the availability of secondary organic vapour by allowing more vapour to be transported to the Arctic in simulation M10_Prsc_SecOrg. Time series and PDFs of surface particle concentration during AO2018 is shown on Fig. 3.6. In the nucleation mode, M10_Prsc_SecOrg produces a concentration of approximately 100 cm^{-3} , behaving similarly to M10_Prsc.

In the Aitken mode, there are periods where M10_Prsc_SecOrg behaves the same as M10_Prsc and brief periods where it produces higher concentrations. For example, on days 223–229, the concentration in M10_Prsc_SecOrg is nearly an order of magnitude greater than that from M10_Prsc, resulting in an overestimation of the observed Aitken concentration.

3.4.4 Combining local and non-local NPF

Overall, M10_ALL performs well in the melt period of AO2018 but still underestimates particle concentration in the freeze period. This suggests that a combination of secondary particles from aloft and local BL NPF involving iodic acid is required to capture the full aerosol time series. The combined simulation of M10_ALL and IA_BL is shown as simulation IA_BL_M10_ALL in Fig. 3.6. IA_BL_M10_ALL captures both the baseline of the nucleation mode in the melt period and the peaks in the freeze period. In the Aitken mode, IA_BL_M10_ALL is within 1 order of magnitude of the observations except for a few brief periods, such as days 253–255 when the observed concentration is overestimated in the model.

The behaviour of the simulations can be summarised by comparing the overlap of PDFs of simulated particle concentration with those from observations (Table 3.2). Simulations with H₂SO₄ or organically-mediated NPF in the BL (K06_BL, M10_BL, M10_ALL, IA_BL_M10_ALL) have higher overlap indices for the nucleation and Aitken modes than CONTROL in the melt period, when the source of secondary particles from the FT has the greatest influence, but lower indices in the freeze period. During freeze-up, IA_BL_M10_ALL slightly overestimates the nucleation mode concentration, meaning that its nucleation mode overlap index in this period (0.51) is lower than that of M10_Prsc (0.52) and M10_Prsc_SecOrg (0.61), which do not overestimate the concentration in the same way. However, it is clear from the time series that the simulation with iodic acid NPF (IA_BL, IA_BL_SecOrg, IA_BL_M10_ALL) capture the nucleation concentration peaks from NPF events in a way that the M10_Prsc simulations do not. Simulation IA_BL_M10_ALL has the highest overlap index of all simulations for the Aitken mode in the freeze period (0.77), as it is the only simulation to capture the highest values of Aitken concentration during that time.

3.5 Discussion and conclusion

We have used field observations and a global aerosol-climate model with an empirical iodic acid nucleation scheme to investigate sources of aerosol in the high Arctic summer. Our results point to a regime transition occurring in late summer from a free-tropospheric source of secondary particles to local boundary layer new particle formation driven by iodic acid. The onset of iodic acid new particle formation (trig-

Vapour species	Change in concentration from Aug to Sep 2018 [%]
DMS	-28.8
SO ₂	135.2
H ₂ SO ₄	-85.2
OH	-87.7
Monoterpenes	31.2
Secondary organics	-5.9

Table 3.3: Table of change in simulated concentrations of different vapours from August to September 2018 in simulation CONTROL. Concentration changes are given as the change in the mean value over gridboxes at the surface with latitude 80–90 N.

gered by sea ice freeze-up) coincides with a decline in the free-tropospheric source rate brought on by declining rates of photochemical production of precursor vapours in the free troposphere. The net effect of the transition from free troposphere to boundary layer nucleation is a fairly constant nucleation and Aitken mode at the surface.

There are several key conclusions we can draw from the simulations we have presented here. They are listed below.

- The default settings of the UKESM1 model cannot capture Arctic aerosol concentrations. The nucleation mode particle concentration at the surface is at least an order of magnitude too low in CONTROL compared to AO2018, ASCOS and ATom observations, sometimes underestimating observed concentrations by as much as 5 orders of magnitude. The surface Aitken mode concentration is also underestimated by up to 3 orders of magnitude. The model performs better at simulating the surface accumulation mode concentration. The accumulation mode concentration in CONTROL is generally within the range of the observations, but does not capture the lowest concentrations (less than 1 cm^{-3}) seen in the time series of AO2018 observations. These periods of low accumulation mode concentration are important in controlling the behaviour and radiative effects of low-level Arctic clouds (Mauritsen et al., 2011; Birch et al., 2012; Loewe et al., 2017; Stevens et al., 2018).
- Simulations with H₂SO₄ or organically-mediated boundary layer new particle formation produce more accurate nucleation and Aitken mode concentrations at the surface during the AO2018 melt period than the CONTROL simulation. However, modelled aerosol concentrations aloft as well as output from a simulation where boundary layer new particle formation is switched on only north of 85°N show that little to no boundary layer new particle formation takes place in situ during the AO2018 before the iodine acid new particle formation events occur. This is in contrast to results from Browse et al. (2012), who found that new particle formation from H₂SO₄ in the Arctic boundary layer was an important source of high Arctic CCN in GLOMAP. Instead, the UKESM simulations with

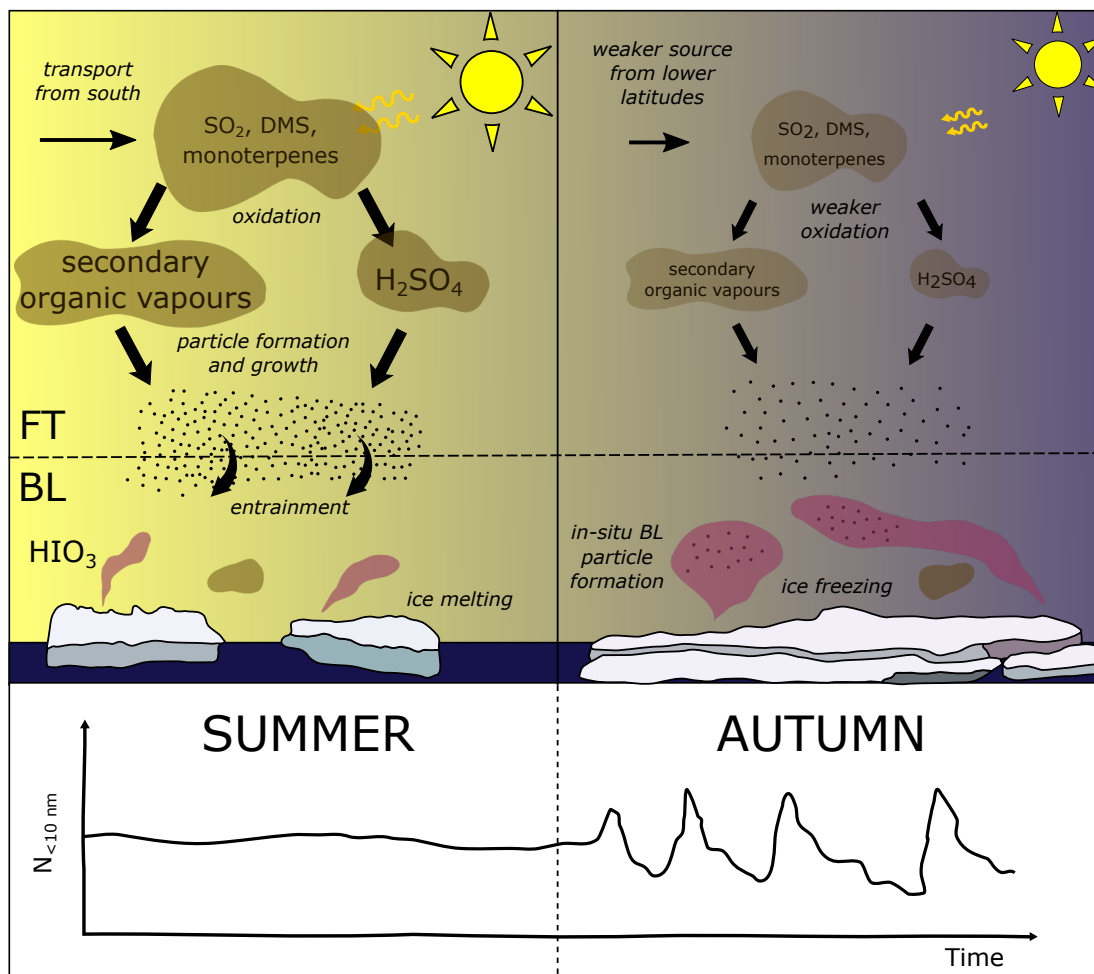


Figure 3.7: Schematic of processes controlling the concentration of nucleation mode particles at the surface in the high Arctic. The summer sea ice melt period is on the left and the freeze-up period in late summer/early autumn is on the right. A cartoon of the nucleation mode particle concentration is shown at the bottom.

boundary layer new particle formation schemes cause more particles to be created at lower latitudes. These small particles are then transported north through the free troposphere, and provide a source of Aitken mode particles to the surface in the high Arctic. Higher concentrations at the surface from a simulation with a prescribed new particle formation rate in the low free troposphere supports the hypothesis of a free-tropospheric source to the surface (Fig. 3.7, left-hand side).

- Our simulations suggest that a seasonal regime shift triggered by changes in photochemistry coincides with the beginning of the iodine season triggered by the sea ice freeze-up. This is portrayed in Fig. 3.7. The net effect of these two changes is a consistent source of particles controlled by new particle formation. Photochemistry declines towards the end of the AO2018 campaign period as a result of the reduction in incoming solar radiation at the end of summer. In the model output from simulation CONTROL, surface concentrations of the OH rad-

ical decline by 87.7% over 80–90°N from August 2018, causing H₂SO₄ to decline by 85.2% while SO₂ increases in concentration in the region by 135.2% over the same period (Table 3.3). The reduction in H₂SO₄ inhibits new particle formation and particle growth (Fig. A.6). In simulation M10.Prsc, the Aitken mode particle concentration declines from August to September 2018 even though the main source of these particles (new particle formation in the free troposphere) is prescribed to be constant. This behaviour highlights the importance of particle growth rates, which can vary alongside the new particle formation rate itself.

Our results have implications for the future Arctic aerosol budget and highlight existing uncertainties that require further attention. The Aitken mode particles produced by new particle formation in the free troposphere and the boundary layer have the potential to affect clouds, since Aitken particles have been observed to act as CCN in the Arctic. However, this is not a process that global models can easily capture. Aitken activation depends on high supersaturations driven by low concentrations of larger particles and/or high updraft velocities. We have shown that UKESM does not capture the lowest measurements of accumulation mode particles in the high Arctic summer. Updraft velocities vary on small spatial scales that are unresolved over the coarse spatial resolution of global model gridboxes. Modelling high updraft velocities and the resulting supersaturations therefore relies on model parameterisations of the sub-grid scale processes. It is not clear whether such parameterisations can capture the conditions that lead to Aitken activation in the Arctic.

A greater understanding of aerosol conditions in the Arctic free troposphere is needed. It is not possible to distinguish from the model output presented here whether particles coming from the free troposphere have been created there by new particle formation or have first been transported from lower latitudes, where they were created in the boundary layer. Our results indicate the importance of obtaining measurements of aerosol size distributions and precursor vapours from above the boundary layer in the high Arctic, which have previously been sparse. Moreover, the Kulmala et al. (2006) H₂SO₄ and Metzger et al. (2010) organically-mediated new particle formation schemes we use produce very similar surface particle concentrations in the region of study, such that we cannot use these datasets to evaluate the accuracy of one over the other. This highlights an open question in modelling of Arctic aerosol. It is crucial to understand which precursor species are important for Arctic aerosol in order to understand how changes to different parts of the climate system will affect the formation and behaviour of Arctic clouds. The production of secondary organic vapour in UKESM1 is crude, accounting only for the oxidation of monoterpenes, and we have not included any effects of ammonia, which has been shown in laboratory and Arctic field studies to contribute to new particle formation. The inclusion of ammonia in the model could lead to more new particle formation in the boundary layer since ammonia can stabilise

H₂SO₄ clusters. However, before these potential sources of model bias can be improved, more observational data is needed about what drives new particle formation throughout the Arctic, both in the free troposphere and at the surface.

Different aerosol sources imply differing sensitivity to regional change in the Arctic aerosol budget. Iodic acid new particle formation in the Arctic boundary layer is strongly coupled to the surface and therefore sensitive to changes in the sea ice. However, our simulations show that entrainment of secondary particles from the free troposphere is also an important source of surface aerosol at Aitken mode sizes. Free-tropospheric new particle formation is unlikely to have such a strong sensitivity to local sea ice changes, since the precursor vapours and background aerosol in the free troposphere are likely to have been transported from other regions. Further work will be required to understand how the balance of boundary layer versus free-tropospheric nucleation will evolve in the changing Arctic, since predictions of cloud behaviour and surface energy balance in the future Arctic depend on knowledge of the Arctic aerosol budget. It is also important to assess the influence of boundary layer versus free-tropospheric sources compared to other uncertain Arctic aerosol processes and their different representations in models, for example sea spray parameterisations and primary marine sources.

Chapter 4

Activation of Aitken mode aerosols into cloud droplets during the high Arctic summer in a high-resolution nested model

Abstract

Arctic aerosol-cloud interactions can modulate the energy budget in the high Arctic, but models have struggled to capture relationships between aerosols, clouds, and the surface. Observations and modelling studies have shown that Aitken mode particles (roughly 10–100 nm diameter) can act as cloud condensation nuclei (CCN) when supersaturations are high. Activation of Aitken mode particles implies a greater sensitivity of Arctic clouds to particles formed by secondary processes, since the low growth rates observed in the Arctic would otherwise prevent such particles from reaching CCN-relevant sizes. In this chapter we use a regional climate model with coupled two-moment cloud and aerosol microphysics. We evaluate the modelled clouds, surface radiative fluxes and aerosol size distribution using measurements from the Arctic Ocean 2018 campaign. We then use an offline version of the model aerosol activation scheme to investigate the effect of aerosol concentration and vertical wind velocity on Aitken activation. We find that the model overestimations of the accumulation mode (100–500 nm) particle concentration inhibits Aitken activation in the model, as well as the unresolved portion of sub-grid scale variability in the vertical wind velocities. Our results point to model processes that require improvement to increase the accuracy of aerosol activation, but also show that biases in the clouds partly stem from the cloud scheme in the model, separately from aerosol processes.

4.1 Introduction

In the Köhler theory of aerosol activation, larger particles activate before smaller particles of the same hygroscopicity. As such, particles in the accumulation mode (larger than about 100 nm dry diameter) are usually considered the most important particles for cloud condensation nuclei (CCN) concentrations and therefore for influencing cloud behaviour. However, the unique environment of the Arctic creates conditions where high supersaturation can occasionally occur, which can allow Aitken mode particles to act as CCN. CCN concentrations can be much lower in the Arctic than in polluted environments at lower latitudes (Bigg and Leck, 2001; Mauritsen et al., 2011). Accumulation mode concentrations can be on the order of 1 cm^{-3} or less, leading to conditions where activation of smaller particles is possible because low droplet concentrations allow supersaturations to reach high levels. Activation of Aitken particles has been observed at Ny Ålesund (Koike et al., 2019; Karlsson et al., 2021), in northern Finland (Komppula et al., 2005) and over the Arctic Ocean (Karlsson et al., 2022). LES modelling studies have also simulated the mechanisms by which Aitken particles can activate in Arctic clouds (Bulatovic et al., 2020; Pöhlker et al., 2021). The occurrence of Aitken activation means that small, newly formed, secondary particles do not need to grow all the way up to accumulation mode sizes to act as CCN in Arctic clouds, making it plausible that such particles could survive long enough in the atmosphere to be important for cloud formation. Because growth rates are usually slow in the high Arctic, particle growth would otherwise act as a considerable limitation for newly formed particles to act as CCN (Schmale and Baccarini, 2021).

The coarse model resolution of our UKESM simulations makes it challenging to simulate the conditions under which Aitken activation takes place in the Arctic. This is because gridbox-mean cloud fractions are used to define the cloud volume for entire grid cells, on the order of 100 km in the horizontal. Variability in cloudiness on sub-grid scales is not explicitly resolved. This invariability in the cloud fields impacts other model processes, such as radiation and precipitation. Behaviour brought on by the extremes in cloud cover is not captured by simulating only the mean state. As such, a higher resolution model is better equipped to capture several processes, for example:

- Higher than average surface radiation fluxes during cloud-free periods has been linked to the onset of melting/freezing of sea ice (Nilsson et al., 2001b; Sedlar et al., 2011), and therefore has a large impact on the Arctic energy budget, but this link will not be captured by UKESM.
- The differences in radiation between a uniformly cloudy gridbox in a global model and cloud-free gridboxes in a high-resolution model could affect the photochemical rates which are strongly linked to the production of Arctic aerosol.
- More variability in precipitation rates creates periods of stronger aerosol removal,

so the variability in the accumulation mode concentration may be better captured in a model with higher resolution. The PDFs of accumulation mode concentration at the surface during AO2018 from our UKESM simulations are systematically narrower than the PDFs of the observed particle concentrations, with the lowest concentrations of 1 cm^{-3} and below not being reproduced in the UKESM output.

- More-variable accumulation mode concentrations will impact the condensation sink of nucleation vapours, affecting new particle formation rates.
- Very low accumulation mode concentrations have been observed to cause the thinning of Arctic clouds, for example during the ASCOS campaign in what was described as a “tenuous” cloud regime (Mauritsen et al., 2011). This reduced cloud cover will not be captured in our UKESM configuration because the low accumulation mode concentrations that drive it are not present.
- Finally, as discussed above and of importance for this chapter, periods of low accumulation mode concentrations can promote the activation of Aitken mode particles into cloud droplets.

Even simulations with higher resolution will struggle to capture the behaviour of clouds if either fixed cloud drop number concentrations (CDNC) or prognostic CDNC from fixed aerosol concentrations are used. Birch et al. (2012) used the UM in a numerical weather prediction (NWP) configuration to study the cloud behaviour during the ASCOS campaign with a resolution on the order of 10 km. The results suggest that overestimations of cloud occurrence during the tenuous regime were improved by changing the fixed CCN concentrations from the default value of 100 cm^{-3} to 1 cm^{-3} , a value more in line with the measured CCN concentrations. The authors thus concluded that a fixed CCN concentration was a key driver of modelled overprediction of cloudiness in that period of the campaign. The same period of the ASCOS campaign was the subject of a multi-model study which included the use of the UM (Stevens et al., 2018). Once again, all models in that study simulated a link between low CCN concentrations and a dissipation of the cloud. In the UM, cloud dissipation was successfully triggered by low CDNC, whether that was achieved by prescribing low CDNC, prescribing low CCN, or by allowing CCN concentrations to vary via aerosol processing. The AO2018 campaign has also been simulated in the UM (Young et al., 2021). The model often failed to simulate cloud-free conditions, like in Birch et al. (2012) for the ASCOS campaign, despite the inclusion of prognostic CDNC in Young et al. (2021), which allows cloud drop number to respond to changes in meteorological conditions. However, the CDNC calculations in Young et al. (2021) used a fixed aerosol concentration of 100 cm^{-3} , so the effect of low aerosol concentrations on the clouds was still not simulated. Young et al. (2021) also ran a sensitivity test with a prescribed aerosol profile with lower concentrations, more in line with typical Arctic conditions.

The lower aerosol concentrations led to lower CDNC and reduced cloud cover. Other than the UM, different models have also been used to confirm the importance of aerosol-cloud interactions in governing the behaviour of Arctic clouds (Sotiropoulou et al., 2016; Loewe et al., 2017; Sterzinger et al., 2022), though these model studies have also lacked the use of coupled aerosol and cloud microphysics. Thus it is clear that three important elements are required for accurate simulations of Arctic clouds: a high enough resolution to resolve variability in the clouds, varying aerosol concentrations, and coupling between the clouds and aerosols that allows non-linear feedbacks between cloud and aerosol behaviour to be simulated.

Here, we use a higher resolution configuration of the model over a limited area that covers the AO2018 drift coordinates. We investigate whether the higher resolution than used in previous chapters is capable of capturing the variability in Arctic clouds and precipitation that leads to low accumulation mode concentrations, thus creating the conditions for activation of Aitken particles in the model. We use UKCA to simulate aerosol microphysics and a two-moment cloud microphysics model to simulate cloud drop formation. Importantly, the aerosol and cloud microphysics are coupled to allow the model to simulate aerosol-cloud interactions and their effects on radiation and precipitation. We introduce the model set-up in section 4.2, the observations of clouds and radiations in section 4.3. The model output of surface radiation and clouds is compared to observations in section 4.4. The behaviour of aerosols in the model is presented in section 4.6. Conclusions are drawn in section 4.7.

4.2 Model description

4.2.1 Regional model configuration

In the previous two chapters we presented results from UKESM in atmosphere-only configuration. UKESM is a global model with coarse horizontal resolution on the order of degrees of latitude and longitude. The UM, used in UKESM to simulate the dynamics of the atmosphere, can be configured as a global model (as in UKESM) or as a regional nested model at high-resolution with explicitly resolved convection. In this chapter, we use the UM in its regional configuration coupled to two modules for aerosol and cloud two-moment microphysics: UKCA and the Cloud AeroSol Interacting Microphysics model (CASIM).

CASIM was designed to provide an accurate representation of the processes important for aerosol-cloud interactions and has been evaluated previously against observations (Grosvenor et al., 2017). It is a two-moment microphysics scheme in that it simulates the total mass and number concentrations of hydrometeors. Aerosol activation is calculated using the method described in Abdul-Razzak and Ghan (2000) (hereafter ARG2000). The method uses vertical wind velocity, humidity and aerosol

information to carry out calculations of activated particle number in line with Köhler theory. This is a different approach from the regional UM without CASIM, which uses a fixed droplet number in clouds, like in Birch et al. (2012). It is also a different approach from UKESM, which runs without CASIM and therefore does not advect cloud drop number concentration as a prognostic variable. Instead, the ARG2000 scheme is used in UKESM to diagnose the cloud drop number each timestep. The CDNC is not carried over to the next timestep and is prescribed as the cloud base concentration throughout the vertical profile of a cloud. By explicitly simulating drop activation depending on updrafts, humidity and aerosols, CASIM provides capability for simulating the effect of aerosols on clouds.

In our configuration, CASIM is additionally coupled to UKCA. The methods used to couple the aerosols from UKCA to the CASIM microphysics are explained in Gordon et al. (2020). In the coupled set-up, the ARG2000 scheme references the size distribution and aerosol composition information simulated by UKCA when calculating the cloud droplet number (which is used to calculate the reflectivity of the cloud). Additionally, the autoconversion and rain rates are passed back to UKCA and used in the calculations of in-cloud and below-cloud scavenging rates. In this way, the simulated aerosol distribution affects the cloud drop number concentration in real time during the simulations, and the clouds in turn affect the aerosol removal. This represents the state of the art in aerosol-cloud interaction modelling. Although these aerosol-radiation and aerosol-precipitation couplings are present in UKESM, they have been absent in previous studies of Arctic clouds using the nested configuration of the UM (Birch et al., 2012; Young et al., 2021).

To simulate the AO2018 campaign period in the regional UM, we use a nest of 150×150 grid points centred on 89°N , 45°E . The horizontal grid resolution is about 4 km, giving a region that is about $600 \text{ km} \times 600 \text{ km}$ in total. The higher resolution in the regional nested model ($\sim 4 \text{ km}$) relative to UKESM ($\sim 150 \text{ km}$ at the equator) will be beneficial for accurate modelling of Arctic clouds and aerosols. Although the regional nested model will still not resolve all of the fine-scale variability in temperature and moisture that lead to inhomogeneities in the cloud field, the km-order resolution makes the presence of model gridboxes where the cloud fraction is at or near 0 more likely. The model uses a “rotated pole” approach to maintain approximately equal grid box areas where the meridians converge at the pole. The boundary conditions for the nest are produced by a global configuration of the UM with horizontal resolution of approximately 0.83° longitude by 0.55° latitude. UKCA is used in both the global model and the nest, while CASIM is used in the nest only. Emissions of anthropogenic carbonaceous aerosol, land-based DMS, monoterpenes, and SO_2 are taken from CMIP5 datasets for the year 2000 (Lamarque et al., 2010). Carbon emissions from biomass burning are from a climatology for the years 2002-2011 from the same CMIP5 dataset.

This configuration also prescribes emissions for oxidants (O_3 , OH, NO_3 , HO_2 , H_2O_2), using output for the years 1988-2010 from model runs used in the Chemistry Climate Model Initiative (CCMI) (Morgenstern et al., 2009; Hardiman et al., 2017). Note that this is different from our UKESM simulations, which used interactive chemistry for these species such that clouds and aerosols could affect photolysis rates via oxidant concentrations. The boundary conditions of the nest are updated from the global driving model every hour. Both the nest and the driving model are initialised from model output.

We ran two simulations using UKCA-CASIM of the AO2018 drift period. The first uses the same set-up as simulation CONTROL in chapter 3 of this document, i.e. with adjustments made to the aerosol ageing scheme as detailed in chapter 3. The second simulation is the same as IA_BLM10_ALL, also presented in chapter 3. Simulation IA_BLM10_ALL uses the Metzger et al. (2010) scheme for organic new particle formation in all model layers and a scheme for boundary layer iodine acid NPF that was described and tested in chapter 3. Simulations CONTROL and IA_BLM10_ALL were selected for use in UKCA-CASIM because they represent the how the model performs with and without our improvements to the Arctic aerosol budget.

4.2.2 Cloud scheme

The cloud scheme calculates the fraction of a model gridbox covered by cloud, accounting for both the gridbox mean values and sub-grid variability in fields such as temperature and humidity. Our simulations use the Van Weverberg et al. (2021) bimodal cloud fraction scheme to diagnose liquid cloud fraction and water content in each gridbox. The Van Weverberg et al. (2021) scheme identifies so-called “entrainment zones” near humidity and temperature inversions and allows for the mixing of moister and drier air (from entrainment) by using a bimodal PDF for the sub-grid scale distribution. Ice and snow water content are calculated by the microphysics scheme and then used to diagnose the frozen cloud fraction.

The cloud fractions are coupled to the radiation and precipitation schemes in the model, such that the radiation can alter the cloud fraction (e.g. via changes in temperature) and the cloud fraction itself can affect the surface energy budget, while precipitation rates can alter the cloud fraction.

4.2.3 Aerosol activation scheme

CASIM uses the ARG2000 scheme to simulate the activation of aerosols into cloud drops. In our configuration, the scheme uses aerosol size distribution and composition from UKCA to calculate a critical supersaturation for each soluble aerosol mode. Following the results of Köhler theory, larger aerosols or more hygroscopic aerosols are

more easily activated and thus have a smaller critical supersaturation that must be reached for them to activate. Once the critical supersaturations have been calculated for each mode, the maximum environmental supersaturation in a gridbox is calculated. The maximum supersaturation is determined according to thermodynamic information (vertical wind velocity, temperature and pressure) and by taking into account the total concentration and critical supersaturation of each soluble mode. Once the critical and maximum environmental supersaturations have been calculated, the activation diameter of each mode is calculated as a function of mean modal diameter and the ratio of the critical and maximum supersaturations. The activation diameter is the minimum diameter above which particles of a given mode will activate for those set of conditions. The activation diameter can be used to calculate the number of particles in each mode that will activate, and the cloud drop number is the sum of activated particles across all modes.

Since there is considerable unresolved, sub-grid variability in the vertical wind velocity, it is not sufficient to use only the gridbox mean of the vertical wind velocity, \bar{w} , in the ARG2000 calculations. Instead, the model uses a characteristic vertical wind velocity in each gridbox, which is the sum of the gridbox mean and a prescribed value to represent the unresolved, sub-grid scale distribution in vertical velocity. This unresolved component, $\sigma_{w,sgs}$, is diagnosed from the simulated boundary layer turbulent kinetic energy (TKE) as

$$\sigma_{w,sgs} = A\sqrt{TKE} \quad (4.1)$$

where A is an empirical constant, often given as $\frac{2}{3}$ derived from an assumption of isotropic turbulence, though set to 1 in our simulations, implying an assumption that the vertical component of turbulence is greater than the horizontal components (Stull, 1988; Morrison and Pinto, 2005). A minimum value of 0.01 m s^{-1} is imposed on $\sigma_{w,sgs}$. So the updraft velocity used by ARG2000 is

$$w_{act} = \bar{w} + \sigma_{w,sgs} \quad (4.2)$$

Note that because the CDNC is a prognostic variable in CASIM, a cloud simulated over several timesteps will “remember” the highest updraft velocity it has seen. The CDNC will only reduce if the cloud partially or totally evaporates from one timestep to the next, i.e. if the cloud fraction goes down. Otherwise, the CDNC will increase if the new CDNC in a timestep is greater than the existing CDNC from the previous timestep.

As well as using ARG2000 to calculate drop number in the model, in this study we

have used a bespoke offline version of the code to make further calculations. We refer to this as ARG2000-offline. There are two advantages of supplementing the model simulations with this offline code. First, we can more easily obtain more outputs that the scheme provides by default in the model, such as the number of activated particles in each mode as opposed to simply the total CDNC. Secondly, by using an offline version of the code we can quickly and easily change the values of certain parameters to run sensitivity tests, without the considerable computational expense of running full UM simulations. Using output from our simulations, we can use ARG2000-offline to prescribe the values of \bar{w} , $\sigma_{w,sgs}$, temperature, pressure and the mass and number of each soluble aerosol mode. The code returns the critical and maximum supersaturations, and the critical diameters and number of activated particles in aerosol each mode.

4.3 Observations

4.3.1 Cloudnet

Cloudnet is an algorithm that uses measurements taken with radar, lidar, ceilometers, microwave radiometers, and radiosondes to produce cloud fractions and liquid water contents on common timesteps and vertical levels (Illingworth et al., 2007). It has previously been applied to measurements of Arctic clouds, by Vüllers et al. (2020) and Young et al. (2021) for measurements from AO2018 and by Achtert et al. (2020) for the Arctic Cloud in Summer Experiment 2014 . The derived variables and common time and altitude coordinates are desirable when performing comparisons between cloud measurements and model output.

Here, we use cloud water contents retrieved using Cloudnet from measurements made during AO2018 (Vüllers et al., 2021). Ice water content is calculated by Cloudnet from measurements of radar reflectivity and temperature. Liquid water path is measured by a radiometer and then partitioned vertically by Cloudnet using lidar measurements of liquid water layers to produce liquid water content. More details of the instruments used to take the measurements that were fed into Cloudnet can be found in Vüllers et al. (2020).

4.3.2 Surface radiation

Surface radiative fluxes were measured during the AO2018 drift period using radiometers located ~ 1.5 m above the ice floe (Vüllers and Brooks, 2021). The radiometers measured up- and downwelling radiation in the solar and infrared bands to produce up, down and net SW and LW radiation fluxes from the snow surface. For more details see Vüllers et al. (2020).

4.3.3 Vertical wind velocity

Vertical wind velocity was measured during AO2018 by the cloud lidar that is used in the water content retrieval. Since the instrument requires the presence of drops, ice crystals or aerosols to reflect the signal, measurements of vertical wind velocity used here are from a case where clouds were present. The measurements from the lidar are limited to cloud base due to the attenuation of the lidar signal in cloud.

The vertical wind velocity measurements we use are from 03:00 to 07:00 and 08:00 to 11:00 UTC on 13th September 2018. A single layer of cloud was present from 03:00 to 07:00, while during 08:00 to 11:00 higher clouds are also present which modify the longwave cooling from the low level cloud. As such, the vertical wind velocity distributions are different between the two cases and we treat them separately here. We will use these measurements to evaluate both model gridbox mean vertical wind velocity, \bar{w} , and the vertical wind velocity used in ARG2000 to calculate aerosol activation, w_{act} .

4.4 Clouds

Since we are investigating aerosol-cloud interactions and the impacts on the surface, we are interested in the modelled cloud microphysics. The surface radiation budget is strongly linked to cloud behaviour, because the presence of clouds reduces incoming SW radiation and increases incoming LW, compared to clear-sky conditions. In this section we evaluate the surface radiation budget, cloud fraction and cloud water contents from UKCA-CASIM compared to observations from the AO2018 campaign.

Figure 4.1 shows SW, LW and total radiation at the surface during the AO2018 drift period from measurements and model output. The measured SW radiation generally shows a downwards trend through the drift period (figure 4.1(a)) which is consistent with the declining solar angle in the end of summer and onset of autumn. At the beginning of the period, the SW measurements are typically between 10–30 W m^{-2} , with occasional peaks of up to 50 W m^{-2} . The peaks suggest increases in incoming solar radiation associated with cloud-free periods. In the second half of the drift period, the SW is frequently less than 10 W m^{-2} and is occasionally close to 0 W m^{-2} (e.g. 7th September). The peaks in the SW time series are evident in the PDF of SW measurements (figure 4.1(b)), which has a peak at 10 W m^{-2} and is skewed in shape with a long tail to the larger values.

The observed LW at the surface is often close to 0 W m^{-2} , with troughs in the time series that can be up to -60 W m^{-2} . The troughs correspond to periods of net LW emission from the surface, which is associated with cloud-free periods. As is expected for cloud-free periods, such troughs in the LW often align with positive peaks in the SW, for example on 24th or 31st August. The distribution of LW measurements peaks

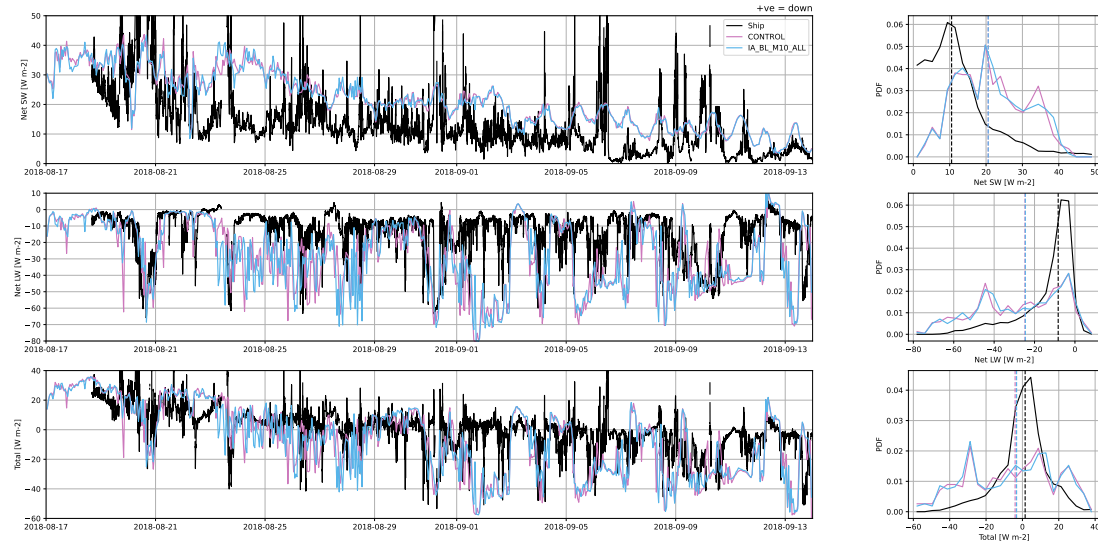


Figure 4.1: Time series and PDFs of measured and simulated (a, b) surface SW radiation, (b, c) surface LW radiation and (d, e) total surface radiation (sum of SW and LW). All values are defined as positive in the downwards direction. Measured values (black lines) are given once a minute. Model output is for simulations CONTROL (pink lines) and IA_BL_M10_ALL (blue lines). Model output is output once an hour and has been colocated with the ship. Dashed lines on the PDFs mark the median of each distribution.

at approximately -5 W m^{-2} with a long negative tail.

The distribution of the total radiation (figure 4.1(e)) peaks at about 5 W m^{-2} and is slightly asymmetrical, with a longer negative than positive tail. The downwards trend seen in the SW is also present in the time series of the net radiation (figure 4.1(d)). The net radiation at the surface is positive at the beginning of the drift period, negative at the end, and fluctuates around 0 W m^{-2} for much of the drift period. Positive net surface radiation, corresponding to net absorption at the surface, is associated with melting sea ice in this region, while negative net surface radiation is associated with freezing. The net radiation time series therefore illustrates the onset of sea ice freezing that was captured by the AO2018 campaign (Vüllers et al., 2020).

Both simulations frequently overestimate the surface SW measurements, though the peaks in the measurements are not captured. Although the model captures the decreasing trend in the SW time series, the absolute values are mostly too high. The positive bias in the model can be seen in the PDF. The observations have a median of about 11 W m^{-2} while the median from the simulations are both nearly double that at 21 W m^{-2} . The PDF of the modelled values are also more symmetrical than the observations, highlighting that the simulations do not have strong peaks in the SW time series like the measurements do.

In the LW, there is a negative model bias. Although some of the troughs in the LW time series are captured by the model, for example on 20th and 31st August, the model

otherwise exhibits troughs in the LW too frequently, creating low biases of up to 50 W m^{-2} . The LW PDF is not captured by either simulation. While the measurements have a peak around -5 W m^{-2} and a median of -9 W m^{-2} , both simulations produce roughly bimodal distributions, reflecting that they simulate too many instances of large negative LW values (associated with cloud-free conditions) and not enough instances of smaller negative or 0 values (associated with cloud cover). The medians are about -25 W m^{-2} for both simulations, nearly 3 times the magnitude of the median in the observations.

The positive model bias in the SW and the negative bias in the LW largely cancel each other out in the time series of total surface radiation, though the shape of the PDF is not captured by either model due to the incorrect behaviour of the SW and the LW. The measured PDF peaks at about 5 W m^{-2} and has a median at 1.5 W m^{-2} . The simulated medians are closer than in the LW or the SW at -4 W m^{-2} for CONTROL and -3 W m^{-2} for IA.BL.M10.ALL. However, the simulated PDFs do not have the peak near 0, instead having peaks close to 30, 10 and -30 W m^{-2} . The transition from sea ice melt to freeze is not as clear in the model as it is in the observed total radiation. The measurements fluctuate around 0 W m^{-2} for much of the drift period whereas the model simulates sustained periods of strongly negative values, e.g. 1st and 2nd September, when the model is 40 W m^{-2} lower than the measurements. The incorrect behaviour in the total surface radiation means the model is not correctly simulating the amount of energy absorbed by the surface. Although our configuration does not simulate a response between surface energy and sea ice melt, this model bias is concerning for coupled configurations such as that of UKESM.

Figure 4.2 shows the mean profile of cloud fraction from observations and model output. Following the method used by Young et al. (2021), a TWC threshold is used to define the cloud fraction in both the model output and the Cloudnet data, facilitating a like-for-like comparison. The threshold is 10^{-3} g m^{-3} below 1 km and 10^{-4} g m^{-3} above 4 km with interpolated values in between. The cloud fraction peaks just above the surface in both simulations at just over 80%, then declines with altitude above this. The measurements also peak in the lowest 500 m but the peak cloud fraction only reaches about 35%, so is less than half of that in the simulations. The model overestimates the mean cloud fraction below 4 km and slightly underestimates mean cloud fraction above this. The overestimation of cloud fraction is counterintuitive to the surface radiation biases (figure 4.1) which showed positive SW and negative LW biases, both consistent with too little cloud cover in the model. It is therefore likely that the biases in surface radiation are driven by the microphysical properties of the clouds, rather than the frequency of cloud occurrence.

Average profiles of LWC and IWC are shown in figure 4.3. The mean is taken over in-cloud values only, i.e. where LWC and IWC are greater than 0. The mean and

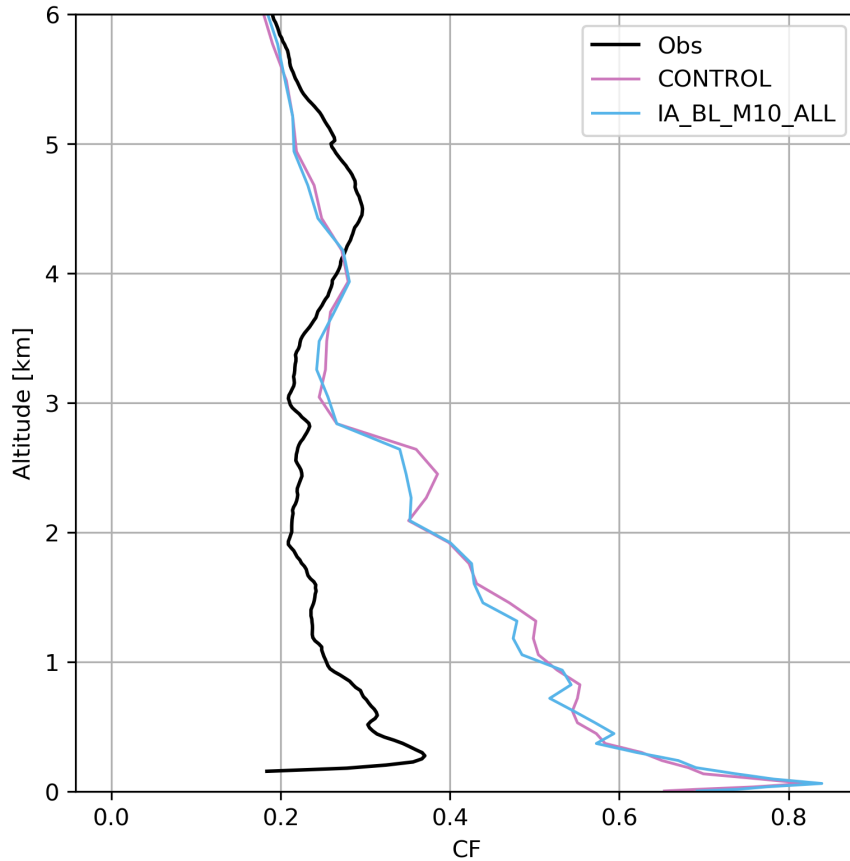


Figure 4.2: Mean cloud fraction from model output and observations over the period 17th August - 13th September 2018. Observations are shown in black. Model output is from CONTROL (pink) and IA_BL_M10_ALL (blue) and was colocated with the ship before taking the average. Cloud fraction is calculated using a mask based on TWC as described in the text.

median of the observations are shown as black solid and dashed lines respectively. The LWC measurements show liquid water throughout the lowest 6 km of the atmosphere. The lowest values occur at about 3.5–5 km, at other altitudes the LWC varies between approximately $0.075\text{--}0.175\text{ g m}^{-3}$ in the median profile, or up to about 0.33 g m^{-3} in the mean. The measured IWC is up to an order of magnitude lower than the LWC, with the mean profile never exceeding 0.01 g m^{-3} and the median values more than 50% lower than the means.

The model produces too much ice and not enough liquid. Both simulations produce no liquid water above 3 km and underestimate the LWC below 3 km. Below 2 km, both the mean and median profiles are underestimated by at least an order of magnitude. Neither simulation produces average LWC values of more than 0.05 g m^{-3} at any altitude. The mean IWC profiles from both simulations peak below 500 m at about 0.04 g m^{-3} , approximately an order of magnitude greater than the measured mean profile. The mean profile is overestimated below 3 km and the median profile is overestimated

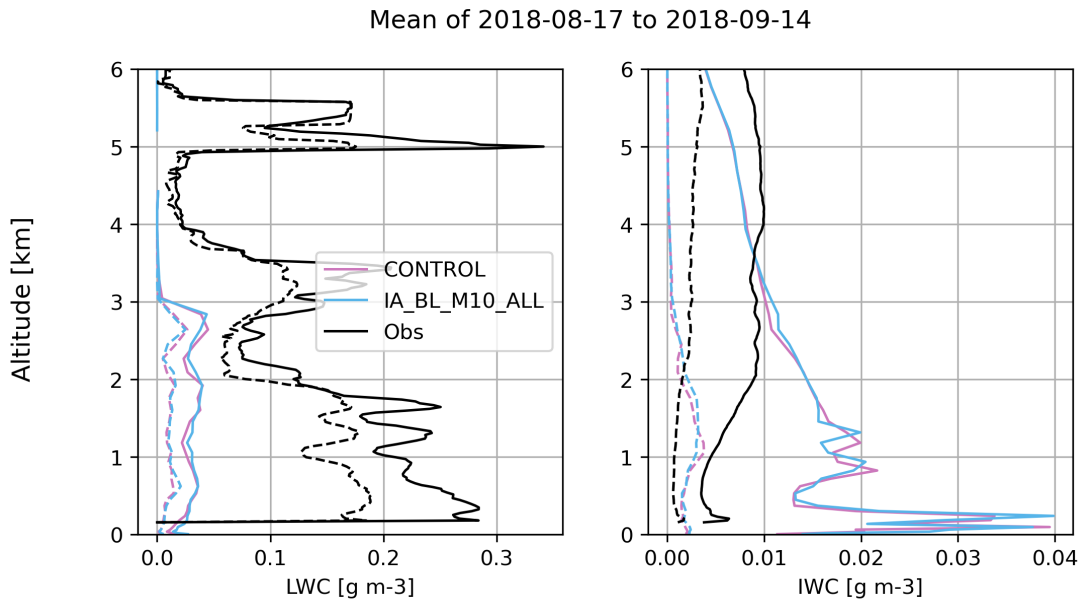


Figure 4.3: Average profiles of (a) LWC and (b) IWC from observations (black) and model output. Mean profiles are shown as solid lines, median profiles are shown as dashed lines. Model output is from simulation CONTROL (pink) and IA_BL_M10_ALL (blue). Averages are taken over non-zero values of LWC and IWC (i.e. values where cloud is present).

below 2 km. The IWC is underestimated aloft.

The mean profiles of cloud fraction, LWC and IWC suggest that the model overestimates cloud occurrence, and simulates clouds that have too much ice and not enough liquid at the surface. This behaviour suggests that the clouds in the model are too optically thin to capture the surface radiation fluxes, which had positive biases in the SW and negative biases in the LW. Since the aerosol and cloud microphysics are coupled in our simulation, the rest of this chapter will explore whether the aerosols are a controlling factor in creating these biases in the clouds and their radiative effects.

4.5 Vertical wind velocity

Since the vertical velocity of air is a controlling factor in the activation of aerosols as calculated by ARG2000, we will now compare the vertical wind speeds from the model and from AO2018 measurements. We will compare measurements to both gridbox mean values, \bar{w} , and to the prescribed sub-grid scale component of vertical wind speed used in ARG2000.

Figure 4.4 shows time series and PDFs of vertical wind velocity measured at cloud base during AO2018. The measurements are from 13th September 2018 and represent a single layer of low-level cloud and the same low-level cloud after another cloud layer formed aloft. The single layer of cloud shows more variability in cloud base updraft

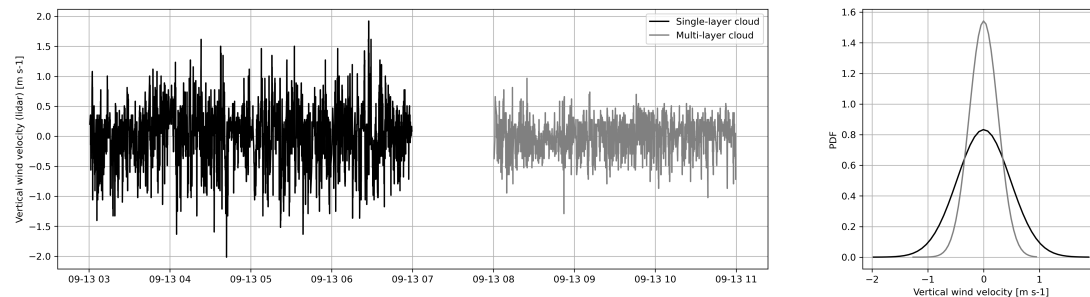


Figure 4.4: Time series and PDFs of vertical wind velocity measured at cloud base by the cloud lidar during AO2018. Measurements are for 03:00–06:00 and 08:00–11:00 UTC on 13th September 2018 and represent a single layer of low level cloud (black lines) and a low level cloud with another cloud layer aloft (grey lines).

velocity than the multi-layered cloud. This is likely related to the reduction in radiative cooling that occurs when the cloud forms aloft, and the resulting reduction in turbulence in the low-level cloud. The standard deviation of the PDF for the single layered cloud is 0.48 m s^{-1} , whereas it is only 0.28 m s^{-1} for the multi-layered cloud.

It is difficult to compare the time series in figure 4.4, which uses data with a time resolution of approximately 5 seconds, with an equivalent time series from the model output, which has a time resolution of 1 hour. However, since we are interested in whether the model captures the highest values in updraft velocity, it is the distribution of values that we are concerned with, so it is sufficient to compare PDFs. We have taken vertical wind velocities from in-cloud gridboxes colocated with AO2018, where we define in-cloud to be gridboxes where TWC is non-zero. We have also taken cloud base gridboxes, defined as boxes that are in-cloud above boxes that are not in-cloud.

Figure 4.5 shows PDFs of gridbox mean updraft velocity (i.e. the resolved component) for cloud and cloud base gridboxes along the AO2018 route. The PDFs of the measurements are also shown. The modelled PDFs are significantly narrower than the observations. This is because the 4 km horizontal resolution of the simulations is not sufficient to capture the variability seen in the point measurements from the ship. Selecting specifically for cloud base rather than all cloud values does not improve the comparison. The PDFs from CONTROL have standard deviations of 0.0141 for cloud values and 0.0114 for cloud base values. The PDFs from IA_BL_M10_ALL have standard deviations of 0.0134 for cloud values and 0.0115 for cloud base values. These are 30–40 times lower than the standard deviations of the measured cloud updraft velocities.

In each in-cloud gridbox, the model prescribes a sub-grid scale component of the vertical wind velocity, $\sigma_{w,sgs}$, diagnosed from the modelled boundary layer TKE (see section 4.2.3). A time series of $\sigma_{w,sgs}$ is shown in figure 4.6. Note that in the model simulations, only in-cloud gridboxes would be prescribed a value for $\sigma_{w,sgs}$, whereas in

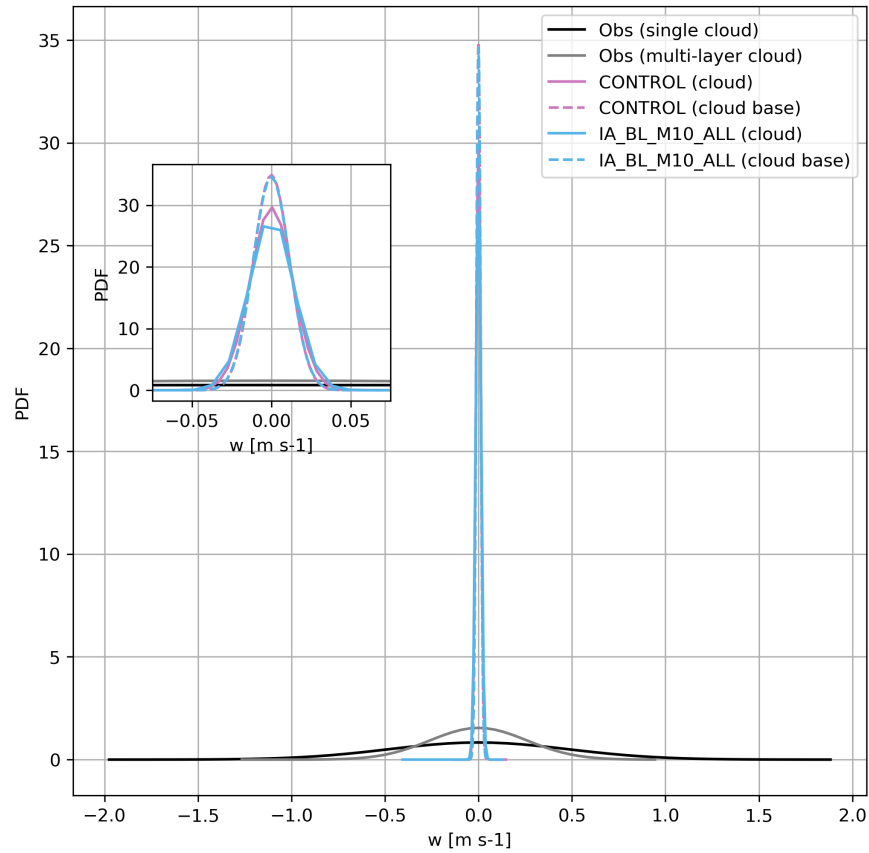


Figure 4.5: PDFs of vertical wind velocity from simulations CONTROL (pink line) and IA_BL_M10_ALL (blue line) and observations (grey and black lines). Model PDFs are shown for in-cloud gridboxes (solid lines) and cloud base gridboxes (dashed lines). Inset shows detail of model PDFs.

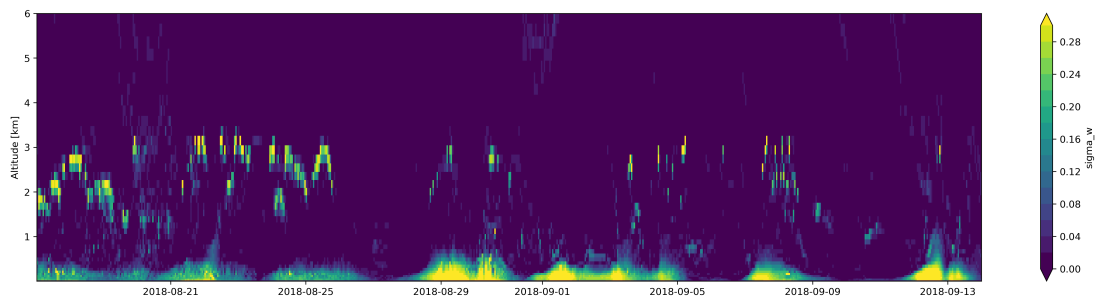


Figure 4.6: Time series of $\sigma_{w,sgs}$, the sub-grid scale component of vertical wind velocity in each gridbox along the AO2018 route, diagnosed from output from simulation IA_BL_M10_ALL.

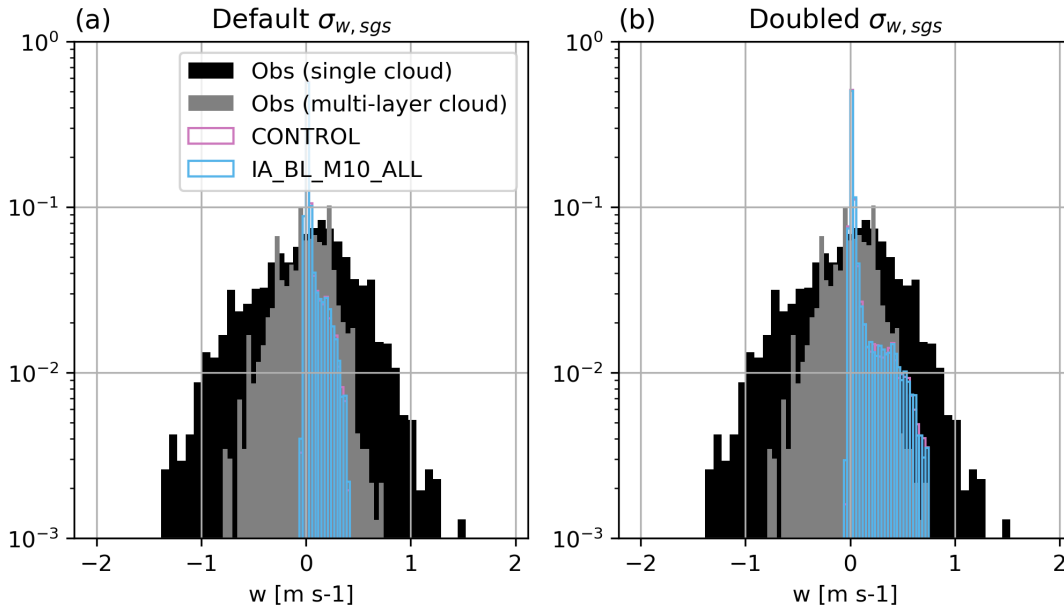


Figure 4.7: Relative frequency distributions of w_{act} for (a) the default values using $\sigma_{w,sgs}$ derived from BL TKE and (b) double the default values. Distributions are shown for in-cloud output from CONTROL (pink bars) and IA_BL_M10_ALL (blue bars). The frequency distributions of vertical wind velocity are also shown for the measurements for the single cloud layer (black bars) and the multi-layer cloud (grey bars).

figure 4.6 we make no such distinction. There are times when $\sigma_{w,sgs}$ is up to 0.3 m s^{-1} , mostly in the lowest 500 m and occasionally between 1.5–3 km. These $\sigma_{w,sgs}$ values represent a sub-grid scale distribution of vertical wind speed that is comparable to that of the multi-layer cloud case in the observations (standard deviation 0.28 m s^{-1}). However, these $\sigma_{w,sgs}$ values are limited in occurrence, and the majority of the colocated gridboxes have the minimum imposed $\sigma_{w,sgs}$ value of 0.01 m s^{-1} . As such, even the sub-grid scale component of vertical wind velocity, which is designed to account for the unresolved velocities, does not typically capture the distributions seen in the observations. The effect of this unresolved variability can be seen in the distribution of w_{act} from in-cloud gridboxes during AO2018, shown in figure 4.7(a). For both simulations, the distributions in 4.7(a) are dominated by occurrences of the minimum $\sigma_{w,sgs}$ value, 0.01 m s^{-1} and the distributions are narrower than the positive half of the observed distributions. Note that because $\sigma_{w,sgs}$ is only designed to capture unresolved updrafts for in-cloud gridboxes, it is only defined for positive values. The simulated distributions in figure 4.7 are therefore skewed to positive values. In the observations, larger vertical wind velocities are more likely to occur. At a relative frequency of 1%, the maximum w_{act} value from the simulations is about 0.4 m s^{-1} , whereas the multi-layer cloud case sees values of about 0.5 m s^{-1} and the single-layer cloud case sees values of nearly 1 m s^{-1} .

In the next section, we will use ARG2000-offline to examine the effect of the updraft

velocity on aerosol activation in our model.

4.6 Aerosols

In the last two sections, we showed that there are model biases in surface radiation, cloud fraction, cloud microphysics and vertical wind velocity. It is likely that the biases in cloud microphysics (i.e. too much ice and too little water) are related to the surface radiation biases. Here, we will investigate the aerosol concentration from both simulations and use ARG2000-offline to examine aerosol activation. We will seek to understand whether the behaviour of aerosols in the model is the cause of biases in the clouds.

4.6.1 Aerosol time series and activated fractions

Figure 4.8 shows time series and PDFs of aerosol at the surface during AO2018. Colocated UKESM output that was shown in the previous chapter is displayed here with UKCA-CASIM output for comparison of the two models. As in UKESM, simulation CONTROL in UKCA-CASIM underestimates the concentration of the nucleation and Aitken modes. The particle concentrations in UKCA-CASIM are up to 5 orders of magnitude too low in the nucleation mode and up to 3 orders of magnitude too low in the Aitken mode. The extra NPF in the boundary layer and free troposphere (IA.BL.M10.ALL relative to CONTROL) increases the nucleation mode concentration by up to 6 orders of magnitude, like in UKESM, vastly improving the agreement of the model with the observations. In the Aitken mode, the concentration in IA.BL.M10.ALL is up to 4 orders of magnitude higher than CONTROL, again improving the model performance and producing PDFs of surface concentration that are much closer to those from the measurements.

The nucleation mode concentrations are occasionally higher in UKCA-CASIM than in UKESM, for example on days 248 and 249 when the output from UKCA-CASIM is about 2 orders of magnitude higher than the UKESM output for both simulations. Conversely, concentrations are occasionally lower in the Aitken mode, sometimes by 2 orders of magnitude (e.g. day 231 for CONTROL relative to UKESM_CONTROL or day 239 for IA.BL.M10.ALL relative to UKESM_IA.BL.M10.ALL).

In the accumulation mode, the concentration does not differ very much between CONTROL and IA.BL.M10.ALL, though both simulations produce lower concentrations than UKESM. The difference between UKCA-CASIM and UKESM in the accumulation mode can be up to an order of magnitude, for example on day 238. The lower concentrations in UKCA-CASIM create some improvement in model performance, since UKESM could not produce the lowest concentrations recorded and had PDFs that were too narrow compared to the observations, centred towards the higher values. The ac-

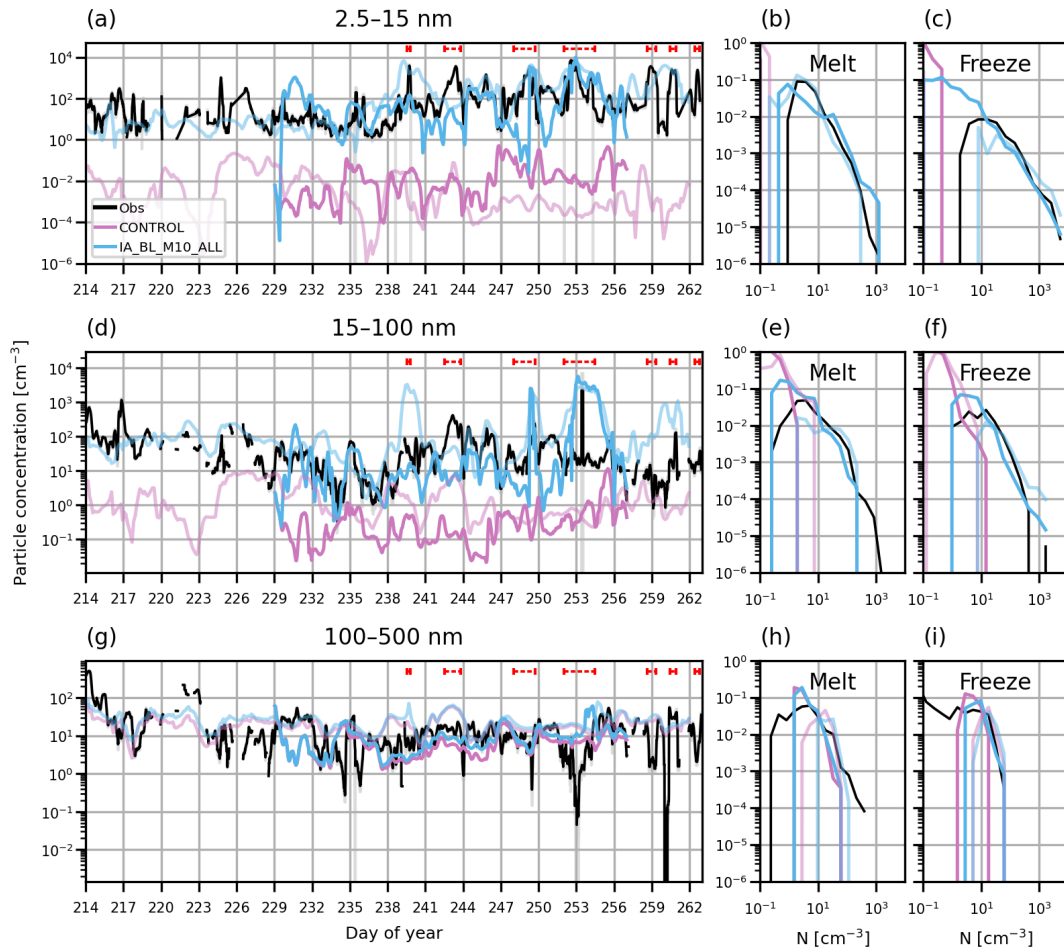


Figure 4.8: Times series and PDFs of aerosol concentration at the surface during AO2018 from observations and model output. Model output is from simulations CONTROL (solid pink lines) and IA_BL_M10_ALL (solid blue lines). UKESM output is also shown, lines have been made slightly transparent for ease of viewing UKCA-CASIM output. Observations are shown as 3-hourly mean (black lines) and standard deviation (grey shading). Aerosol concentrations are shown for particles with diameter (a-c) 2.5-15 nm, (d-f) 15-100 nm and (g-i) 100-500 nm. Red dashed lines in (a, d, g) show observed NPF events. PDFs are separated by observed sea ice freeze-up date, 27th August 2018 (day 239).

cumulation mode concentrations in UKCA-CASIM have a larger range and thus wider PDFs, except for simulation CONTROL in the freeze period which is narrower than that from UKESM but is shifted to smaller values. Despite the lower accumulation mode concentrations from UKCA-CASIM, the model still fails to capture the minimum values recorded. The lowest concentration from UKCA-CASIM is about 10 cm^{-3} whereas concentrations of less than 0.01 cm^{-3} were recorded during the campaign.

Figure 4.9 shows colocated aerosol profiles of the accumulation mode up to 6 km from simulation IA_BL_M10_ALL. The concentration is generally higher aloft and at the beginning of the drift period. Concentrations in the boundary layer typically vary

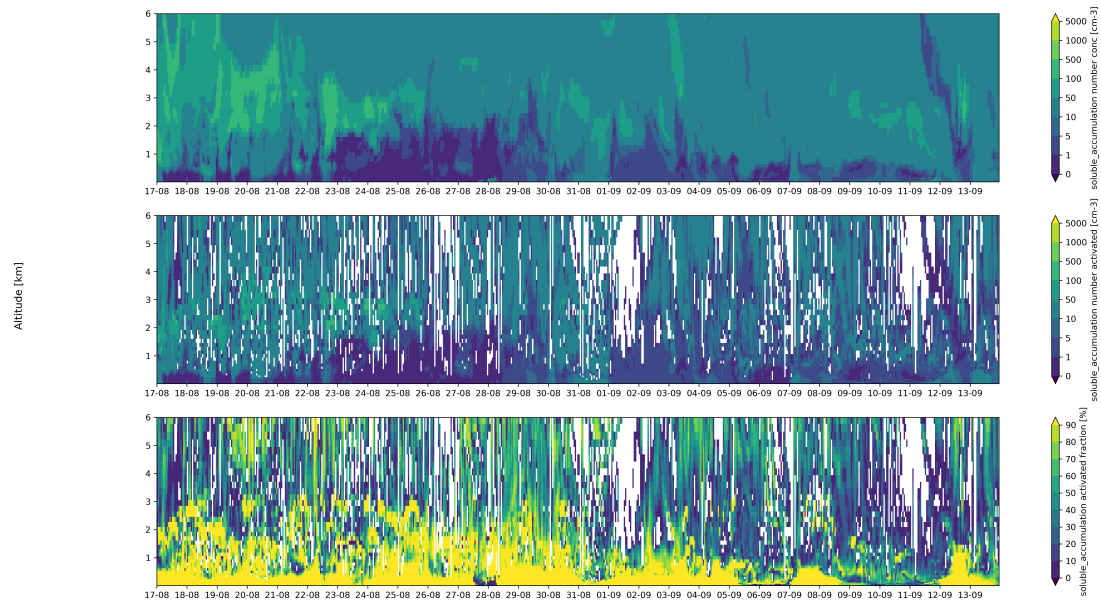


Figure 4.9: Profiles of (a) accumulation mode total concentration, (b) accumulation mode activated concentration and (c) fraction of activated accumulation mode particles from ARG2000-offline output, run using model output from IA_BLM10_ALL.

between $0\text{--}10\text{ cm}^{-3}$, with higher values occurring occasionally, for example at the surface on 28th August or below 1 km on 31st August and 1st September. The highest concentrations are simulated between about 2–4 km, where values are over 100 cm^{-3} , e.g. between 19th and 21st August.

Figure 4.9 also shows the number of activated particles in the accumulation mode as calculated in each timestep by ARG2000-offline, and the fraction of particles in the accumulation mode that are activated. Missing data corresponds to gridboxes with negative values of w_{act} , which occur since we have not selected for in-cloud gridboxes in figure 4.9. Below 1 km, where the accumulation mode concentrations are typically lowest, most accumulation particles are activated and the activated fraction at this altitude is usually 90%. Above 1 km, where the total accumulation mode concentration is higher, the activated fraction is more variable and reaches lower values than nearer the surface.

Total and activated concentrations for the Aitken mode are given in figure 4.10, along with the activated fraction of particles. The concentration of Aitken mode particles is generally lowest near the surface, though there are periods of high concentration at the surface, on the order of 1000 cm^{-3} , resulting from the iodic acid NPF, e.g. 28th August or 10th and 11th September. Outside of these events, Aitken concentrations in the boundary layer are on the order of 1 cm^{-3} . In the first few days of the simulation (up to 21st August), these low concentrations extend up to about 3 km. After the 21st August, concentrations above the boundary layer are higher, increasing with altitude

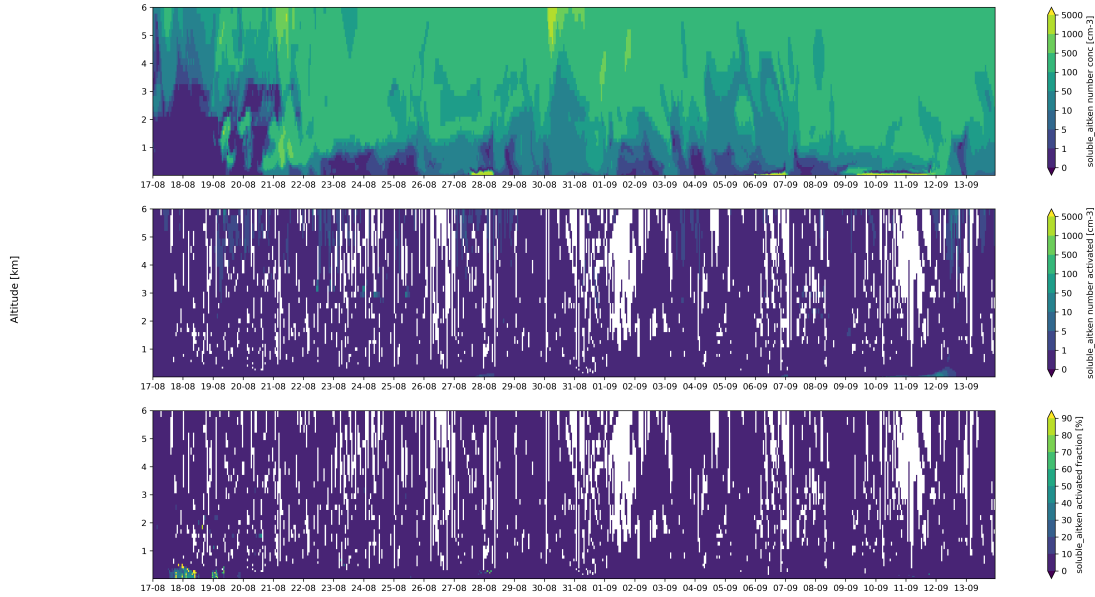


Figure 4.10: Profiles of (a) Aitken mode total concentration, (b) Aitken mode activated concentration and (c) fraction of activated Aitken mode particles from ARG2000-offline output, run using model output from IA_BLM10_ALL.

from the surface. Above 1 km, concentrations are on the order of between 10–100 cm^{-3} , reaching 1000 cm^{-3} above 5 km on 30th August. The gradient of Aitken mode concentrations with altitude reflects the free-tropospheric source of secondary particles.

Very few particles are activated in the Aitken mode. Most Aitken activation occurs above 4 km, where the concentration of activated particles occasionally reaches 50 cm^{-3} . The activated fraction remains below 10% through the drift period at all altitudes, except for a brief period at the surface on 17–19th August, where there are a few timesteps with high activated fractions. Since these timesteps occur when both total and activated concentrations are low ($< 1 \text{ cm}^{-3}$), these high fractions can be considered noise.

The activation of accumulation and Aitken mode particles at the surface is summarised in figure 4.11. The total number of activated particles from ARG2000-offline is shown for the surface. Note that in the model, the total number of activated particles could be larger since CDNC is prognostic and will only reduce during cloud evaporation. The activated concentration from ARG2000-offline varies over 3 orders of magnitude, from 10^{-2} – 10 cm^{-3} . The fractional contribution of activated particles from the accumulation and Aitken modes reflects that very few Aitken particles are activated at the surface (figure 4.10) and so most activated particles are from the accumulation mode. Note that the contribution from the coarse mode is not shown, but the total concentration of the coarse mode is low, so the contribution from the coarse mode is also small. There are only brief periods on the order of a few hours where the contribution

from the Aitken mode is non-zero and only 2 occasions where the contribution from the Aitken mode is larger than that from the accumulation mode. These are on 27th August and 6th September. The fraction of activated particles from the Aitken mode is below 80% on 27th August and below 60% on 6th September. The total number of activated particles drops by about an order of magnitude in both of these periods of Aitken activation. Figure 4.11 also shows the number of activated particles predicted by ARG2000-offline without any contribution from the Aitken mode (blue dashed line). The number of activated particles with and without Aitken activation are similar, reflecting the fact that the Aitken mode is not contributing much to the surface CDNC on these occasions.

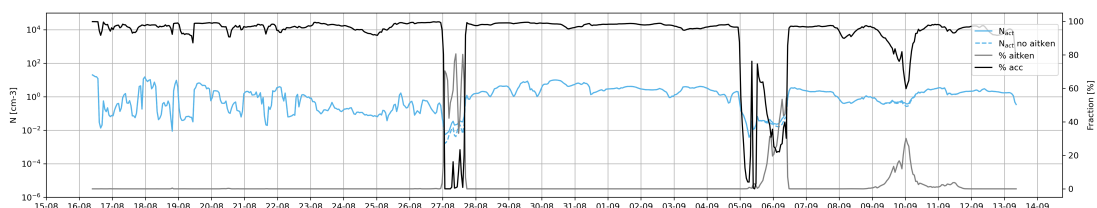


Figure 4.11: Time series of the total number concentration of activated particles at the surface (blue line) as predicted by ARG2000-offline, using model output from IA_BL_M10_ALL, with the fraction of activated particles coming from the accumulation mode (black line) and Aitken mode (grey line). The predicted number concentration of activated particles excluding those from the Aitken mode is also shown (blue dashed line).

4.6.2 Sensitivity of aerosol activation to accumulation mode concentration and updraft velocity

Figures 4.9, 4.10 and 4.11 show that the majority of the activated particles as calculated by ARG2000-offline are from the accumulation mode. However, it was clear from the results presented in Baccarini et al. (2020) that particles as small as 40 nm were activated during AO2018. The low activated concentration in the Aitken mode from ARG2000-offline therefore suggests that the model is not capturing the conditions required for activation of small particles. Activation of small particles requires a high supersaturation. Field measurements and LES studies have shown that the high supersaturations required can typically occur in two ways: in high-updraft regimes, or when the concentration of large aerosols is low (1 cm^{-3} or less). In this section, we will run sensitivity tests with the ARG2000-offline code to investigate how the activated fractions respond to higher updraft velocities and lower accumulation mode concentrations.

As shown in figure 4.8, the measured accumulation mode at the surface reached 1 cm^{-3} on multiple occasions during AO2018, but the model does not capture such low concentrations in the accumulation mode. The lowest concentration in the model output is 10 cm^{-3} , and the troughs in the observed concentration are overestimated

by 1–2 orders of magnitude (e.g. days 249, 253). Rather than re-run the model with numerous sensitivity tests, we can use ARG2000-offline to examine what happens to the activated particle concentration from each mode when the accumulation mode concentration is lower. We do this by prescribing the accumulation mode concentration in ARG2000-offline to be a factor of 100 lower than that of the model output. We use a factor of 100 since this brings the modelled concentration in line with the accumulation mode concentration on day 253, when the accumulation mode concentration was at its lowest in the drift period.

We showed in section 4.5 that neither the gridbox mean vertical wind velocity nor the prescribed sub-grid scale component is capable of capturing the observed distribution in cloud updraft velocities. As such, the strongest updrafts will not be simulated and the calculations in ARG2000 will use updraft velocities that are too low. This limits the maximum supersaturation of the model and therefore impacts on the activation of Aitken mode particles as calculated by ARG2000. To test the sensitivity of Aitken activation to the variability in the updraft velocities, we ran the offline code with a prescribed sub-grid component double that of the default value calculated from TKE. The distribution of w_{act} during AO2018 using the doubled $\sigma_{w,sgs}$ values is shown in figure 4.7(b). Note that we apply the minimum value after doubling, so the minimum standard deviation is still 0.01 m s^{-1} . The distribution in w_{act} after doubling roughly captures the width of the vertical wind velocity distribution during the multi-layer cloud case, so higher updraft velocities will be more likely to occur. The distribution for the single-layer cloud is still wider than the the simulated distribution, and the simulated distribution is still dominated by the minimum value of $\sigma_{w,sgs}$. However, since the perturbed updraft velocity distribution is wider, it provides a sensitivity test of how activation responds in ARG2000-offline when higher updraft velocities are more likely to occur. Note that in the model, the CDNC calculated by ARG2000 “remembers” the highest updraft velocity seen by a cloud, as discussed in section 4.2.3. As such, the effect of increasing w_{act} as we do here would potentially have less of an effect in the model than it does in ARG2000-offline, where we do not use the prognostic CDNC information.

Figure 4.12 shows the results of activated particle concentration at the surface from ARG2000-offline using the more realistic updraft distribution and lower accumulation mode concentration. In general, the activated concentration is 1–2 orders of magnitude lower than the results from ARG2000-offline using unadjusted model output (figure 4.11). This is because the lower accumulation mode concentration leads to fewer activated particles overall. A larger fraction of the activated particles are from the Aitken mode than when unadjusted model output is used. With the more realistic updraft distribution and accumulation mode concentration, the fraction of activated particles coming from the accumulation mode is rarely greater than 60%. The fraction from the

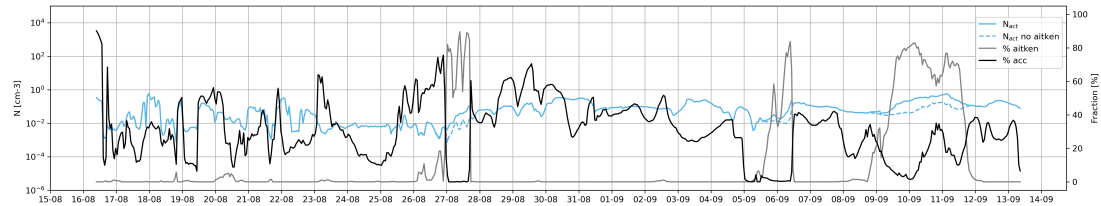


Figure 4.12: Time series of the total number concentration of activated particles at the surface (blue line) as predicted by ARG2000-offline, using model output from IA_BLM10_ALL with the number concentration of the accumulation mode reduced by a factor of 100 and the width of the updraft PDF increased by a factor of 2. The fraction of activated particles are shown for particles from the accumulation mode (black line) and Aitken mode (grey line). The predicted number concentration of activated particles excluding those from the Aitken mode is also shown (blue dashed line).

Aitken mode does not always increase sufficiently to account for the deficit, indicating a greater fraction from the coarse mode which is not shown, but the fractions from the Aitken mode increase as well. On three occasions, e.g. between 9th and 12th September, the Aitken mode is larger than the accumulation mode fraction. This behaviour suggests that the Aitken mode could sustain cloud drop number concentrations when the accumulation concentration is low. Moreover, it shows that the activation scheme of ARG2000 is able to capture such behaviour, but only when the model captures the corresponding dynamic conditions.

4.7 Discussion and conclusions

We have used the regional configuration of the UM with UKCA and CASIM to investigate aerosol activation in the Arctic. We have shown that incorrect behaviour of clouds is linked to biases in the surface radiation budget. Our simulations have identified three areas of the model that require improvements to enable UKCA-CASIM to capture the activation of Aitken mode particles in the Arctic summer boundary layer:

- Like in UKESM, the model baseline simulation underestimates the concentration of nucleation and Aitken mode particles at the surface by several orders of magnitude. Secondary particles, both entrained from the free troposphere and created in the boundary layer from iodic acid, are required as a source of particles for the model to reproduce the concentrations measured during AO2018.
- The model does not simulate periods during which accumulation mode concentrations are very low, as were observed during AO2018. The lowest measured concentrations of 1 cm^{-3} and below are overestimated by the model by about 2 orders of magnitude. Since lower concentrations of larger particles leads to higher supersaturations, lower accumulation mode concentrations can promote the activation of Aitken particles. This is seen in the results from the ARG2000

code. When we remove the model bias in accumulation mode, ARG2000 simulates periods when the Aitken mode is the main source of CCN.

- The model does not resolve the updraft velocities. Although ARG2000 uses a sub-grid component in the vertical winds, we have shown that this method is still not able to capture the observed distribution of updrafts. The lower variability in the model means that higher values of vertical wind velocity are sampled less frequently, and since high updrafts cause higher supersaturation, the lower variability results in lower supersaturations in the model. More Aitken particles are therefore activated when we tune the vertical wind velocity distribution to measurements by increasing the width of the distribution.

We have shown that when all three of these factors (Aitken mode particle concentration, accumulation mode particle concentration and sub-grid scale vertical wind velocity) are improved in the activation scheme, Aitken particles can occasionally be the dominant source of CCN, as was observed Karlsson et al. (2022). The results reflect other studies where it has been shown that Aitken mode particles can sustain Arctic clouds during periods of low accumulation mode concentration. However, our results have also highlighted biases in the model that cannot be fixed by focusing on aerosol activation alone. Since the cloud formation in the model is controlled by the large-scale cloud scheme, problems of too-high cloud fraction are not caused by the aerosols. Our simulations produce similar values for surface radiation fluxes, cloud fraction, LWC, and IWC. Higher Aitken and nucleation mode particle concentrations from new particle formation (simulation IA_BL_M10_ALL) are therefore not influencing cloud behaviour in the simulations.

The results from these high-resolution simulations have implications for global models and Arctic climate projections. Clouds in the Arctic are both a controlling factor and a source of uncertainty in the future energy budget of the region. Aerosols constitute a large part of this uncertainty, since the future aerosol budget is very difficult to model, as are the impacts and feedbacks relating to such change. Since the coarse resolution of global Earth system models cannot resolve important cloud processes, we use high-resolution configurations such as the one used here to gain a process-level understanding with the aim of creating parameterisations that can more accurately capture cloud and aerosol behaviour in global models that are used to predict long-term climate change. In this study we aimed to investigate the activation of small particles, such as those created by new particle formation, in Arctic clouds. We have shown that we will not be able to quantify the frequency or importance of Aitken activation on a large scale until the parameterisations used to simulate cloud formation are improved.

Chapter 5

Conclusions

The interactions of aerosols and clouds in the Arctic climate system contribute to the significant uncertainty in projections of Arctic warming and sea ice loss. In this thesis, we have used global and regional models to investigate the Arctic aerosol budget and Arctic aerosol-cloud interactions. In this chapter we will summarise the results of the thesis and their implications. We will then give suggestions for future work that follows from areas where open questions remain.

This thesis has showed that we can improve the simulation of the high Arctic summertime aerosol size distribution in regional and global modelling set-ups by including new particle formation in the free troposphere as a source of particles to the surface. However, our ability to investigate the interactions of this particle source with Arctic clouds has been hindered by biases in the simulation of Arctic clouds by the regional model. The clouds in our regional simulations are too frequently occurring and contain too much ice, resulting in too much incoming solar radiation and too much outgoing longwave radiation compared to observations. Also, the simulated accumulation mode concentrations do not reach the lowest observed values. Too high accumulation mode concentrations affect the new particle formation rates via the condensation sink of precursor vapours, and inhibit the activation of Aitken particles that can otherwise occur during high supersaturation regimes when accumulation mode concentrations are low (about 1 cm^{-3} and below).

5.1 Summary of findings

The concentration of nucleation and Aitken mode particles in the high Arctic summertime is underestimated in the default configurations of both the global and regional models. In the global model, the Aitken mode concentration at the surface is up to 3 orders of magnitude too low; the nucleation mode concentration is up to 5 orders of magnitude too low. Such poor model-observation agreement implies that the balance

of sources and sinks of Arctic aerosol is not captured by the model. This is likely as a result of the uncertainty in model parameterisations of aerosol processes such as new particle formation, primary emissions, and wet removal. If the aerosol budget is incorrect in the model, the sensitivity of the Arctic region to climate change will also be subject to biases. The higher resolution of the regional model does not correct the underestimations in nucleation and Aitken mode particle concentrations.

The concentration of the accumulation mode is in closer agreement with observations than the smaller modes, but the lowest observed concentrations are not captured by the model. In the observations, the accumulation mode concentration at the surface is occasionally on the order of 1 cm^{-3} or below for hours at a time. During such events, both models typically overestimate the accumulation mode concentration by 1–2 orders of magnitude. Such periods of low accumulation mode concentrations have been associated with cloud dissipation or tenuous cloud regimes, and therefore could have significant effects on the surface radiation budget that the models will fail to capture. Moreover, the accumulation mode particles act as a sink of condensable vapours, so the formation and growth of smaller particles in the model could also be affected by biases in the accumulation mode.

In chapter 2, we showed that neither the wet removal of aerosols nor the emissions of primary marine organic particles could be modified to account for the underestimation of nucleation and Aitken mode particle concentrations in our configuration of UKESM. We tested a source of primary marine organic carbon emitted at a size of 20 nm diameter. We found that for this source of 20 nm particles to explain the observations from the high Arctic summer, the flux of particles from the Arctic Ocean would need to be a factor of 200 higher than observed fluxes from the same region during summer. It is possible that an increase in particle number after emission due to particle break-up, as has been proposed in literature, could account for the difference in modelled and observed fluxes, though measurements of such a process are currently lacking. Moreover, both the Aitken and accumulation mode particle concentrations were overestimated when this 20 nm primary marine source was included, but peaks in the nucleation mode concentration that were observed to occur during new particle events were not captured. Because we could not reconcile the modelled aerosol size distribution with observations using either a primary marine source or by adjusting wet removal, we investigated secondary sources in chapter 3.

The results presented in chapter 3 show a transition at the end of summer from a free-tropospheric source of particles to a boundary layer source. We implemented an empirical iodic acid scheme based on in-situ measurements, and particle formation and growth rates from a recent laboratory study. The results showed that iodic acid can be a source of small particles in the boundary layer, as was observed. Prior to the onset of sea ice freezing, the principal source of particles to the surface was entrainment of particles

from the free troposphere. It is unclear whether such particles were created in the high Arctic free troposphere or were transported there after being created at lower latitudes. This seasonal transition in Arctic new particle formation was surprising given results from previous studies that have highlighted the importance of new particle formation in the boundary layer as a source of Arctic aerosol (Browse et al., 2014). A free-tropospheric source of particles would have implications for the future Arctic aerosol budget, because it would be less sensitive to changes taking place at the surface (i.e. sea ice retreat) than particle formation in the boundary layer.

In chapter 4, we used the regional model to investigate the activation of Aitken mode particles into cloud droplets. We found that modifications are required to get the model activation scheme to simulate the observed behaviour of Aitken activation. The model could only simulate Aitken activation when we reduced the accumulation mode concentration by a factor of 100 to capture the lowest observed concentrations, and increased the sub-grid scale component of the updraft velocities by a factor of 2 to improve the model-observation agreement in the distribution of updraft velocities. The results therefore show that biases in the accumulation mode concentration are preventing the model from capturing the correct behaviour in the Aitken mode, both via the effect on new particle formation from the condensation sink and also by influencing aerosol activation. In addition, the parameterisation used to simulate sub-grid scale variations in the updraft velocity is still not capturing the distribution of updrafts as measured in the field.

Chapter 4 also revealed model biases in cloud fraction, cloud water contents, and the surface radiative fluxes. Modifications to the aerosol sources did not mitigate these biases. The overestimated shortwave flux and underestimated longwave flux are likely related to the biases in clouds. The simulated clouds contain too much ice and not enough liquid water, which would make them too optically thin, therefore increasing incoming shortwave and outgoing longwave relative to the observations. Our improvements to the nucleation and Aitken mode concentrations do not correct these biases in the model, although as we have already discussed, the activation of Aitken particles into cloud drops is not captured in the model, so the influence of the improved Aitken mode concentration on clouds is limited. However, Aitken activation alone is unlikely to be the source of the problems in the simulated clouds. Previous studies have reported issues in the regional model when it comes to simulating clouds in the Arctic (Birch et al., 2012; Young et al., 2021). For example, the model struggles to simulate the decoupled conditions that are typical in the high Arctic summer, instead producing boundary layers that are too well mixed. Mixing in the boundary layer affects the transport of heat and moisture from the surface to the cloud layer, and so can influence the behaviour of clouds, including the phase partitioning. In our simulations, the formation of cloud ice is temperature dependent.

5.2 Future work

This thesis has provided information on the behaviour of Arctic aerosol in the UKCA model, both in a global climate configuration and in a regional model, coupled to two-moment cloud microphysics. It has also highlighted several questions which remain open. The rest of this chapter describes such questions and recommends topics for future work.

A primary marine source of carbonaceous aerosol was ruled out in chapter 2 as the source of model-observation bias in the high Arctic summer size distribution. However, the results did suggest that the relationship between wind speed and primary marine aerosol emissions is not captured in the model for gridboxes containing sea ice. Observations from the Arctic have shown a weaker wind speed dependence for particle flux from open leads than the flux from open ocean. This is likely because of the smaller fetch over a lead compared to open ocean, something the model does not take account of by using only a linear scaling of particle flux to gridbox open water fraction. The incorrect relationship of particle emissions to sea ice fraction is likely to create biases in projections of the Arctic aerosol budget, since the expansion of the MIZ and loss of ice in the pack ice region will perturb emission fluxes from the Arctic Ocean. If the model does not capture the present day baseline in Arctic Ocean particle emissions, any potential cloud adjustments or climate feedbacks from this change in behaviour will not be simulated. We suggest that the wind speed dependence of primary emissions from open leads should be parameterised separately from that of the open ocean.

Further to the incorrect wind speed dependence of primary emissions from open leads, the size distribution of primary marine organic carbon warrants further attention. UKESM uses a single log-normal mode. We tested the effects of changing the mean size of the mode for the Arctic, but did not examine other functional forms of the size distribution. Complex microphysical processes, such as the particle break-up theory proposed by Leck and Bigg (2010) and Lawler et al. (2021) are unlikely to produce a particle size distribution as straightforward as a single mode. Given the knowledge gaps surrounding primary marine organics in the Arctic, a synthesis of field measurements, laboratory work and modelling studies is required to improve the representation of this process in global climate and Earth system models.

In chapter 2, we used a threshold for the ratio of ice to liquid in clouds above which to suppress aerosol scavenging. This mechanism was designed to represent the lower efficiency of scavenging from ice and mixed-phase clouds than liquid clouds. Although the use of the threshold led to model overestimations in sulphate mass concentrations at Arctic ground stations, the output also showed slight improvements in the seasonal cycle of the measurements. It is therefore possible that a combination of the ice water content fraction and a higher scavenging efficiency could improve model skill overall

when evaluated against Arctic aerosol mass concentrations. This possibility should be investigated.

Chapter 3 revealed the importance of the free troposphere as a source of secondary particles to the surface during Arctic summer. Particle formation in the Arctic free troposphere is less well understood than at the surface. More observations of size-resolved aerosol concentrations and vapour concentrations from above the boundary layer are critical to shed more light on this free-tropospheric secondary source. Moreover, we used an empirical iodic acid new particle formation scheme to show that it is a source of particles in the boundary layer during the sea ice freeze period. The exact mechanisms controlling the formation of iodic acid during sea ice freezing are not understood, and should be investigated to understand how widespread this particle source is, and how it is sensitive to changes in the region. Also, we did not include cloud or fog droplets as a sink of iodic acid in our simulations, since the representation of the clouds in the coarse global gridboxes was not accurate. Future investigations of iodic acid new particle formation should include the effect of cloud drops as a sink of iodic acid.

Bibliography

- Abdul-Razzak, H. and Ghan, S. J. 2000. “A parameterization of aerosol activation 2. Multiple aerosol types”. *Journal of Geophysical Research Atmospheres* **105**(D5), pp. 6837–6844.
- Achtert, P., Oconnor, E. J., Brooks, I. M., Sotiropoulou, G., Shupe, M. D., Pospichal, B., Brooks, B. J., and Tjernström, M. 2020. “Properties of Arctic liquid and mixed-phase clouds from shipborne Cloudnet observations during ACSE 2014”. *Atmospheric Chemistry and Physics* **20**(23), pp. 14983–15002.
- Albert, M. F., Schaap, M., Manders, A. M., Scannell, C., O’Dowd, C. D., and Leeuw, G. de 2012. “Uncertainties in the determination of global sub-micron marine organic matter emissions”. *Atmospheric Environment* **57**, pp. 289–300.
- Albrecht, B. A. 1989. “Aerosols, Cloud Microphysics, and Fractional Cloudiness”. *Science* **245**(4923), pp. 1227–1230.
- Allan, J. D., Williams, P. I., Najera, J., Whitehead, J. D., Flynn, M. J., Taylor, J. W., Liu, D., Darbyshire, E., Carpenter, L. J., Chance, R., Andrews, S. J., Hackenberg, S. C., and McFiggans, G. 2015. “Iodine observed in new particle formation events in the Arctic atmosphere during ACCACIA”. *Atmospheric Chemistry and Physics* **15**(10), pp. 5599–5609.
- Baccarini, A., Karlsson, L., Dommen, J., Duplessis, P., Vüllers, J., Brooks, I. M., Saiz-Lopez, A., Salter, M., Tjernström, M., Baltensperger, U., Zieger, P., and Schmale, J. 2020. “Frequent new particle formation over the high Arctic pack ice by enhanced iodine emissions”. *Nature Communications* **11**(1), p. 4924.
- Baccarini, A. and Schmale, J. 2020. *Ultrafine particle concentration measured during the Arctic Ocean 2018 expedition [data set]*.
- Beck, L. J., Sarnela, N., Junninen, H., Hoppe, C. J. M., Garmash, O., Bianchi, F., Riva, M., Rose, C., Peräkylä, O., Wimmer, D., Kausiala, O., Jokinen, T., Ahonen, L., Mikkilä, J., Hakala, J., He, X.-C., Kontkanen, J., Wolf, K. K. E., Cappelletti, D., Mazzola, M., Traversi, R., Petroselli, C., Viola, A. P., Vitale, V., Lange, R., Massling, A., Nøjgaard, J. K., Krejci, R., Karlsson, L., Zieger, P., Jang, S., Lee, K., Vakkari, V., Lampilahti, J., Thakur, R. C., Leino, K., Kangasluoma, J., Duplissy, E.-M., Siivola, E., Marbouti, M., Tham, Y. J., Saiz-Lopez, A., Petäjä, T., Ehn, M.,

- Worsnop, D. R., Skov, H., Kulmala, M., Kerminen, V.-M., and Sipilä, M. 2020. “Differing mechanisms of new particle formation at two Arctic sites.” *Geophysical Research Letters*.
- Bigg, E. K. and Leck, C. 2001. “Cloud-active particles over the central Arctic Ocean”. *Journal of Geophysical Research Atmospheres*.
- Bigg, K. E., Leck, C., and Nilsson, D. E. 1996. “Sudden changes in arctic atmospheric aerosol concentrations during summer and autumn”. *Tellus B: Chemical and Physical Meteorology* **48**(2), pp. 254–271.
- Bintanja, R. 2018. “The impact of Arctic warming on increased rainfall”. *Scientific Reports* **8**(1), p. 16001.
- Birch, C. E., Brooks, I. M., Tjernström, M., Shupe, M. D., Mauritsen, T., Sedlar, J., Lock, A. P., Earnshaw, P., Persson, P. O. G., Milton, S. F., and Leck, C. 2012. “Modelling atmospheric structure, cloud and their response to CCN in the central Arctic: ASCOS case studies”. *Atmospheric Chemistry and Physics* **12**(7), pp. 3419–3435.
- Boeke, R. C. and Taylor, P. C. 2016. “Evaluation of the Arctic surface radiation budget in CMIP5 models”. *Journal of Geophysical Research* **121**(14), pp. 8525–8548.
- Brock, C. A., Williamson, C., Kupc, A., Froyd, K. D., Erdesz, F., Wagner, N., Richardson, M., Schwarz, J. P., Gao, R. S., Katich, J. M., Campuzano-Jost, P., Nault, B. A., Schroder, J. C., Jimenez, J. L., Weinzierl, B., Dollner, M., Bui, T., and Murphy, D. M. 2019. “Aerosol size distributions during the Atmospheric Tomography Mission (ATom): Methods, uncertainties, and data products”. *Atmospheric Measurement Techniques* **12**(6), pp. 3081–3099.
- Browse, J., Carslaw, K. S., Arnold, S. R., Pringle, K., and Boucher, O. 2012. “The scavenging processes controlling the seasonal cycle in Arctic sulphate and black carbon aerosol”. *Atmospheric Chemistry and Physics*.
- Browse, J., Carslaw, K. S., Mann, G. W., Birch, C. E., Arnold, S. R., and Leck, C. 2014. “The complex response of Arctic aerosol to sea-ice retreat”. *Atmospheric Chemistry and Physics*.
- Bulatovic, I., Igel, A. L., Leck, C., Heintzenberg, J., Riipinen, I., Ekman, A. M. L., and Bulatovic, I. 2020. “The importance of Aitken mode aerosol particles for cloud sustenance in the summertime high Arctic: A simulation study supported by observational data”.
- Cai, Z., You, Q., Wu, F., Chen, H. W., Chen, D., and Cohen, J. 2021. “Arctic warming revealed by multiple CMIP6 models: Evaluation of historical simulations and quantification of future projection uncertainties”. *Journal of Climate* **34**(12), pp. 4871–4892.
- Carslaw, K. S., Boucher, O., Spracklen, D. V., Mann, G. W., Rae, J. G. L., Woodward, S., and Kulmala, M. 2010. *Atmospheric Chemistry and Physics A review of natural*

- aerosol interactions and feedbacks within the Earth system*. Tech. rep., pp. 1701–1737.
- Chang, R. Y., Sjostedt, S. J., Pierce, J. R., Papakyriakou, T. N., Scarratt, M. G., Michaud, S., Levasseur, M., Leaitch, W. R., and Abbatt, J. P. 2011. “Relating atmospheric and oceanic DMS levels to particle nucleation events in the Canadian Arctic”. *Journal of Geophysical Research Atmospheres* **116**(21).
- Cohen, J., Zhang, X., Francis, J., Jung, T., Kwok, R., Overland, J., Ballinger, T. J., Bhatt, U. S., Chen, H. W., Coumou, D., Feldstein, S., Gu, H., Handorf, D., Henderson, G., Ionita, M., Kretschmer, M., Laliberte, F., Lee, S., Linderholm, H. W., Maslowski, W., Peings, Y., Pfeiffer, K., Rigor, I., Semmler, T., Stroeve, J., Taylor, P. C., Vavrus, S., Vihma, T., Wang, S., Wendisch, M., Wu, Y., and Yoon, J. 2020. “Divergent consensus on Arctic amplification influence on midlatitude severe winter weather”. *Nature Climate Change* **10**(1), pp. 20–29.
- Coopman, Q., Riedi, J., Finch, D. P., and Garrett, T. J. 2018. “Evidence for Changes in Arctic Cloud Phase Due to Long-Range Pollution Transport”. *Geophysical Research Letters* **45**(19), pp. 709–710.
- Croft, B., Wentworth, G. R., Martin, R. V., Leaitch, W. R., Murphy, J. G., Murphy, B. N., Kodros, J. K., Abbatt, J. P., and Pierce, J. R. 2016a. “Contribution of Arctic seabird-colony ammonia to atmospheric particles and cloud-albedo radiative effect”. *Nature Communications* **7**.
- Croft, B., Martin, R. V., Leaitch, W. R., Burkart, J., Chang, R. Y.-W., Collins, D. B., Hayes, P. L., Hodshire, A. L., Huang, L., Kodros, J. K., Moravek, A., Mungall, E. L., Murphy, J. G., Sharma, S., Tremblay, S., Wentworth, G. R., Willis, M. D., Abbatt, J. P. D., and Pierce, J. R. 2019. “Arctic marine secondary organic aerosol contributes significantly to summertime particle size distributions in the Canadian Arctic Archipelago”. *Atmospheric Chemistry and Physics* **19**(5), pp. 2787–2812.
- Croft, B., Martin, R. V., Leaitch, W. R., Tunved, P., Breider, T. J., D’Andrea, S. D., and Pierce, J. R. 2016b. “Processes controlling the annual cycle of Arctic aerosol number and size distributions”. *Atmospheric Chemistry and Physics* **16**(6), pp. 3665–3682.
- Curry, J. A., Schramm, J. L., and Ebert, E. E. 1993. “Impact of clouds on the surface radiation balance of the Arctic Ocean”. *Meteorology and Atmospheric Physics* **51**(3–4), pp. 197–217.
- Curry, J. A., Ebert, E. E., Curry, J. A., and Ebert, E. E. 1992. “Annual Cycle of Radiation Fluxes over the Arctic Ocean: Sensitivity to Cloud Optical Properties”. *Journal of Climate* **5**(11), pp. 1267–1280.
- Dall’Osto, M., Beddows, D. C. S., Tunved, P., Krejci, R., Ström, J., Hansson, H.-C., Yoon, Y. J., Park, K.-T., Becagli, S., Udisti, R., Onasch, T., O’Dowd, C. D., Simó, R., and Harrison, R. M. 2017. “Arctic sea ice melt leads to atmospheric new particle formation”. *Scientific Reports* **7**(1), p. 3318.

- Dall'Osto, M., Geels, C., Beddows, D. C., Boertmann, D., Lange, R., Nøjgaard, J. K., Harrison, R. M., Simo, R., Skov, H., and Massling, A. 2018. "Regions of open water and melting sea ice drive new particle formation in North East Greenland". *Scientific Reports* **8**(1).
- De Leeuw, G., Andreas, E. L., Anguelova, M. D., Fairall, C. W., Lewis, E. R., O'Dowd, C., Schulz, M., and Schwartz, S. E. 2011. "Production flux of sea spray aerosol". *Reviews of Geophysics* **49**(2).
- Dunne, E. M., Gordon, H., Kürten, A., Almeida, J., Duplissy, J., Williamson, C., Ortega, I. K., Kirsty, —., Pringle, J., Adamov, A., Baltensperger, U., Barmet, P., Benduhn, F., Bianchi, F., Breitenlechner, M., Clarke, A., Curtius, J., Dommen, J., Donahue, N. M., Ehrhart, S., Flagan, R. C., Franchin, A., Guida, R., Hakala, J., Hansel, A., Heinritzi, M., Jokinen, T., Kangasluoma, J., Kirkby, J., Kulmala, M., Kupc, A., Michael, Lawler, J., Lehtipalo, K., Makhmutov, V., Mann, G., Mathot, S., Merikanto, J., Miettinen, P., Nenes, A., Onnela, A., Rap, A., Reddington, C. L. S., Riccobono, F., Richards, N. A. D., Rissanen, M. P., Rondo, L., Sarnela, N., Schobesberger, S., Sengupta, K., Simon, M., Sipilä, M., Smith, J. N., Stozkhov, Y., Tomé, A., Tröstl, J., Wagner, P. E., Wimmer, D., Winkler, P. M., Worsnop, D. R., and Carslaw, K. S. 2016. "Global atmospheric particle formation from CERN CLOUD measurements". *Science* **354**(6316), pp. 1119–1124.
- Eneroth, K., Kjellström, E., and Holmén, K. 2003. "A trajectory climatology for Svalbard; investigating how atmospheric flow patterns influence observed tracer concentrations". *Physics and Chemistry of the Earth* **28**(28-32), pp. 1191–1203.
- Engvall, A.-C., Krejci, R., Ström, J., Treffeisen, R., Scheele, R., Hermansen, O., and Paatero, J. 2008a. "Changes in aerosol properties during spring-summer period in the Arctic troposphere". *Atmospheric Chemistry and Physics* **8**(3), pp. 445–462.
- Engvall, A.-C., Krejci, R., Ström, J., Minikin, A., Treffeisen, R., Stohl, A., and Herber, A. 2008b. "In-situ airborne observations of the microphysical properties of the Arctic tropospheric aerosol during late spring and summer". *Tellus B: Chemical and Physical Meteorology* **60**(3), pp. 392–404.
- Gantt, B., Johnson, M. S., Crippa, M., Prévôt, A. S., and Meskhidze, N. 2015. "Implementing marine organic aerosols into the GEOS-Chem model". *Geoscientific Model Development* **8**(3), pp. 619–629.
- Garrett, T., Zhao, C., and Novelli, P. 2010. "Assessing the relative contributions of transport efficiency and scavenging to seasonal variability in Arctic aerosol". *Tellus B: Chemical and Physical Meteorology* **62**(3), pp. 190–196.
- Garrett, T. J., Brattström, S., Sharma, S., Worthy, D. E. J., and Novelli, P. 2011. "The role of scavenging in the seasonal transport of black carbon and sulfate to the Arctic". *Geophysical Research Letters*.
- Garrett, T. J., Radke, L. F., and Hobbs, P. V. 2002. *Aerosol Effects on Cloud Emissivity and Surface Longwave Heating in the Arctic*. Tech. rep.

- Garrett, T. J. and Zhao, C. 2006. “Increased Arctic cloud longwave emissivity associated with pollution from mid-latitudes”. *Nature* **440**(7085), pp. 787–789.
- Gilgen, A., Ting Katty Huang, W., Ickes, L., Neubauer, D., and Lohmann, U. 2018. “How important are future marine and shipping aerosol emissions in a warming Arctic summer and autumn?” *Atmospheric Chemistry and Physics* **18**(14), pp. 10521–10555.
- Gong, S. L. 2003. “A parameterization of sea-salt aerosol source function for sub- and super-micron particles”. *Global Biogeochemical Cycles* **17**(4).
- Gordon, H., Field, P. R., Abel, S. J., Barrett, P., Bower, K., Crawford, I., Cui, Z., Grosvenor, D. P., Hill, A. A., Taylor, J., Wilkinson, J., Wu, H., and Carslaw, K. S. 2020. “Development of aerosol activation in the double-moment Unified Model and evaluation with CLARIFY measurements”. *Atmospheric Chemistry and Physics* **20**(18), pp. 10997–11024.
- Gordon, H., Kirkby, J., Baltensperger, U., Bianchi, F., Breitenlechner, M., Curtius, J., Dias, A., Dommen, J., Donahue, N. M., Dunne, E. M., Duplissy, J., Ehrhart, S., Flanagan, R. C., Frege, C., Fuchs, C., Hansel, A., Hoyle, C. R., Kulmala, M., Kürten, A., Lehtipalo, K., Makhmutov, V., Molteni, U., Rissanen, M. P., Stozkhov, Y., Tröstl, J., Tsagkogeorgas, G., Wagner, R., Williamson, C., Wimmer, D., Winkler, P. M., Yan, C., and Carslaw, K. S. 2017. “Causes and importance of new particle formation in the present-day and preindustrial atmospheres”. *Journal of Geophysical Research: Atmospheres* **122**(16), pp. 8739–8760.
- Grosvenor, D. P., Field, P. R., Hill, A. A., and Shipway, B. J. 2017. “The relative importance of macrophysical and cloud albedo changes for aerosol-induced radiative effects in closed-cell stratocumulus: Insight from the modelling of a case study”. *Atmospheric Chemistry and Physics* **17**(8), pp. 5155–5183.
- Hardiman, S. C., Butchart, N., O’Connor, F. M., and Rumbold, S. T. 2017. “The Met Office HadGEM3-ES chemistry-climate model: Evaluation of stratospheric dynamics and its impact on ozone”. *Geoscientific Model Development* **10**(3), pp. 1209–1232.
- He, X.-C. et al. 2021. *Role of iodine oxoacids in atmospheric aerosol nucleation*. Tech. rep.
- Held, A., Brooks, I. M., Leck, C., and Tjernström, M. 2011. “On the potential contribution of open lead particle emissions to the central Arctic aerosol concentration”. *Atmospheric Chemistry and Physics* **11**(7), pp. 3093–3105.
- Heslin-Rees, D., Burgos, M., Hansson, H. C., Krejci, R., Ström, J., Tunved, P., and Zieger, P. 2020. “From a polar to a marine environment: Has the changing Arctic led to a shift in aerosol light scattering properties?” *Atmospheric Chemistry and Physics* **20**(21), pp. 13671–13686.

- Hodson, D. L., Keeley, S. P., West, A., Ridley, J., Hawkins, E., and Hewitt, H. T. 2013. “Identifying uncertainties in Arctic climate change projections”. *Climate Dynamics* **40**(11-12), pp. 2849–2865.
- Hoesly, R. M., Smith, S. J., Feng, L., Klimont, Z., Janssens-Maenhout, G., Pitkanen, T., Seibert, J. J., Vu, L., Andres, R. J., Bolt, R. M., Bond, T. C., Dawidowski, L., Kholod, N., Kurokawa, J. I., Li, M., Liu, L., Lu, Z., Moura, M. C., O’Rourke, P. R., and Zhang, Q. 2018. “Historical (1750-2014) anthropogenic emissions of reactive gases and aerosols from the Community Emissions Data System (CEDS)”. *Geoscientific Model Development* **11**(1), pp. 369–408.
- Igel, A. L., Ekman, A. M., Leck, C., Tjernström, M., Savre, J., and Sedlar, J. 2017. “The free troposphere as a potential source of arctic boundary layer aerosol particles”. *Geophysical Research Letters*.
- Illingworth, A. J., Hogan, R. J., O’Connor, E. J., Bouniol, D., Brooks, M. E., Delanoë, J., Donovan, D. P., Eastment, J. D., Gaussiat, N., Goddard, J. W., Haeffelin, M., Klein Baltinik, H., Krasnov, O. A., Pelon, J., Piriou, J. M., Protat, A., Russchenberg, H. W., Seifert, A., Tompkins, A. M., Zadelhoff, G. J. van, Vinit, F., Willen, U., Wilson, D. R., and Wrench, C. L. 2007. “Cloudnet: Continuous evaluation of cloud profiles in seven operational models using ground-based observations”. *Bulletin of the American Meteorological Society* **88**(6), pp. 883–898.
- Intrieri, J. M., Shupe, M. D., Uttal, T., and McCarty, B. J. 2002. “An annual cycle of Arctic cloud characteristics observed by radar and lidar at SHEBA”. *Journal of Geophysical Research* **107**(C10), p. 8030.
- Jones, A., Haywood, J. M., and Boucher, O. 2007. “Aerosol forcing, climate response and climate sensitivity in the Hadley Centre climate model”. *Journal of Geophysical Research* **112**(D20), p. D20211.
- Karl, M., Leck, C., Coz, E., and Heintzenberg, J. 2013. “Marine nanogels as a source of atmospheric nanoparticles in the high Arctic”. *Geophysical Research Letters* **40**(14), pp. 3738–3743.
- Karl, M., Leck, C., Gross, A., and Pirjola, L. 2012. “A study of new particle formation in the marine boundary layer over the central Arctic Ocean using a flexible multi-component aerosol dynamic model”. *Tellus B: Chemical and Physical Meteorology* **64**(1), p. 17158.
- Karlsson, L., Baccarini, A., Duplessis, P., Baumgardner, D., Brooks, I. M., Chang, R. Y.-W., Dada, L., Dällenbach, K. R., Heikkinen, L., Krejci, R., Leaitch, W. R., Leck, C., Partridge, D. G., Salter, M. E., Wernli, H., Wheeler, M. J., Schmale, J., and Zieger, P. 2022. “Physical and Chemical Properties of Cloud Droplet Residuals and Aerosol Particles During the Arctic Ocean 2018 Expedition”. *Journal of Geophysical Research: Atmospheres* **127**(11).

- Karlsson, L., Krejci, R., Koike, M., Ebell, K., and Zieger, P. 2021. “A long-term study of cloud residuals from low-level Arctic clouds”. *Atmospheric Chemistry and Physics* **21**(11), pp. 8933–8959.
- Karlsson, L. and Zieger, P. 2020. *Aerosol particle number size distribution data collected during the Arctic Ocean 2018 expedition [data set]*.
- Kay, J. E., L’Ecuyer, T., Chepfer, H., Loeb, N., Morrison, A., and Cesana, G. 2016. *Recent Advances in Arctic Cloud and Climate Research*.
- Kerminen, V.-M. and Kulmala, M. 2002. *Analytical formulae connecting the “real” and the “apparent” nucleation rate and the nuclei number concentration for atmospheric nucleation events*. Tech. rep., pp. 609–622.
- Koike, M., Ukita, J., Ström, J., Tunved, P., Shiobara, M., Vitale, V., Lupi, A., Baumgardner, D., Ritter, C., Hermansen, O., Yamada, K., and Pedersen, C. A. 2019. “Year-Round In Situ Measurements of Arctic Low-Level Clouds: Microphysical Properties and Their Relationships With Aerosols”. *Journal of Geophysical Research: Atmospheres* **124**(3), pp. 1798–1822.
- Komppula, M., Lihavainen, H., Kerminen, V. M., Kulmala, M., and Viisanen, Y. 2005. “Measurements of cloud droplet activation of aerosol particles at a clean subarctic background site”. *Journal of Geophysical Research D: Atmospheres* **110**(6), pp. 1–10.
- Korhonen, H., Carslaw, K. S., and Romakkaniemi, S. 2010. “Enhancement of marine cloud albedo via controlled sea spray injections: A global model study of the influence of emission rates, microphysics and transport”. *Atmospheric Chemistry and Physics* **10**(9), pp. 4133–4143.
- Korhonen, H., Carslaw, K. S., Spracklen, D. V., Mann, G. W., and Woodhouse, M. T. 2008a. “Influence of oceanic dimethyl sulfide emissions on cloud condensation nuclei concentrations and seasonality over the remote Southern Hemisphere oceans: A global model study”. *Journal of Geophysical Research Atmospheres* **113**(15).
- Korhonen, H., Carslaw, K. S., Spracklen, D. V., Ridley, D. A., and Ström, J. 2008b. “A global model study of processes controlling aerosol size distributions in the Arctic spring and summer”. *Journal of Geophysical Research* **113**(D8), p. D08211.
- Kulmala, M., Lehtinen, K. E. J., and Laaksonen, A. 2006. *Atmospheric Chemistry and Physics Cluster activation theory as an explanation of the linear dependence between formation rate of 3 nm particles and sulphuric acid concentration*. Tech. rep., pp. 787–793.
- Kupiszewski, P., Leck, C., Tjernström, M., Sjogren, S., Sedlar, J., Graus, M., Müller, M., Brooks, B., Swietlicki, E., Norris, S., and Hansel, A. 2013. “Vertical profiling of aerosol particles and trace gases over the central Arctic Ocean during summer”. *Atmospheric Chemistry and Physics* **13**(24), pp. 12405–12431.
- Lamarque, J. F., Bond, T. C., Eyring, V., Granier, C., Heil, A., Klimont, Z., Lee, D., Liousse, C., Mieville, A., Owen, B., Schultz, M. G., Shindell, D., Smith, S. J., Stehfest,

- E., Van Aardenne, J., Cooper, O. R., Kainuma, M., Mahowald, N., McConnell, J. R., Naik, V., Riahi, K., and Van Vuuren, D. P. 2010. “Historical (1850-2000) gridded anthropogenic and biomass burning emissions of reactive gases and aerosols: Methodology and application”. *Atmospheric Chemistry and Physics* **10**(15), pp. 7017–7039.
- Lance, S., Shupe, M. D., Feingold, G., Brock, C. A., Cozic, J., Holloway, J. S., Moore, R. H., Nenes, A., Schwarz, J. P., Spackman, J. R., Froyd, K. D., Murphy, D. M., Brioude, J., Cooper, O. R., Stohl, A., and Burkhardt, J. F. 2011. “Cloud condensation nuclei as a modulator of ice processes in Arctic mixed-phase clouds”. *Atmospheric Chemistry and Physics* **11**(15), pp. 8003–8015.
- Lawler, M. J., Saltzman, E. S., Karlsson, L., Zieger, P., Salter, M., Baccarini, A., Schmale, J., and Leck, C. 2021. “New insights into the composition and origins of ultrafine aerosol in the summertime high Arctic”. *Geophysical Research Letters*.
- Leck, C. and Svensson, E. 2015. “Importance of aerosol composition and mixing state for cloud droplet activation over the Arctic pack ice in summer”. *Atmospheric Chemistry and Physics* **15**(5), pp. 2545–2568.
- Leck, C. and Bigg, E. K. 2010. “New particle formation of marine biological origin”. *Aerosol Science and Technology*. **Vol. 44**. 7, pp. 570–577.
- Leck, C. and Keith Bigg, E. 1999. “Aerosol production over remote marine areas - A new route”. *Geophysical Research Letters* **26**(23), pp. 3577–3580.
- Loewe, K., Ekman, A. M. L., Paukert, M., Sedlar, J., Tjernström, M., and Hoose, C. 2017. “Modelling micro- and macrophysical contributors to the dissipation of an Arctic mixed-phase cloud during the Arctic Summer Cloud Ocean Study (ASCOS)”. *Atmospheric Chemistry and Physics* **17**(11), pp. 6693–6704.
- Lubin, D. and Vogelmann, A. M. 2006. “A climatologically significant aerosol longwave indirect effect in the Arctic”. *Nature* **439**(7075), pp. 453–456.
- Lupikasza, E. B. and Cielecka-Nowak, K. 2020. “Changing probabilities of days with snow and rain in the atlantic sector of the arctic under the current warming trend”. *Journal of Climate* **33**(7), pp. 2509–2532.
- Mahmood, R., Salzen, K. von, Norman, A.-L., Galí, M., and Levasseur, M. 2019. “Sensitivity of Arctic sulfate aerosol and clouds to changes in future surface seawater dimethylsulfide concentrations”. *Atmospheric Chemistry and Physics* **19**(9), pp. 6419–6435.
- Mann, G. W., Carslaw, K. S., Spracklen, D. V., Ridley, D. A., Manktelow, P. T., Chipperfield, M. P., Pickering, S. J., and Johnson, C. E. 2010. “Description and evaluation of GLOMAP-mode: A modal global aerosol microphysics model for the UKCA composition-climate model”. *Geoscientific Model Development* **3**(2), pp. 519–551.
- Mårtensson, E. M., Nilsson, E. D., Leeuw, G. de, Cohen, L. H., and Hansson, H. C. 2003. “Laboratory simulations and parameterization of the primary marine aerosol production”. *Journal of Geophysical Research: Atmospheres* **108**(9).

- Mauritsen, T., Sedlar, J., Tjernström, M., Leck, C., Martin, M., Shupe, M., Sjogren, S., Sierau, B., Persson, P. O., Brooks, I. M., and Swietlicki, E. 2011. “An Arctic CCN-limited cloud-aerosol regime”. *Atmospheric Chemistry and Physics*.
- McCrystall, M. R., Stroeve, J., Serreze, M., Forbes, B. C., and Screen, J. A. 2021. “New climate models reveal faster and larger increases in Arctic precipitation than previously projected”. *Nature Communications* **12**(1).
- Meinander, O., Dagsson-Waldhauserova, P., Amosov, P., Aseyeva, E., Atkins, C., Baklanov, A., Baldo, C., Barr, S. L., Barzycka, B., Benning, L. G., Cvetkovic, B., Enchilik, P., Frolov, D., Gassó, S., Kandler, K., Kasimov, N., Kavan, J., King, J., Koroleva, T., Krupskaya, V., Kulmala, M., Kusiak, M., Lappalainen, H. K., Laska, M., Lasne, J., Lewandowski, M., Luks, B., McQuaid, J. B., Moroni, B., Murray, B., Möhler, O., Nawrot, A., Nickovic, S., O’neill, N. T., Pejanovic, G., Popovicheva, O., Ranjbar, K., Romanias, M., Samonova, O., Sanchez-Marroquin, A., Schepanski, K., Semenov, I., Sharapova, A., Shevnina, E., Shi, Z., Sofiev, M., Thevenet, F., Thorsteinsson, T., Timofeev, M., Umo, N. S., Uppstu, A., Urupina, D., Varga, G., Werner, T., Arnalds, O., and Vukovic Vimic, A. 2022. “Newly identified climatically and environmentally significant high-latitude dust sources”. *Atmospheric Chemistry and Physics* **22**(17), pp. 11889–11930.
- Merikanto, J., Spracklen, D. V., Mann, G. W., Pickering, S. J., and Carslaw, K. S. 2009. *Atmospheric Chemistry and Physics Impact of nucleation on global CCN*. Tech. rep., pp. 8601–8616.
- Metzger, A., Verheggen, B., Dommen, J., Duplissy, J., Prevot, A. S., Weingartner, E., Riipinen, I., Kulmala, M., Spracklen, D. V., Carslaw, K. S., and Baltensperger, U. 2010. “Evidence for the role of organics in aerosol particle formation under atmospheric conditions”. *Proceedings of the National Academy of Sciences of the United States of America* **107**(15), pp. 6646–6651.
- Monahan, E. C., Spiel, D. E., and Davidson, K. L. 1986. *A MODEL OF MARINE AEROSOL GENERATION VIA WHITECAPS AND WAVE DISRUPTION*. Tech. rep.
- Morgenstern, O., Braesicke, P., O’connor, F. M., Bushell, A. C., Johnson, C. E., Osprey, S. M., and Pyle, J. A. 2009. *Evaluation of the new UKCA climate-composition model-Part 1: The stratosphere*. Tech. rep., pp. 43–57.
- Morrison, H. and Pinto, J. O. 2005. “Mesoscale Modeling of Springtime Arctic Mixed-Phase Stratiform Clouds Using a New Two-Moment Bulk Microphysics Scheme”. *Journal of the Atmospheric Sciences*.
- Morrison, H., Zuidema, P., Ackerman, A. S., Avramov, A., Boer, G. de, Fan, J., Fridlind, A. M., Hashino, T., Harrington, J. Y., Luo, Y., Ovchinnikov, M., and Shipway, B. 2011. “Intercomparison of cloud model simulations of Arctic mixed-phase boundary layer clouds observed during SHEBA/FIRE-ACE”. *Journal of Advances in Modeling Earth Systems* **3**(2), n/a–n/a.

- Mulcahy, J. P., Johnson, C., Jones, C. G., Povey, A. C., Scott, C. E., Sellar, A., Turnock, S. T., Woodhouse, M. T., Abraham, N. L., Andrews, M. B., Bellouin, N., Browse, J., Carslaw, K. S., Dalvi, M., Folberth, G. A., Glover, M., Grosvenor, D. P., Hardacre, C., Hill, R., Johnson, B., Jones, A., Kipling, Z., Mann, G., Mollard, J., O'Connor, F. M., Palmiéri, J., Reddington, C., Rumbold, S. T., Richardson, M., Schutgens, N. A., Stier, P., Stringer, M., Tang, Y., Walton, J., Woodward, S., and Yool, A. 2020. “Description and evaluation of aerosol in UKESM1 and HadGEM3-GC3.1 CMIP6 historical simulations”. *Geoscientific Model Development* **13**(12), pp. 6383–6423.
- Nilsson, E. D., Rannik, Ü., Swietlicki, E., Leck, C., Aalto, P. P., Zhou, J., and Norman, M. 2001a. “Turbulent aerosol fluxes over the Arctic Ocean 2. Wind-driven sources from the sea”. *Journal of Geophysical Research Atmospheres* **106**(D23), pp. 32139–32154.
- Nilsson, E. D., Rannik, Ü., and Håkansson, M. 2001b. “Surface energy budget over the central Arctic Ocean during late summer and early freeze-up”. *Journal of Geophysical Research Atmospheres* **106**(D23), pp. 32187–32205.
- Norgren, M. S., De Boer, G., and Shupe, M. D. 2018. “Observed aerosol suppression of cloud ice in low-level Arctic mixed-phase clouds”. *Atmospheric Chemistry and Physics*.
- Notz, D. and SIMIP Community 2020. “Arctic Sea Ice in CMIP6”. *Geophysical Research Letters* **47**(10).
- Notz, D. and Stroeve, J. 2018. *The Trajectory Towards a Seasonally Ice-Free Arctic Ocean*.
- O'Connor, F. M., Johnson, C. E., Morgenstern, O., Abraham, N. L., Braesicke, P., Dalvi, M., Folberth, G. A., Sanderson, M. G., Telford, P. J., Voulgarakis, A., Young, P. J., Zeng, G., Collins, W. J., and Pyle, J. A. 2014. “Evaluation of the new UKCA climate-composition model-Part 2: The troposphere”. *Geoscientific Model Development* **7**(1), pp. 41–91.
- Orellana, M. V., Matrai, P. A., Leck, C., Rauschenberg, C. D., Lee, A. M., and Coz, E. 2011. “Marine microgels as a source of cloud condensation nuclei in the high arctic”. *Proceedings of the National Academy of Sciences of the United States of America* **108**(33), pp. 13612–13617.
- Ovchinnikov, M., Ackerman, A. S., Avramov, A., Cheng, A., Fan, J., Fridlind, A. M., Ghan, S., Harrington, J., Hoose, C., Korolev, A., McFarquhar, G. M., Morrison, H., Paukert, M., Savre, J., Shipway, B. J., Shupe, M. D., Solomon, A., and Sulia, K. 2014. “Intercomparison of large-eddy simulations of Arctic mixed-phase clouds: Importance of ice size distribution assumptions”. *Journal of Advances in Modeling Earth Systems* **6**(1), pp. 223–248.
- Overland, J. E. and Wang, M. 2010. “Large-scale atmospheric circulation changes are associated with the recent loss of Arctic sea ice”. *Tellus, Series A: Dynamic Meteorology and Oceanography* **62**(1), pp. 1–9.

- Pan, S., Dou, T., Lin, L., Yang, J., Zhang, F., Duan, M., Zhao, C., Liao, H., and Xiao, C. 2020. “Larger Sensitivity of Arctic Precipitation Phase to Aerosol than Greenhouse Gas Forcing”. *Geophysical Research Letters* **47**(23).
- Pastore, M. and Calcagnì, A. 2019. “Measuring distribution similarities between samples: A distribution-free overlapping index”. *Frontiers in Psychology* **10**.
- Pernov, J. B., Beddows, D., Thomas, D. C., Dall’Osto, M., Harrison, R. M., Schmale, J., Skov, H., and Massling, A. 2022. “Increased aerosol concentrations in the High Arctic attributable to changing atmospheric transport patterns”. *npj Climate and Atmospheric Science* **5**(1), p. 62.
- Pistone, K., Eisenman, I., and Ramanathan, V. 2019. “Radiative Heating of an Ice-Free Arctic Ocean”. *Geophysical Research Letters* **46**(13), 2019GL082914.
- Pithan, F. and Mauritsen, T. 2014. “Arctic amplification dominated by temperature feedbacks in contemporary climate models”. *Nature Geoscience* **7**(3), pp. 181–184.
- Pöhlker, M. L., Zhang, M., Campos Braga, R., Krüger, O. O., Pöschl, U., and Ervens, B. 2021. “Aitken mode particles as CCN in aerosol- and updraft-sensitive regimes of cloud droplet formation”. *Atmospheric Chemistry and Physics* **21**(15), pp. 11723–11740.
- Porter, G. C., Adams, M. P., Brooks, I. M., Ickes, L., Karlsson, L., Leck, C., Salter, M. E., Schmale, J., Siegel, K., Sikora, S. N., Tarn, M. D., Vüllers, J., Wernli, H., Zieger, P., Zinke, J., and Murray, B. J. 2022. “Highly Active Ice-Nucleating Particles at the Summer North Pole”. *Journal of Geophysical Research: Atmospheres* **127**(6).
- Possner, A., Ekman, A. M., and Lohmann, U. 2017. “Cloud response and feedback processes in stratiform mixed-phase clouds perturbed by ship exhaust”. *Geophysical Research Letters*.
- Prenni, A. J., Harrington, J. Y., Tjernström, M., DeMott, P. J., Avramov, A., Long, C. N., Kreidenweis, S. M., Olsson, P. Q., Verlinde, J., Prenni, A. J., Harrington, J. Y., Michael, T., DeMott, P. J., Avramov, A., Long, C. N., Kreidenweis, S. M., Olsson, P. Q., and Verlinde, J. 2007. “Can Ice-Nucleating Aerosols Affect Arctic Seasonal Climate?” *Bulletin of the American Meteorological Society* **88**(4), pp. 541–550.
- Ramachandran, S., Rupakheti, M., and Cherian, R. 2022. “Insights into recent aerosol trends over Asia from observations and CMIP6 simulations”. *Science of the Total Environment* **807**.
- Rantanen, M., Karpechko, A. Y., Lipponen, A., Nordling, K., Hyvärinen, O., Ruosteenoja, K., Vihma, T., and Laaksonen, A. 2022. “The Arctic has warmed nearly four times faster than the globe since 1979”. *Communications Earth & Environment* **3**(1), p. 168.
- Rosenblum, E. and Eisenman, I. 2017. “Sea Ice Trends in Climate Models Only Accurate in Runs with Biased Global Warming”.

- Samset, B. H., Lund, M. T., Bollasina, M., Myhre, G., and Wilcox, L. 2019. *Emerging Asian aerosol patterns*.
- Sanchez-Marroquin, A., Arnalds, O., Baustian-Dorsi, K. J., Browse, J., Dagsson-Waldhauserova, P., Harrison, A. D., Maters, E. C., Pringle, K. J., Vergara-Temprado, J., Burke, I. T., McQuaid, J. B., Carslaw, K. S., and Murray, B. J. 2020. *Iceland is an episodic source of atmospheric ice-nucleating particles relevant for mixed-phase clouds*. Tech. rep., pp. 8137–8161.
- Schmale, J. and Baccarini, A. 2021. *Progress in Unraveling Atmospheric New Particle Formation and Growth Across the Arctic*.
- Schmale, J., Sharma, S., Decesari, S., Pernov, J., Massling, A., Hansson, H. C., Von Salzen, K., Skov, H., Andrews, E., Quinn, P. K., Upchurch, L. M., Eleftheriadis, K., Traversi, R., Gilardoni, S., Mazzola, M., Laing, J., and Hopke, P. 2022. “Pan-Arctic seasonal cycles and long-term trends of aerosol properties from 10 observatories”. *Atmospheric Chemistry and Physics* **22**(5), pp. 3067–3096.
- Sedlar, J., Tjernström, M., Mauritsen, T., Shupe, M. D., Brooks, I. M., Persson, P. O. G., Birch, C. E., Leck, C., Sirevaag, A., and Nicolaus, M. 2011. “A transitioning Arctic surface energy budget: the impacts of solar zenith angle, surface albedo and cloud radiative forcing”. *Climate Dynamics* **37**(7-8), pp. 1643–1660.
- Sellar, A. A., Jones, C. G., Mulcahy, J. P., Tang, Y., Yool, A., Wiltshire, A., O’Connor, F. M., Stringer, M., Hill, R., Palmieri, J., Woodward, S., Mora, L. de, Kuhlbrodt, T., Rumbold, S. T., Kelley, D. I., Ellis, R., Johnson, C. E., Walton, J., Abraham, N. L., Andrews, M. B., Andrews, T., Archibald, A. T., Berthou, S., Burke, E., Blockley, E., Carslaw, K., Dalvi, M., Edwards, J., Folberth, G. A., Gedney, N., Griffiths, P. T., Harper, A. B., Hendry, M. A., Hewitt, A. J., Johnson, B., Jones, A., Jones, C. D., Keeble, J., Liddicoat, S., Morgenstern, O., Parker, R. J., Predoi, V., Robertson, E., Siahhaan, A., Smith, R. S., Swaminathan, R., Woodhouse, M. T., Zeng, G., and Zerroukat, M. 2019. “UKESM1: Description and Evaluation of the U.K. Earth System Model”. *Journal of Advances in Modeling Earth Systems* **11**(12), pp. 4513–4558.
- Sharma, S., Barrie, L. A., Magnusson, E., Brattström, G., Leitch, W. R., Steffen, A., and Landsberger, S. 2019. “A Factor and Trends Analysis of Multidecadal Lower Tropospheric Observations of Arctic Aerosol Composition, Black Carbon, Ozone, and Mercury at Alert, Canada”. *Journal of Geophysical Research: Atmospheres* **124**(24), pp. 14133–14161.
- Sharma, S., Brook, J. R., Cachier, H., Chow, J., Gaudenzi, A., and Lu, G. 2002. “Light absorption and thermal measurements of black carbon in different regions of Canada”. *Journal of Geophysical Research Atmospheres* **107**(24).
- Shaw, G. E. 1995. “The Arctic Haze Phenomenon”. *Bulletin of the American Meteorological Society* **76**(12), pp. 2403–2413.

- Shu, Q., Wang, Q., Song, Z., Qiao, F., Zhao, J., Chu, M., and Li, X. 2020. “Assessment of Sea Ice Extent in CMIP6 With Comparison to Observations and CMIP5”. *Geophysical Research Letters* **47**(9).
- Shupe, M. D. 2011. “Clouds at Arctic Atmospheric Observatories. Part II: Thermodynamic Phase Characteristics”. *Journal of Applied Meteorology and Climatology* **50**(3), pp. 645–661.
- Shupe, M. D., Walden, V. P., Eloranta, E., Uttal, T., Campbell, J. R., Starkweather, S. M., and Shiobara, M. 2011. “Clouds at Arctic atmospheric observatories. Part I: Occurrence and macrophysical properties”. *Journal of Applied Meteorology and Climatology*.
- Sindelarova, K., Granier, C., Bouarar, I., Guenther, A., Tilmes, S., Stavrou, T., Müller, J. F., Kuhn, U., Stefani, P., and Knorr, W. 2014. “Global data set of biogenic VOC emissions calculated by the MEGAN model over the last 30 years”. *Atmospheric Chemistry and Physics* **14**(17), pp. 9317–9341.
- Sipilä, M., Sarnela, N., Jokinen, T., Henschel, H., Junninen, H., Kontkanen, J., Richters, S., Kangasluoma, J., Franchin, A., Peräkylä, O., Rissanen, M. P., Ehn, M., Vehkamäki, H., Kurten, T., Berndt, T., Petäjä, T., Worsnop, D., Ceburnis, D., Kerminen, V. M., Kulmala, M., and O’Dowd, C. 2016. “Molecular-scale evidence of aerosol particle formation via sequential addition of HIO₃”. *Nature* **537**(7621), pp. 532–534.
- Solomon, A., Shupe, M. D., Persson, P. O., and Morrison, H. 2011. “Moisture and dynamical interactions maintaining decoupled Arctic mixed-phase stratocumulus in the presence of a humidity inversion”. *Atmospheric Chemistry and Physics*.
- Sotiropoulou, G., Sedlar, J., Forbes, R., and Tjernström, M. 2016. “Summer Arctic clouds in the ECMWF forecast model: an evaluation of cloud parametrization schemes”. *Quarterly Journal of the Royal Meteorological Society* **142**(694), pp. 387–400.
- Spracklen, D. V., Carslaw, K. S., Kulmala, M., Kerminen, V.-M., Mann, G. W., and Sihto, S.-L. 2006. *Atmospheric Chemistry and Physics*. Tech. rep. 12, pp. 5631–5648.
- Sterzinger, L. J., Sedlar, J., Guy, H., Neely III, R. R., and Igel, A. L. 2022. “Do Arctic mixed-phase clouds sometimes dissipate due to insufficient aerosol? Evidence from comparisons between observations and idealized simulations”. *Atmospheric Chemistry and Physics* **22**(13), pp. 8973–8988.
- Stevens, R. G., Loewe, K., Dearden, C., Dimitrellos, A., Possner, A., Eirund, G. K., Raatikainen, T., Hill, A. A., Shipway, B. J., Wilkinson, J., Romakkaniemi, S., Tonttila, J., Laaksonen, A., Korhonen, H., Connolly, P., Lohmann, U., Hoose, C., Ekman, A. M., Carslaw, K. S., and Field, P. R. 2018. “A model intercomparison of CCN-limited tenuous clouds in the high Arctic”. *Atmospheric Chemistry and Physics*.
- Stier, P., Feichter, J., Kinne, S., Kloster, S., Vignati, E., Wilson, J., Ganzeveld, L., Tegen, I., Werner, M., Balkanski, Y., Schulz, M., Boucher, O., Minikin, A., and

- Petzold, A. 2005. *The aerosol-climate model ECHAM5-HAM*. Tech. rep., pp. 1125–1156.
- Stohl, A. 2006. “Characteristics of atmospheric transport into the Arctic troposphere”. *Journal of Geophysical Research* **111**(D11), p. D11306.
- Ström, J., Umegård, J., Tørseth, K., Tunved, P., Hansson, H.-C., Holmén, K., Wismann, V., Herber, A., and König-Langlo, G. 2003. “One year of particle size distribution and aerosol chemical composition measurements at the Zeppelin Station, Svalbard, March 2000–March 2001”. *Physics and Chemistry of the Earth, Parts A/B/C* **28**(28-32), pp. 1181–1190.
- Strong, C. and Rigor, I. G. 2013. “Arctic marginal ice zone trending wider in summer and narrower in winter”. *Geophysical Research Letters* **40**(18), pp. 4864–4868.
- Struthers, H., Ekman, A. M. L., Glantz, P., Iversen, T., Kirkevåg, A., Mårtensson, E. M., Seland, Ø., and Nilsson, E. D. 2011. “The effect of sea ice loss on sea salt aerosol concentrations and the radiative balance in the Arctic”. *Atmos. Chem. Phys* **11**, pp. 3459–3477.
- Stull, R. B. 1988. *An Introduction to Boundary Layer Meteorology*. KLUWER ACADEMIC PUBLISHERS.
- Tjernström, M., Leck, C., Birch, C. E., Bottenheim, J. W., Brooks, B. J., Brooks, I. M., Bäcklin, L., Chang, R. Y., De Leeuw, G., Di Liberto, L., De La Rosa, S., Granath, E., Graus, M., Hansel, A., Heintzenberg, J., Held, A., Hind, A., Johnston, P., Knulst, J., Martin, M., Matrai, P. A., Mauritsen, T., Müller, M., Norris, S. J., Orellana, M. V., Orsini, D. A., Paatero, J., Persson, P. O., Gao, Q., Rauschenberg, C., Ristovski, Z., Sedlar, J., Shupe, M. D., Sierau, B., Sirevaag, A., Sjogren, S., Stetzer, O., Swietlicki, E., Szczodrak, M., Vaattovaara, P., Wahlberg, N., Westberg, M., and Wheeler, C. R. 2014. *The Arctic Summer Cloud Ocean Study (ASCOS): Overview and experimental design*.
- Tobo, Y., Adachi, K., DeMott, P. J., Hill, T. C., Hamilton, D. S., Mahowald, N. M., Nagatsuka, N., Ohata, S., Uetake, J., Kondo, Y., and Koike, M. 2019. “Glacially sourced dust as a potentially significant source of ice nucleating particles”. *Nature Geoscience* **12**(4), pp. 253–258.
- Tsigaridis, K., Koch, D., and Menon, S. 2013. “Uncertainties and importance of sea spray composition on aerosol direct and indirect effects”. *Journal of Geophysical Research Atmospheres* **118**(1), pp. 220–235.
- Tunved, P., Ström, J., and Krejci, R. 2013. “Arctic aerosol life cycle: Linking aerosol size distributions observed between 2000 and 2010 with air mass transport and precipitation at Zeppelin station, Ny-Ålesund, Svalbard”. *Atmospheric Chemistry and Physics*.
- Turetsky, M. R., Kane, E. S., Harden, J. W., Ottmar, R. D., Manies, K. L., Hoy, E., and Kasischke, E. S. 2011. “Recent acceleration of biomass burning and carbon losses in Alaskan forests and peatlands”. *Nature Geoscience* **4**(1), pp. 27–31.

- Twomey, S. 1977. “The Influence of Pollution on the Shortwave Albedo of Clouds”. *Journal of the Atmospheric Sciences* **34**(7), pp. 1149–1152.
- Van Marle, M. J., Kloster, S., Magi, B. I., Marlon, J. R., Daniau, A. L., Field, R. D., Arneth, A., Forrest, M., Hantson, S., Kehrwald, N. M., Knorr, W., Lasslop, G., Li, F., Mangeon, S., Yue, C., Kaiser, J. W., and Van Der Werf, G. R. 2017. *Historic global biomass burning emissions for CMIP6 (BB4CMIP) based on merging satellite observations with proxies and fire models (1750-2015)*.
- Van Weverberg, K., Morcrette, C. J., Boutle, I., Furtado, K., and Field, P. R. 2021. “A bimodal diagnostic cloud fraction parameterization. Part I: Motivating analysis and scheme description”. *Monthly Weather Review* **149**(3), pp. 841–857.
- Vehkamäki, H., Kulmala, M., Napari, I., Lehtinen, K. E. J., Timmreck, C., Noppel, M., and Laaksonen, A. 2002. “An improved parameterization for sulfuric acid–water nucleation rates for tropospheric and stratospheric conditions”. *Journal of Geophysical Research* **107**(D22), p. 4622.
- Veraverbeke, S., Rogers, B. M., Goulden, M. L., Jandt, R. R., Miller, C. E., Wiggins, E. B., and Randerson, J. T. 2017. “Lightning as a major driver of recent large fire years in North American boreal forests”. *Nature Climate Change* **7**(7), pp. 529–534.
- Vihma, T., Pirazzini, R., Fer, I., Renfrew, I. A., Sedlar, J., Tjernström, M., Lüpkes, C., Nygård, T., Notz, D., Weiss, J., Marsan, D., Cheng, B., Birnbaum, G., Gerland, S., Chechin, D., and Gascard, J. C. 2014. *Advances in understanding and parameterization of small-scale physical processes in the marine Arctic climate system: A review*.
- Vüllers, J., Achter, P., Brooks, I., Neely III, R., and Brooks, B. 2021. *Cloudnet remote sensing retrievals of cloud properties during the Arctic Ocean 2018 expedition [dataset]*.
- Vüllers, J., Achtert, P., Brooks, I., Tjernström, M., Prytherch, J., and Neely III, R. 2020. “Meteorological and cloud conditions during the Arctic Ocean 2018 expedition”. *Atmospheric Chemistry and Physics*, pp. 1–43.
- Vüllers, J. and Brooks, I. M. 2021. *Microbiology-Ocean-Cloud Coupling in the High Arctic (MOCCHA): Meteorological data from the measurement station on the ice floe [dataset]*.
- Walker, X. J., Baltzer, J. L., Cumming, S. G., Day, N. J., Ebert, C., Goetz, S., Johnstone, J. F., Potter, S., Rogers, B. M., Schuur, E. A., Turetsky, M. R., and Mack, M. C. 2019. “Increasing wildfires threaten historic carbon sink of boreal forest soils”. *Nature* **572**(7770), pp. 520–523.
- Walters, D., Baran, A. J., Boutle, I., Brooks, M., Earnshaw, P., Edwards, J., Furtado, K., Hill, P., Lock, A., Manners, J., Morcrette, C., Mulcahy, J., Sanchez, C., Smith, C., Stratton, R., Tennant, W., Tomassini, L., Van Weverberg, K., Vosper, S., Willett, M., Browse, J., Bushell, A., Carslaw, K., Dalvi, M., Essery, R., Gedney, N., Hardiman, S., Johnson, B., Johnson, C., Jones, A., Jones, C., Mann, G., Milton, S.,

- Rumbold, H., Sellar, A., Ujiie, M., Whittall, M., Williams, K., and Zerroukat, M. 2019. “The Met Office Unified Model Global Atmosphere 7.0/7.1 and JULES Global Land 7.0 configurations”. *Geoscientific Model Development* **12**(5), pp. 1909–1963.
- Wang, X., Key, J. R., Wang, X., and Key, J. R. 2005. “Arctic Surface, Cloud, and Radiation Properties Based on the AVHRR Polar Pathfinder Dataset. Part I: Spatial and Temporal Characteristics”. *Journal of Climate* **18**(14), pp. 2558–2574.
- Wex, H., Huang, L., Zhang, W., Hung, H., Traversi, R., Becagli, S., Sheesley, R. J., Moffett, C. E., Barrett, T. E., Bossi, R., Skov, H., Hünerbein, A., Lubitz, J., Löffler, M., Linke, O., Hartmann, M., Herenz, P., and Stratmann, F. 2019. “Annual variability of ice-nucleating particle concentrations at different Arctic locations”. *Atmospheric Chemistry and Physics* **19**(7), pp. 5293–5311.
- Willis, M. D., Burkart, J., Thomas, J. L., Köllner, F., Schneider, J., Bozem, H., Hoor, P. M., Aliabadi, A. A., Schulz, H., Herber, A. B., Leaitch, W. R., and Abbatt, J. P. D. 2016. “Growth of nucleation mode particles in the summertime Arctic: a case study”. *Atmospheric Chemistry and Physics* **16**(12), pp. 7663–7679.
- Willis, M. D., Köllner, F., Burkart, J., Bozem, H., Thomas, J. L., Schneider, J., Aliabadi, A. A., Hoor, P. M., Schulz, H., Herber, A. B., Leaitch, W. R., and Abbatt, J. P. 2017. “Evidence for marine biogenic influence on summertime Arctic aerosol”. *Geophysical Research Letters* **44**(12), pp. 6460–6470.
- Willis, M. D., Leaitch, W. R., and Abbatt, J. P. 2018. *Processes Controlling the Composition and Abundance of Arctic Aerosol*.
- Young, G., Connolly, P. J., Jones, H. M., and Choulaton, T. W. 2017. “Microphysical sensitivity of coupled springtime Arctic stratocumulus to modelled primary ice over the ice pack, marginal ice, and ocean”. *Atmospheric Chemistry and Physics* **17**(6), pp. 4209–4227.
- Young, G., Vüllers, J., Achtert, P., Field, P., Day, J. J., Forbes, R., Tjernström, M., Prytherch, J., Neely III, R., and Brooks, I. M. 2021. “Evaluating Arctic clouds modelled with the Unified Model and Integrated Forecasting System 2 [preprint]”. *Atmospheric Chemistry and Physics Discussions*.
- Zinke, J., Nilsson, E. D., Zieger, P., and Salter, M. E. 2022. “The Effect of Seawater Salinity and Seawater Temperature on Sea Salt Aerosol Production”. *Journal of Geophysical Research: Atmospheres* **127**(16).

Appendix A

Appendix

A.1 Particle ageing

In Sect. 3.4.2 we show that K06_BL and M10_BL simulate more accurate concentrations of the nucleation and Aitken modes during AO2018 than simulation CONTROL (figure 3.2). Figure A.1 shows the surface aerosol concentrations for simulations BIOMASS and CONTROL, K06_BL_default and K06_BL, and M10_BL_default and M10_BL. The simulations with the ageing change produce higher concentrations in the nucleation and Aitken modes than the DEFAULT simulations, and this difference is greater in the simulations with BL NPF than it is between UKESM_DEFAULT and CONTROL. This is because the mode merging described in Sect. 3.3.1 affects the Aitken mode concentration more when there is a stronger source of smaller particles. In the Aitken mode, the concentrations from simulations K06_BL and M10_BL are typically higher than K06_BL_DEFAULT and M10_BL_DEFAULT by a factor of 2–10. The model-observation agreement is therefore improved in simulations with the ageing change.

A.2 Latitude limit for prescribed FT NPF rate

In simulation M10_Prsc, we impose an NPF rate of $10^{-2} \text{ cm}^{-3} \text{ s}^{-1}$ in model levels between the top of the boundary layer and 7.5 km altitude. The rate is imposed in gridboxes north of 80°N . In Sect. 3.4.3 we compare the M10_Prsc output to aerosol profiles from the ASCOS and ATom campaigns to test how realistic such a NPF rate may be. However, the data we use from ATom was taken further south, between approximately 60 – 80°N . To test our prescribed FT NPF rate using ATom observations we therefore ran another simulation, M10_Prsc_60N, where the rate is imposed north of 60°N .

Figures A.2 and A.3 show output from M10_Prsc and M10_Prsc_60N with observations from ASCOS and ATom. Aerosol concentrations from the two simulations are

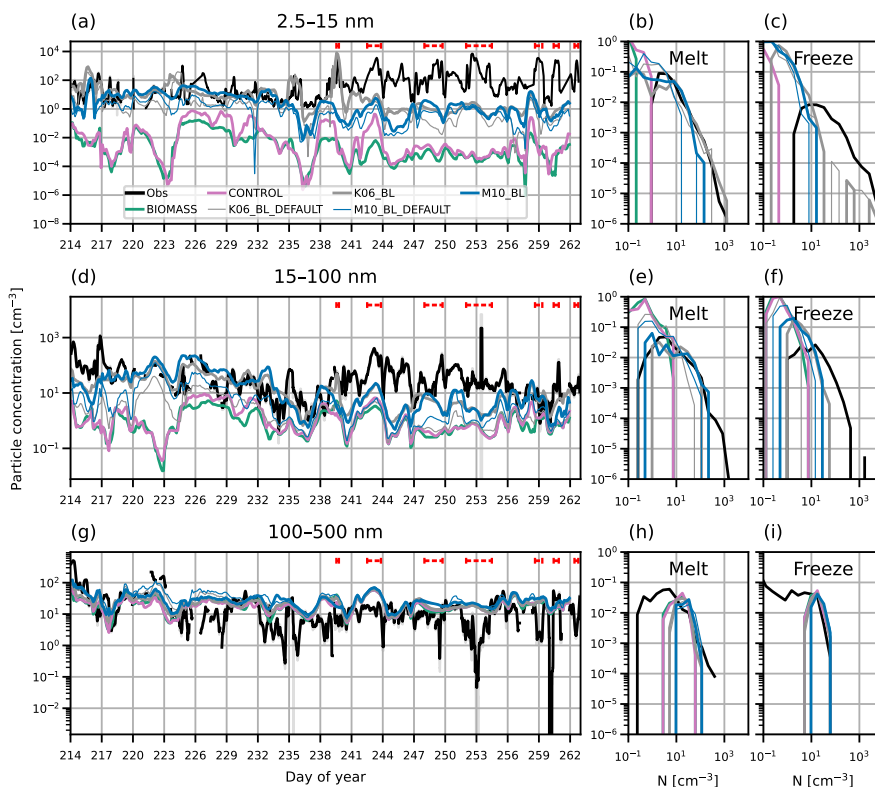


Figure A.1: Time series and PDFs of surface aerosol concentration during AO2018 from observations and model output. Model output is from simulations BIOMASS (green lines), CONTROL (pink lines), K06_BL_DEFAULT (thin grey lines), K06_BL (thick grey lines), M10_BL_DEFAULT (thin blue lines) and M10_BL (thick blue lines). Observations are shown as 3-hourly mean (black lines) and standard deviation (grey shading). Aerosol concentrations are shown for particles with diameter (a–c) 2.5–15 nm, (d–f) 15–100 nm and (g–i) 100–500 nm. Red dashed lines in (a, d, g) show observed NPF events. PDFs are separated by observed sea ice freeze-up date, 27th August 2018 (day 239).

within an order of magnitude of each other. While the prescribed rate increases aerosol concentrations relative to CONTROL in the ASCOS region (Sect. 3.4.3), it makes little difference in the AToM region even when we extend the region in which the rate is applied. This is likely because NPF rates are already higher in the AToM region than the ASCOS region due to the relative proximity of AToM to open water and boreal forests, both of which supply precursor vapours to the atmosphere.

A.3 Aerosol precursor vapours and growth rate

Figures A.4 and A.5 show maps and zonal means of H_2SO_4 and secondary organic vapour concentration from simulation CONTROL. In August, Arctic H_2SO_4 concentration peaks just above the surface and at approximately 8 km (Fig. A.4(a)). The concentration decreases throughout most of the troposphere from August to September by at least an order of magnitude. In August, the secondary organics have a maximum

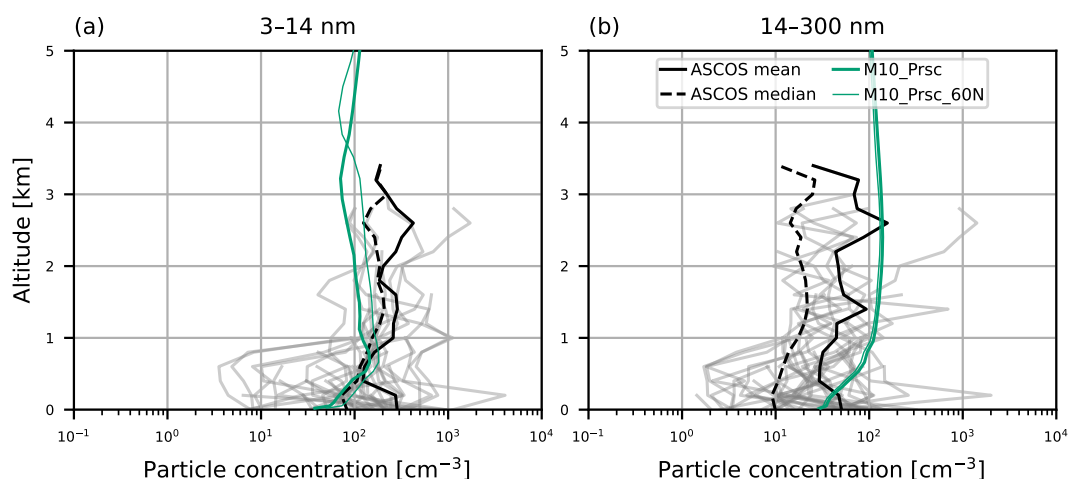


Figure A.2: Aerosol vertical profiles from model output and ASCOS campaign observations. Model output is from colocated monthly mean values from simulations M10_Prsc (thick dark green) and M10_Prsc_60N (thin dark green). Observed values are given as the mean profile from each ASCOS flight (grey lines), overall mean (solid black) and overall median (dashed black). Profiles are for particles with size (a) 3–14 nm, measured during ASCOS using a UCPC and (b) 14–300 nm, measured using a CPC (particles greater than 14 nm) and a CLASP instrument (particles greater than 300 nm).

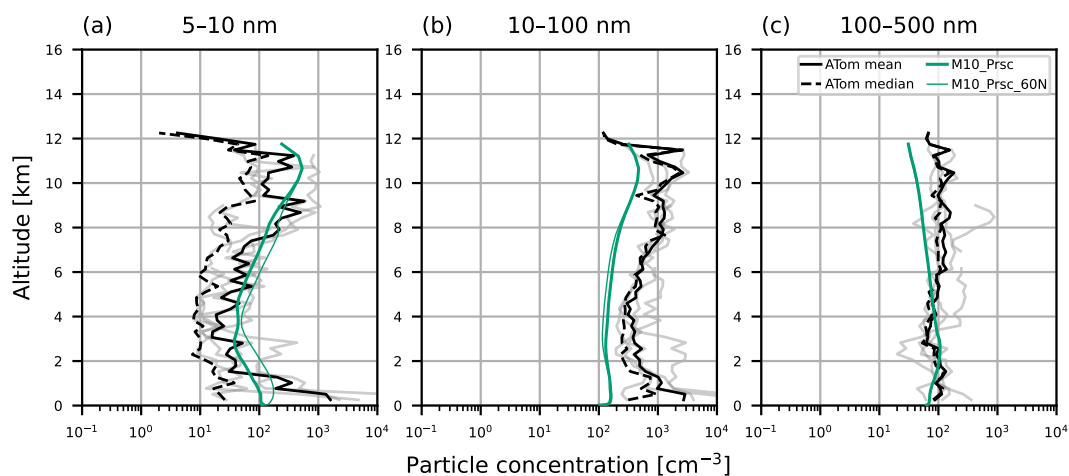


Figure A.3: Aerosol vertical profiles from model output and ATom campaign observations. Model output is from colocated monthly mean values from simulations M10_Prsc (thick dark green) and M10_Prsc_60N (thin dark green). ATom observations are taken from leg 1 of the campaign and restricted to measurements that were taken north of 60°N. Observations correspond to mean profiles from different days (grey lines), the overall mean (black solid lines) and overall median (black dashed lines). Profiles are for particles with size (a) 5–10 nm, (b) 10–100 nm and (c) 100–500 nm. Observations were recorded at standard temperature and pressure, model output has been adjusted to account for this.

at the surface from 60–70°N and some of this plume spreads north to the high Arctic. Unlike H_2SO_4 , concentrations do not significantly reduce from August to September. The mean surface concentration of H_2SO_4 for 80–90°N reduces by 85.2% from August

to September, while for secondary organics the reduction is only 5.9%. Percentage changes for other vapours are given in Table 3.3.

The decline in vapour concentration from August to September drives a reduction in the growth rate of aerosols from condensation of vapour. Figure A.6 shows aerosol growth rates calculated from model output from simulation CONTROL. Arctic growth rates are lower than in the mid-latitudes and tropics, where H_2SO_4 and secondary organics have higher concentrations. In the central Arctic, the decreasing growth rate is driven by the decrease in H_2SO_4 . Secondary organic vapours contribute little to the growth rate in the central Arctic region, but dominate in the continental Arctic in North America and northern Eurasia, where concentrations are high near the boreal forest source regions.

In Sect. 3.4.3 we showed that the source of aerosols from FT NPF weakens towards the end of summer. This occurs even when the FT NPF rate is held constant in time as in simulation M10_Prsc. The slower aerosol growth rate shown in Fig. A.6 curbs FT NPF in September. This highlights that it is important to understand the growth of new particles as well as their formation.

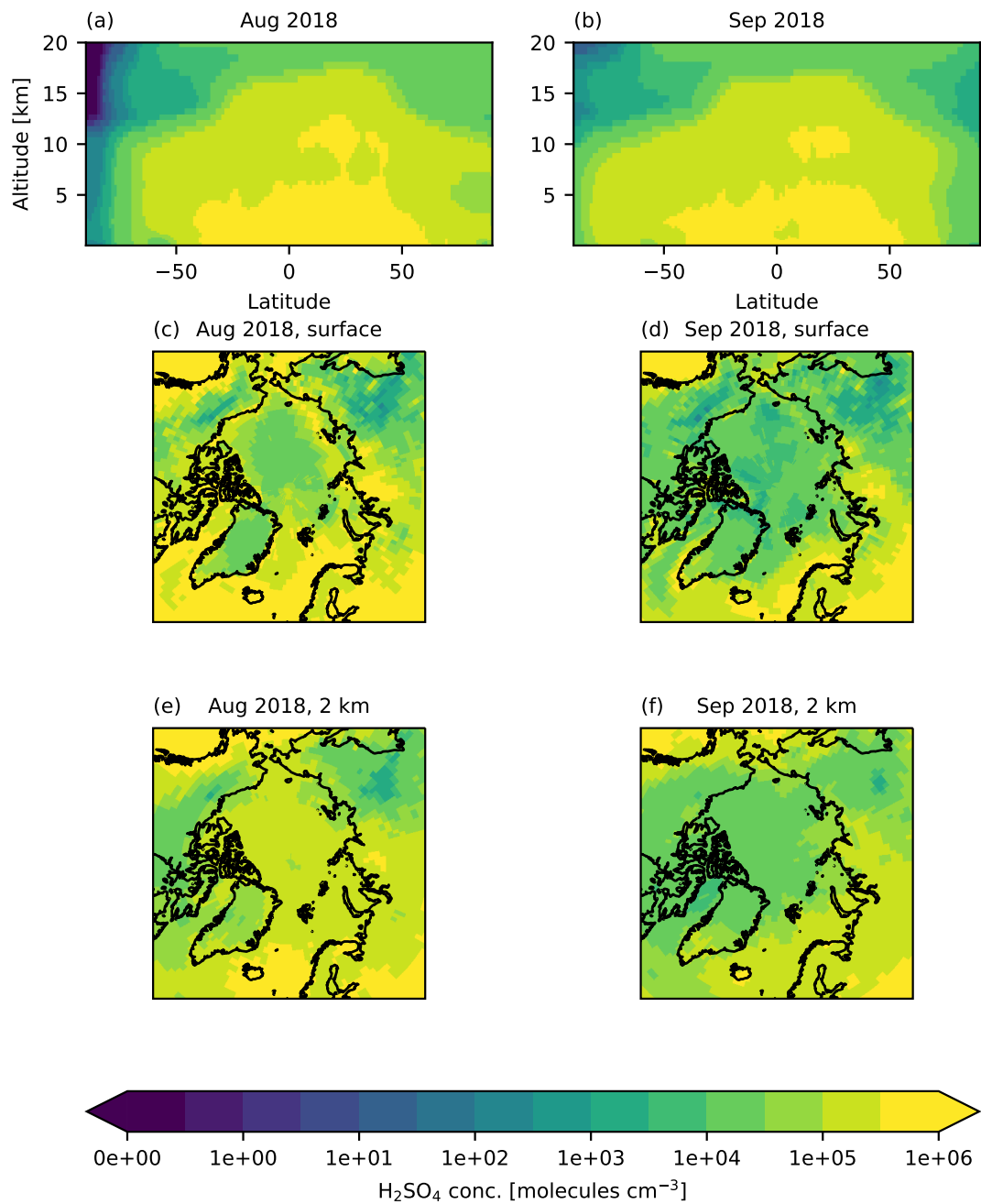


Figure A.4: Zonal means and maps of simulated monthly mean H_2SO_4 concentration from simulation CONTROL. Maps are taken from model level (c-d) at surface and (e-f) with altitude 2 km.

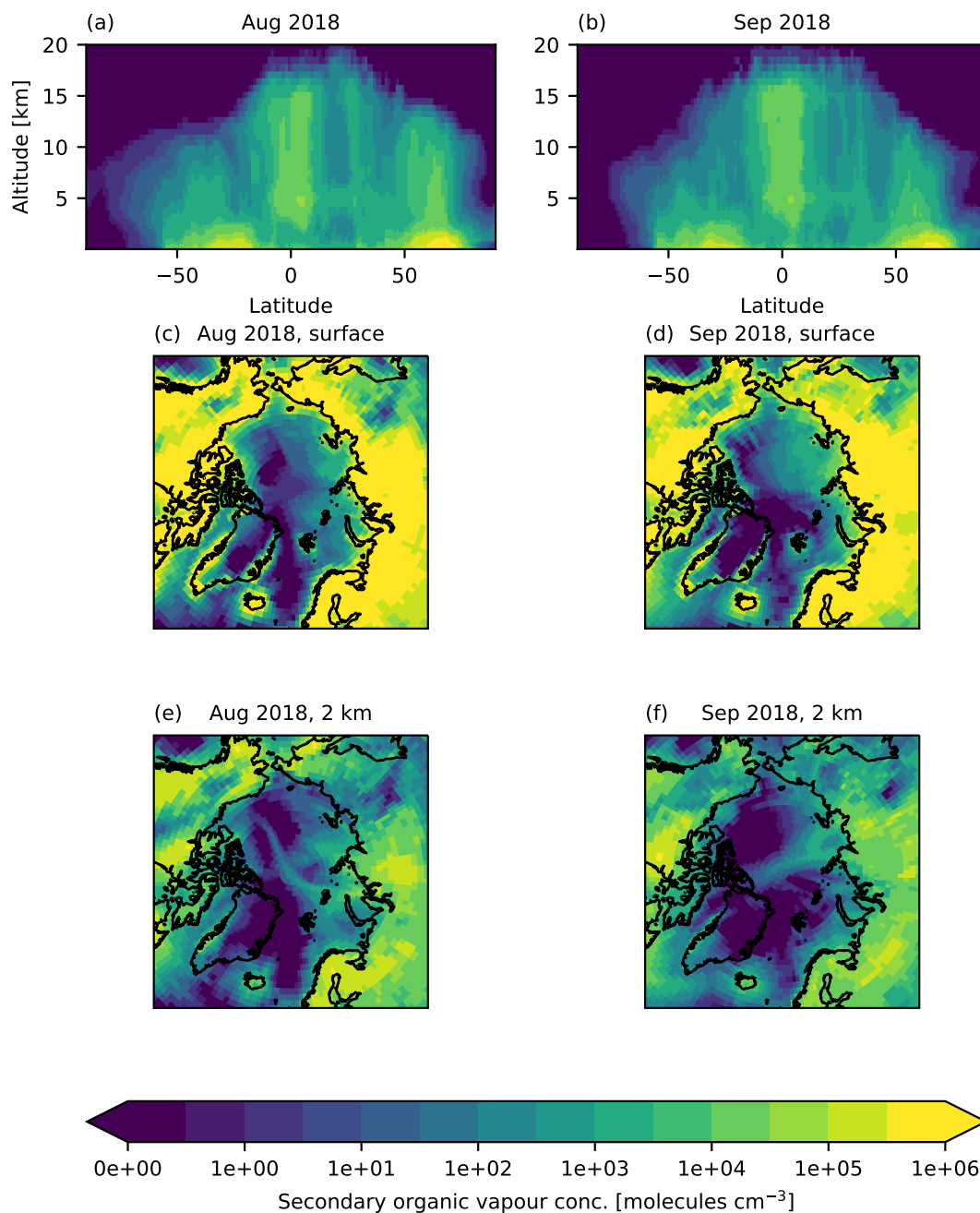


Figure A.5: Zonal means and maps of simulated monthly mean secondary organic vapour concentration from simulation CONTROL. Maps are taken from model level (c-d) sat surface and (e-f) with altitude 2 km.

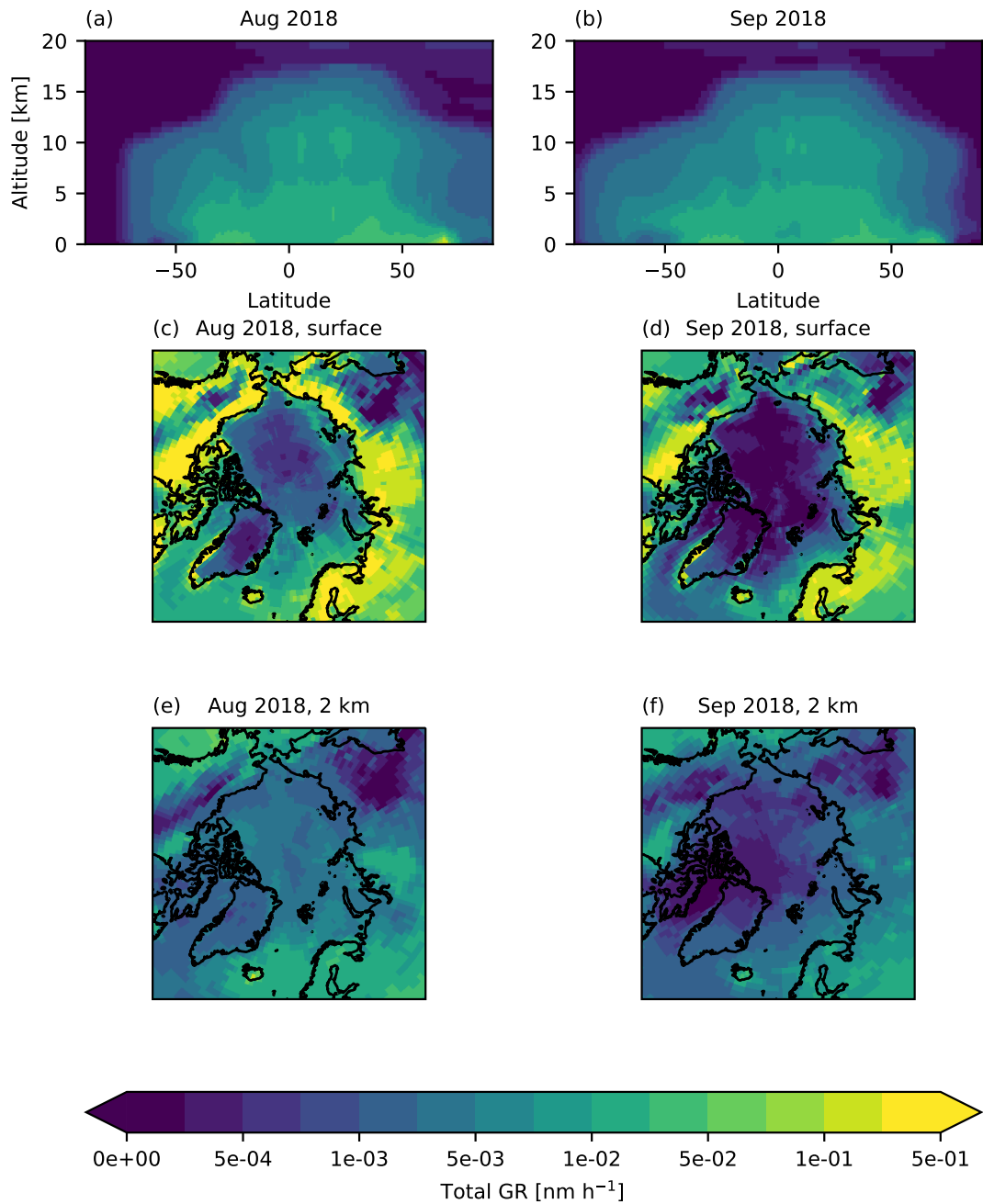


Figure A.6: Zonal means and maps of aerosol growth rates from simulation CONTROL. Growth rates are calculated offline using model output of temperature and concentrations of H_2SO_4 and secondary organic vapour. Maps are taken from model level (c-d) at surface and (e-f) with altitude 2 km.

